Trends in Plant Science

CellPress

Opinion

Bending to auxin: fast acid growth for tropisms

Lanxin Li, [1] Michelle Gallei, [1] and Jiří Friml [1,*]

The phytohormone auxin is the major growth regulator governing tropic responses including gravitropism. Auxin build-up at the lower side of stimulated shoots promotes cell expansion, whereas in roots it inhibits growth, leading to upward shoot bending and downward root bending, respectively. Yet it remains an enigma how the same signal can trigger such opposite cellular responses. In this review, we discuss several recent unexpected insights into the mechanisms underlying auxin regulation of growth, challenging several existing models. We focus on the divergent mechanisms of apoplastic pH regulation in shoots and roots revisiting the classical Acid Growth Theory and discuss coordinated involvement of multiple auxin signaling pathways. From this emerges a more comprehensive, updated picture how auxin regulates growth.

Highlights

The Acid Growth Theory applies to both shoots and roots but the mechanisms of auxin-triggered apoplastic pH regulations are different.

Auxin activates plasma membrane (PM) H^+-ATPases both in shoots and roots, contributing to shoot growth promotion while counteracting root growth inhibition.

Cell surface TMK1 signaling directly activates PM H^+-ATPases for apoplast acidification in both shoots and roots.

Intracellular TIR1/AFB auxin signaling, besides transcriptional regulation, has a non-transcriptional branch mediating apoplast alkalinization in roots.

Auxin-induced rapid apoplast alkalinization in roots occurs not through PM H^+-ATPase regulation, but by an unidentified mechanism of H^+ influx.

Directional growth as key mechanism for plant adaptive development

Plant cells do not migrate during tissue patterning and the whole body plan results from orientated cell division and growth. This puts the regulation of cell expansion at the center of plant development and its adaptation to the environment [1], with tropisms being spectacular examples. During gravitropism, the phytohormone auxin is transported to the lower side of the stimulated organ, where the cell growth is promoted (in shoots) or inhibited (in roots). The resulting differential growth rate between the lower and upper side of the organ leads to upward or downward bending, respectively [2]. This is a prime example of the contribution of regulated cell expansion to general plant development and adaptive behavior. Despite the importance of auxin in cell signaling, how it regulates cell expansion oppositely in shoots and roots remains largely unknown. Several contemporary studies focusing on the mechanism of auxin-induced rapid root growth inhibition and shoot growth promotion, as well as novel auxin signaling pathways provide cutting-edge insights into this topic.

Main entry points for the regulation of cell expansion

To understand how the growth of plant cells is regulated, one must consider their special features. Distinct from animal cells, plant cells have a high turgor pressure ranging between 0.6 and 1 MPa [3], and are encased by a structural layer of the cell wall. Plant cell growth is the consequence of the balance between the driving force (turgor pressure) and the limiting force (cell wall). The turgor pressure increases by osmosis-driven water uptake driven by the membrane potential, which is built up by the difference in the ion concentrations across the plasma membrane (PM) resulting from the active H^+ pumping out of the cell. The vacuole which accumulates water and osmotic compounds possibly also contributes to turgor-driven growth regulation [4]. The robust cell wall limits expansion of the pressurized cells. The cell wall rigidity depends not only on the composition and structural arrangements, which are regulated by cortical microtubules (CMTs), but also on the cell wall-based enzymes, whose activities are regulated by the apoplastic pH [5–7]. Hence, ion fluxes, apoplastic pH, CMTs, and vacuoles, are all potentially contributing to the regulation of cell growth.

[1]Institute of Science and Technology Austria, 3400 Klosterneuburg, Austria

*Correspondence: jiri.friml@ist.ac.at (J. Friml).

© 2021 Elsevier Ltd. All rights reserved.

Auxin: one signal with manifold performances

Auxin is the main endogenous signal regulating cell growth across the plant with shoots and roots having distinct sensitivities. Exogenous auxin promotes the elongation of arabidopsis (*Arabidopsis thaliana*) hypocotyl segments even at 10 μM [8], whereas it already inhibits root growth at 5 nM [9]. Similarly, following gravistimulation, auxin accumulation stimulates cell expansion in shoots, whereas inhibits it in roots [10,11]. The timing of growth responses in the two organs is also different. Following gravistimulation, arabidopsis hypocotyl starts bending after 1–2 hours and it takes *circa* 4–6 hours to reach the half-bending angle [12]. By comparison, the root starts bending visibly already 10 minutes after gravistimulation and it takes *circa* 40–60 minutes to reach the half-bending angle [13,14]. Similarly, exogenous auxin application promotes the growth of etiolated hypocotyl segments in about 20 minutes [15], whereas inhibits it in intact roots in less than 30 seconds [9,16], despite that the organs transcription responds to auxin in a similar time scale of *circa* 20 minutes as reported by DR5::LUC reporters [9,15]. These differences in concentration and timing suggest that the mechanism of auxin-triggered cell growth regulation differs between shoots and roots.

To understand how auxin regulates cell growth in different tissues, we focus on: (i) auxin-triggered cellular responses; and (ii) upstream auxin signaling. During auxin-induced root growth regulation, auxin triggers a series of cellular responses, such as cortical microtubule (CMT) reorientation, vacuole constriction, Ca^{2+} transients, apoplast alkalinization, membrane depolarization, and K^{+} efflux. We critically examine the involvement of those cellular responses and upstream signaling in growth regulation.

CMT reorientation: a consequence not the cause

CMTs are microtubule arrays located close to the PM. In elongating cells, they colocalize with and are required for guiding the cellulose synthase complex, which produces cellulose fibrils building the main structure of the cell wall [17,18]. The orientation of CMTs thus determines the anisotropy of the cell wall, to either restrict or allow cell expansion in a certain direction. Therefore, CMTs contribute to growth regulation and may be, potentially, part of the mechanism by which auxin regulates growth.

In response to auxin, CMTs reorient from longitudinal to transversal in respect to the growth axis in etiolated arabidopsis hypocotyls and oppositely in roots. In both organs, the CMT orientation correlates with the growth regulation. Nonetheless, the causal relationship has remained a matter of debate over the years [19,20]. Recent pharmacological and genetic studies in arabidopsis hypocotyls consistently argued that CMT reorientation is not a crucial part of the auxin-triggered mechanism for growth regulation [8]. For example, auxin can promote growth normally, even when CMTs are depolymerized, confirming that intact CMTs are not essential. Conversely, auxin treatment in hyperosmotic conditions that prevent growth, does not lead to CMT reorientation. This shows that in shoots CMT reorientation responds to the growth promotion but not to auxin itself [8]. Similarly in roots, kinetic analysis of CMTs after auxin treatment demonstrated that a significant CMT reorientation occurred later than growth inhibition [16]. Furthermore, the inhibition of auxin-triggered CMT reorientation by the microtubule (MT) stabilizer Taxol does not influence the growth inhibition by auxin [16]. Collectively, in both shoots and roots, CMT reorientation is the indirect consequence rather than cause of the auxin-induced growth change (Figure 1).

Vacuolar constriction: too late for the show

Vacuoles are unique plant organelles. Their development is a dynamic combination of fusion and fragmentation of liquid pouches, the size of which can take up to 90% of a mature plant cell [21].

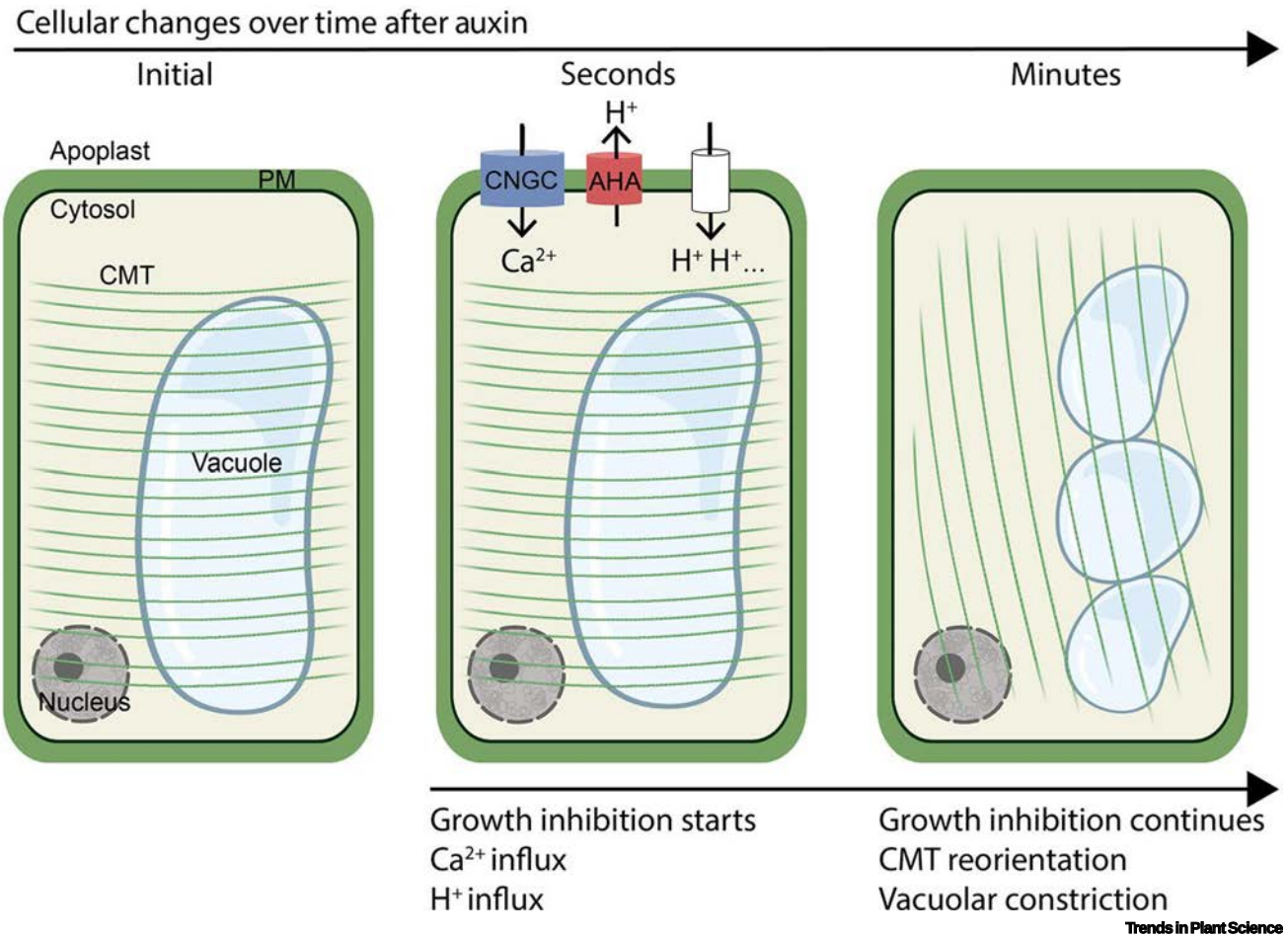

Figure 1. The time scale of auxin-triggered fast cellular responses in arabidopsis roots. In response to increased auxin levels, root cells show a rapid H^+ influx. This is contributed by CNGC14-mediated Ca^{2+} transient, but not by PM H^+-ATPases. The resulting apoplastic alkalinization causes root growth inhibition within seconds. Responding to the growth inhibition, the cortical microtubules (CMTs), green lines, are then reoriented from transversal to longitudinal/oblique. The vacuoles are constricted at later time points; not consistent with their direct involvement in rapid auxin-induced growth inhibition. Abbreviations: AHA, PM H^+-ATPase; CNGC, cyclic nucleotide-gated channel; PM, plasma membrane.

Due to their potential contribution to the osmotic properties of cells, vacuoles have been linked to the regulation of cell growth [4,22].

During auxin-triggered root growth inhibition, a concomitant constriction of vacuoles has been observed [4]. Similar to CMT reorientation, the question remains whether the vacuolar constriction contributes to or is only the consequence of growth inhibition. The kinetics of vacuole morphology and cell length in roots after auxin treatment revealed that vacuole changes take place within 15–25 minutes, thus seemingly preceding cell length changes, which were visible in the late meristematic zone by the applied method only after about 45–55 minutes. All genetic and pharmacological manipulations however of auxin signaling and cellular processes were analyzed only after 20 hours of the respective treatment [4,22] not allowing for definite statements about time dynamics. Also, there was no obvious auxin-triggered change in the vacuole morphology in the elongating cells [16], which have the highest capacity of growth regulation by auxin [23,24]. This puts the process of vacuolar morphology changes well outside the time scale of auxin-

triggered root growth inhibition, which occurs faster than 30 seconds [9], arguing against its direct involvement in the mechanism of immediate auxin-induced root growth inhibition (Figure 1).

Early auxin birds: Ca^{2+}, H^+, and K^+ fluxes across the PM

Unlike CMT reorientation and vacuole constriction, ion fluxes across the PM in root cells change almost immediately after auxin application. The most significant ones are Ca^{2+} and H^+ influxes (Figure 1). Specifically, a cytosolic Ca^{2+} transient and a rhizospheric pH increase occurred within 7–14 seconds and 15 seconds, respectively, after auxin treatment [25]. Consistently, the apoplast pH was increased upon auxin application in 30 seconds or earlier [16]. During gravitropism, both cytosolic Ca^{2+} levels and the rhizospheric pH changed in both upper (decreased Ca^{2+} and pH) and lower (increased Ca^{2+} and pH) flank 2–6 minutes after gravistimulation [25]. Therefore, the Ca^{2+} transient and external pH changes are very early responses to auxin and closely correlate with auxin-induced rapid root growth inhibition [16] (Figure 1).

The possible causal relationship between the auxin-induced Ca^{2+} transient, extracellular alkalinization, and root growth inhibition has been addressed pharmacologically and genetically. The Ca^{2+} channel inhibitor $LaCl_3$ interferes with auxin-induced rhizosphere alkalinization [25]. Similarly, mutation of the Ca^{2+} permeable cation channel Cyclic NUCLEOTIDE-GATED CHANNEL 14 (CNGC14) leads to a delay of apoplast alkalinization and growth inhibition of *circa* 6 minutes after auxin application [16,26]. Besides, depletion of Ca^{2+} in the medium results in a diminished Ca^{2+} transient as well as a delay of pH and growth responses of *circa* 4–6 minutes [16]. This suggests that CNGC14-mediated Ca^{2+} transients contribute to early auxin response by apoplast alkalinization and growth inhibition.

In contrast to an influx of Ca^{2+} and H^+, K^+ is transported out of root cells after auxin [16]. The efflux of K^+ leads to less water uptake [27], in line with less cell expansion. Besides, the total net ion fluxes across the PM after auxin result in a rapid membrane depolarization [28,29], contributing to the growth inhibition.

In the driver's seat: apoplastic pH changes and the Acid Growth Theory

Auxin application leads to apoplastic pH changes simultaneously with the growth regulation in both shoots and roots. Not only the time scale, but also the trend of the change in the apoplastic pH and growth regulation coincide. In shoots, auxin leads to slower acidification and growth promotion [15,30]; while in roots, it results in rapid alkalinization and growth inhibition [16,25,31]. The long-standing Acid Growth Theory suggests that the apoplastic pH directly regulates the cell growth. Acidification of the apoplast activates pH-dependent expansins that loosen the otherwise rigid cell wall allowing for cell expansion. Concomitantly, the H^+ efflux builds up a higher membrane potential that drives the secondary ion influx, leading to an increase in turgor pressure and water uptake [27]. In this theory, H^+ flux across the PM coordinates both the cell wall rigidity and turgor pressure to regulate cell growth [27].

The molecular mechanism of the Acid Growth Theory has been well established in the arabidopsis hypocotyl. Auxin transcriptionally upregulates the expression level of SMALL AUXIN Up-RNA 19 (SAUR19), which binds to and inhibits the TYPE 2C PROTEIN PHOSPHATASES (PP2C). PP2C normally dephosphorylates and inhibits the activity of the PM H^+-ATPases [30,32]. By inhibiting the PM H^+-ATPases inhibitor, this auxin-induced activation of the PM H^+-ATPases leads to apoplast acidification and thus promotes shoot growth [15,33]. In addition, recent discoveries revealed that the PM H^+-ATPases can be directly phosphorylated and activated by the cell surface kinase TRANSMEMBRANE KINASE 1 (TMK1) in both shoots and roots [16,34]. Particularly in shoots, auxin induces interaction between TMK1 and AHA1 in 10 seconds, and auxin-induced

acidification requires TMK1 and TMK4 [34]. This adds a missing mechanism in shoots for initial phosphorylation and activation of PM H^+-ATPases before the SAUR-mediated transcriptional mechanism sets in. Nonetheless, the relevance of this mechanism for shoot growth is not entirely clear, considering that auxin induces apoplast acidification and growth in hypocotyl segments with a delay of about 20 minutes, and it strongly relies on transcriptional TRANSPORT INHIBITOR RESPONSE1/AUXIN-SIGNALLING F-BOX protein (TIR1/AFB)-mediated signaling [15].

In roots, the situation is more complex. Here, auxin induces apoplast alkalinization leading to growth inhibition, thus also following the main premise of the Acid Growth Theory. However, the auxin-triggered, TMK1-mediated activation of PM H^+-ATPases, mediates apoplast acidification also in the root [16,35]. This counteracts the observed more dominant apoplast alkalinization [16]. The physiological meaning of these antagonistic gas–brake growth regulations is unclear, but it might be important to fine-tune the root growth during navigating a complex soil environment.

The mechanism underlying TIR1/AFB-mediated apoplast alkalinization remains unclear. Besides alkalinization of the apoplast, auxin triggers simultaneously acidification in the cytosol next to the PM and increases net H^+ influx, suggesting that auxin promotes H^+ influx to alkalinize the apoplast and depolarize the PM for rapid root growth inhibition [16,28]. The question of how this is achieved remains. One possibility is that this inward H^+ flow is directly symported by the active auxin importer AUX1/LAX, with 2 H^+ per IAA molecule [29]. However, a conserved estimation does not favor it; the amount of auxin-induced H^+ influx measured in primary roots or root hairs is a magnitude higher than the maximum amount of H^+ symported by the overexpressed AUX1 in *Xenopus laevis* oocytes [16]. Additionally, bypassing auxin import by directly injecting auxin into root hair cytosol still led to a consistent membrane depolarization, though with a transient hyperpolarization [29]. This suggests that auxin-induced membrane depolarization or H^+ influx is not contributed significantly by auxin import itself.

Other possibilities include that auxin regulates an ion transporter or channel that symports H^+, or actively opens a H^+ channel, or creates a H^+ leak in the membrane by some other mechanism. Considering that this process seems to be linked to cytosolic Ca^{2+} transients [36], it is possible that the H^+ symporter might be a Ca^{2+} transporter or channel. Nonetheless, the Ca^{2+} transient and pH change displayed different kinetics following auxin treatment or gravistimulation [25] not supporting the hypothesis that Ca^{2+} and H^+ are symported. Therefore, it is likely that auxin actively opens an unknown H^+ channel that may be Ca^{2+}-dependent.

In summary, following the classical Acid Growth Theory, the auxin-induced apoplastic pH changes are the major cellular mechanism of the growth regulation in both shoots and roots. In shoots, auxin acidifies the apoplast via transcriptional activation [15,30] and post-translationally by maintaining the activation of PM H^+-ATPases [34]. In roots, though this post-translational activation of PM H^+-ATPases also applies, a more dominant process is immediate, auxin-triggered apoplast alkalinization, mediated by a non-transcriptional branch of the TIR1/AFB signaling (see next section), possibly occurring through non-transcriptional activation of a H^+ channel for a rapid H^+ influx [16].

Not so canonical: TIR1/AFB-mediated non-transcriptional responses

The canonical, nuclear auxin signaling pathway, is well characterized and has been for decades thought, rather exclusively, to be the mechanism mediating auxin effect on gene transcription. It begins with the auxin perception facilitating the binding between the co-receptors, SCF-TIR1/AFB ubiquitin ligases and the Aux/IAA transcriptional repressors. This leads to the ubiquitination of the Aux/IAAs and their further degradation via the 26S proteasome. Consequently, the

repression of AUXIN RESPONSE FACTOR (ARFs) is released and they are free to act on auxin response genes [37–39] (Figure 2).

The exception has been discovered in roots, where auxin alkalinizes the apoplast and inhibits growth faster than 30 seconds. This response time is far too fast for the transcriptional regulation to be involved and, in addition, the rapid auxin effects are observed also when transcription is inhibited [9,16], altogether suggesting a non-transcriptional signaling mechanism.

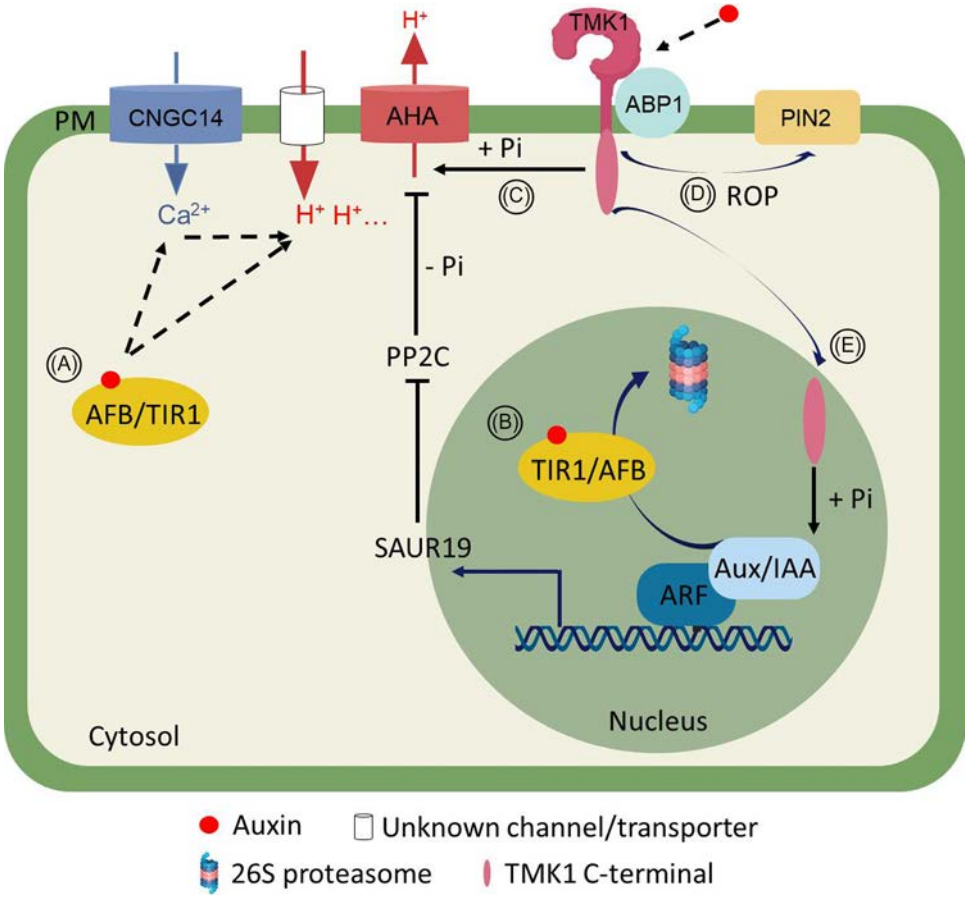

Figure 2. Auxin signalling pathways in arabidopsis. (A) Non-transcriptional branch of the TIR1/AFB pathway in roots. Intracellular auxin perceived by the cytosolic fraction of TIR1/AFB triggers a rapid CNGC14-mediated Ca^{2+} influx and an unknown channel or transporter-mediated H^+ influx across the PM. The H^+ influx, contributed by the Ca^{2+} transient, leads to apoplast alkalinization and thus rapid root growth inhibition. (B) The canonical, transcriptional TIR1/AFB pathway. Intracellular auxin perceived by the nuclear fraction of TIR1/AFB and Aux/IAAs leads to ubiquitination and 26S proteasome-mediated degradation of Aux/IAAs. Consequently, the inhibition of Aux/IAAs on the ARF-regulated downstream gene transcription is released including SAUR19, which inhibits PP2C that normally dephosphorylates and thus deactivates AHA. Thereby, AHA becomes activated. (C) The PM-localized TMK1, directly phosphorylates and activates AHA in both shoots and roots. (D) The PM-localized TMK1, which might perceive external auxin through ABP1, activates ROPs for pavement cell expansion and regulates PIN2 during root gravitropic response. (E) The PM-localized TMK1, in response to auxin, has its C-terminal kinase domain cleaved and translocated to the nucleus for phosphorylating and stabilizing non-canonical Aux/IAAs, regulating gene transcription in the apical hook. Abbreviations: ABP1, AUXIN BINDING PROTEIN 1; AHA, PM H^+-ATPase; ARF, AUXIN RESPONSE FACTOR; CNGC14, Cyclic NUCLEOTIDE-GATED CHANNEL 14; PIN2, PIN-FORMED 2; PM, plasma membrane; PP2C, type 2C protein phosphatases; ROP, RHO-RELATED PROTEIN FROM PLANTS; SAUR19, SMALL AUXIN Up-RNA 19; TIR1/AFB, TRANSPORT INHIBITOR RESPONSE1/AUXIN-SIGNALLING F-BOX protein; TMK1, TRANSMEMBRANE KINASE 1.

Nonetheless, several observations clearly show that this signaling is still dependent on TIR1/AFB receptors. For example, the *tir1* and *afb* mutants display less auxin sensitivity in terms of apoplast alkalinization, membrane depolarization, cytosolic Ca^{2+} increase, and root growth inhibition [9,16,29]. Furthermore, using an engineered ccvTIR1 and cvxIAA pair system, which allows for specific and selective activation of TIR1/AFB signaling [35], the cvxIAA-mediated ccvTIR1 activation is sufficient to trigger apoplast alkalinization, cytosolic Ca^{2+} transients, and root growth inhibition [9,16]. These observations lead to the conclusion that TIR1/AFB signaling has a non-transcriptional branch mediating auxin effect on rapid responses including CNGC14-mediated Ca^{2+} transients, apoplast alkalinization, and rapid root growth inhibition [40] (Figure 2).

Recent observations provide initial insights into this novel branch of the TIR1/AFB pathway. First, the subcellular localization of all six TIR1/AFB proteins in arabidopsis was examined. In roots, AFB1 is most abundant in the cytosol while TIR1 is mainly found in the nucleus [41]. It has been proposed that the cytosolic fraction of TIR1/AFBs may contribute to the fast non-transcriptional regulation for the rapid growth response while the nuclear fraction is more responsible for the slower, transcriptional regulation (Figure 2). Accordingly, the *afb1* mutant is less auxin-sensitive than wild type (WT) and *tir1* in terms of root growth inhibition, membrane potential decrease, or apoplast alkalinization [16,28,41]; while *tir1* is more auxin-resistant to root growth inhibition than *afb1* in a longer term (>6h) [16].

Thus, an unknown branch of auxin signaling pathway starting presumably with cytosolic TIR1/AFB receptors mediates rapid apoplast alkalinization, membrane depolarization, and growth inhibition in roots. It remains unclear, at which point the branching occurs and whether the known downstream components such as Aux/IAAs and ARFs are involved. The key question is, however, the mechanism, by which this pathway promotes influx of H^+ into the cell leading to collapse of the H^+ gradient across the PM, apoplast alkalinization, and membrane depolarization. It remains a challenge for future investigations to establish what this molecular mechanism of apoplast alkalinization may be and how it is activated by the fast TIR1/AFB signaling.

TMKs: receptors or receptor-likes?

Four leucine-rich receptor-like kinases, which form the TMK family, have been proposed as components of a largely elusive auxin signaling initiated at the cell surface. TMKs act in general growth regulation and downstream of auxin [42,43]. At the concave side of the apical hook, TMK1 in response to auxin has its C-terminal kinase domain cleaved and translocated to the nucleus, where it phosphorylates and stabilizes noncanonical Aux/IAAs, resulting in gene transcription regulation [44] (Figure 2). This provides a mechanism, by which TMK1 and TIR1/AFB-Aux/IAA signaling mechanisms converge on transcriptional regulation.

Conversely, TMKs contribute also to non-transcriptional regulation of cell growth. TMKs are required for the auxin-induced rapid activation (within 30 seconds) of RHO-RELATED PROTEIN FROM PLANTS 2 (ROP2) and ROP6 GTPases during pavement cell expansion [45–47]. A similar mechanism may act during root gravitropism, where TMK1 is important for ROP6 activation, which regulates PIN-FORMED 2 (PIN2) localization to affect root gravitropic response [48,49] (Figure 2). Notably, both TMK and ROPs have been shown to localize into nanocluster structures presumably dependent on lipid membrane composition [47,50] but physiological relevance of this localization remains unclear.

A mechanism emerges, by which the TMK pathway regulates apoplastic pH and cell growth via activating H^+ export. As mentioned before, TMK1 activation of PM H^+-ATPases [16,34] in shoots maintains the initial phosphorylation of PM H^+-ATPases presumably aiding the TIR1/

AFB-mediated transcriptional regulation for a slow apoplast acidification and growth promotion [34]. Conversely, in roots, the TMK1–AHA2 mechanism acts antagonistically to the rapid, non-transcriptional branch of the TIR1/AFB pathway, fine-tuning the root growth regulation [16] (Figure 2).

Another TMK family member, TMK4, was identified to have a distinctive role in regulating auxin biosynthesis. In response to auxin, TMK4 phosphorylates the TRYPTOPHAN AMINOTRANSFERASE OF ARABIDOPSIS (TAA1), a key enzyme in the auxin biosynthesis pathway, leading to a suppression of auxin biosynthesis [51]. Therefore, downstream of the auxin pathway, TMK4 acts as negative feedback in the regulation of root meristem size and root hair development.

Taken together, TMKs regulate the general and the auxin-regulated cell expansion in multiple ways (Figure 2), however, the details of the downstream mechanisms are largely unknown. For example, whether auxin-triggered cleavage of TMKs' C terminus occurs and regulates other processes besides the apical hook, or how the downstream ROP activation participates in auxin-induced growth regulation, remains to be investigated.

The main open question concerns how auxin activates the TMK pathway. One possibility would be that auxin binds directly to extracellular domain of TMKs and activates them but there are no observations supporting this scenario. A more plausible possibility is that another protein that binds auxin interacts with TMKs and activates them. The candidate for such 'co-receptor' is AUXIN BINDING PROTEIN 1 (ABP1), which has been shown to interact with TMK1 [45]. ABP1 has been considered for decades as a possible auxin receptor, based on the ability of the maize ABP1 to bind to auxin [52,53]. Any function of ABP1 however was put into doubt due to a lack of obvious phenotypic defects in the verified knockout mutants [54]. A systematic analysis confirmed only minor defects in the *abp1* loss-of-function mutants, whereas gain-of-function alleles showed a broad spectrum of growth and developmental aberrations [55]. This discrepancy might be caused by functional gene redundancy, presumably from the germin superfamily, to which ABP1 belongs [52,56]. Nonetheless, until these potentially redundant proteins are identified and/or involvement of both ABP1 and TMK in some process(es) are genetically verified, the role of ABP1 as auxin receptor for the TMK-mediated auxin signaling remains hypothetical (Figure 2).

Concluding remarks

Auxin regulates cell expansion and triggers various short and long-term cellular responses. Some are direct parts of the mechanism for auxin-induced growth regulation, others the indirect consequences of the growth regulation *per se*. Auxin-induced CMT reorientation and vacuole fragmentation belong to the latter case. Still, they regulate the capacity of cell growth and contribute to the control of the eventual cell size. By contrast, the auxin-induced Ca^{2+} transient is an instant response, which may be linked to auxin-triggered H^+ flux across the PM and the apoplastic pH change. The auxin-induced apoplastic pH change regulates cell growth following the Acid Growth Theory, with acidification promoting and alkalinization inhibiting growth. However, the mechanisms of how auxin regulates apoplastic pH varies between shoots and roots.

In shoots, auxin acidifies the apoplast through PM H^+-ATPase activation, the process mediated by both (i) the nuclear TIR1/AFB transcriptional pathway via inhibiting of PP2C phosphatase acting on PM H^+-ATPases; and (ii) direct phosphorylation and activation by the cell surface-based TMK1 receptor-like kinase. By contrast, in roots, auxin alkalinizes the apoplast via rapid activation of H^+ influx, a process, which is mediated through an unknown, non-transcriptional branch of the cytosolic TIR1/AFB auxin pathway. Meanwhile, the nuclear fraction of TIR1/AFB presumably mediates the sustained and long-term effect of root growth inhibition. Conversely,

Outstanding questions

What is the molecular mechanism of auxin-triggered H^+ influx for root growth inhibition?

How does the non-transcriptional AFBs/TIR1 signaling branch look like?

Does it involve AUX/IAAs' ubiquitination and degradation?

Do cytosolic and nuclear fractions of TIR1/AFBs mediate distinct functions?

How does the TMK pathway perceive auxin?

the cell surface-based TMK1 directly binds and activates PM H^+-ATPase also in roots; their functioning antagonistic to the apoplast alkalinization, fine-tuning the root growth regulation. A future challenge will be to unravel the mechanism of rapid H^+ influx and better characterize all various auxin signaling mechanisms (see Outstanding questions).

Acknowledgments

The authors thank Alexandra Mally for editing the text. This work was supported by the Austrian Science Fund (FWF) I 3630-B25 to Jiří Friml and the DOC Fellowship of the Austrian Academy of Sciences to Lanxin Li. All figures were created with BioRender.com.

Author Contributions

Lanxin Li and Jiří Friml wrote the manuscript. Michelle Gallei helped with corrections.

Declaration of interests

No interests to declare.

References

1. Su, S.-H. *et al.* (2017) Molecular mechanisms of root gravitropism. *Curr. Biol.* 27, R964–R972
2. Nakamura, M. *et al.* (2019) Bridging the gap between amyloplasts and directional auxin transport in plant gravitropism. *Curr. Opin. Plant Biol.* 52, 54–60
3. Schopfer, P. (2006) Biomechanics of plant growth. *Am. J. Bot.* 93, 1415–1425
4. Löfke, C. *et al.* (2015) Auxin regulates SNARE-dependent vacuolar morphology restricting cell size. *Elife* 4, e05868
5. Atanasova, L. *et al.* (2018) Evolution and functional characterization of pectate lyase PEL12, a member of a highly expanded *Clonostachys rosea* polysaccharide lyase 1 family. *BMC Microbiol.* 18, 178
6. Hocq, L. *et al.* (2017) Connecting homogalacturonan-type pectin remodeling to acid growth. *Trends Plant Sci.* 22, 20–29
7. Samalova, M. *et al.* (2020) Expansin-controlled cell wall stiffness regulates root growth in Arabidopsis. *bioRxiv* Published online July 31, 2020. https://doi.org/10.1101/2020.06.25.170969
8. Adamowski, M. *et al.* (2019) Reorientation of cortical microtubule arrays in the hypocotyl of *Arabidopsis thaliana* is induced by the cell growth process and independent of auxin signalling. *Int. J. Mol. Sci.* 20, 3337
9. Fendrych, M. *et al.* (2018) Rapid and reversible root growth inhibition by TIR1 auxin signalling. *Nat. Plants* 4, 453
10. Rakusová, H. *et al.* (2016) Termination of shoot gravitropic responses by auxin feedback on PIN3 polarity. *Curr. Biol.* 26, 3026–3032
11. Pařízková, B. *et al.* (2017) What has been seen cannot be unseen—detecting auxin *in vivo*. *Int. J. Mol. Sci.* 18, 2736
12. Rakusová, H. *et al.* (2011) Polarization of PIN3-dependent auxin transport for hypocotyl gravitropic response in *Arabidopsis thaliana*. *Plant J.* 67, 817–826
13. Taniguchi, M. *et al.* (2017) The Arabidopsis LAZY1 family plays a key role in gravity signalling within statocytes and in branch angle control of roots and shoots. *Plant Cell* 29, 1984–1999
14. Bailly, A. *et al.* (2008) Modulation of P-glycoproteins by auxin transport inhibitors is mediated by interaction with immunophilins. *J. Biol. Chem.* 283, 21817–21826
15. Fendrych, M. *et al.* (2016) TIR1/AFB-Aux/IAA auxin perception mediates rapid cell wall acidification and growth of Arabidopsis hypocotyls. *Elife* 5, e19048
16. Li, L. *et al.* (2021) Cell surface and intracellular auxin signalling for H^+ fluxes in root growth. *Nature* 599, 273–277
17. Paredez, A.R. *et al.* (2006) Visualization of cellulose synthase demonstrates functional association with microtubules. *Science* 312, 1491–1495
18. Li, S. *et al.* (2012) Cellulose synthase interactive protein 1 (CSI1) links microtubules and cellulose synthase complexes. *Proc. Natl. Acad. Sci. U. S. A.* 109, 185–190
19. Chen, X. *et al.* (2014) Inhibition of cell expansion by rapid ABP1-mediated auxin effect on microtubules. *Nature* 516, 90
20. Le, J. *et al.* (2005) Cell elongation and microtubule behavior in the Arabidopsis hypocotyl: responses to ethylene and auxin. *J. Plant Growth Regul.* 24, 166–178
21. Tan, X. *et al.* (2019) A review of plant vacuoles: formation, located proteins, and functions. *Plants* 8, 327
22. Kaiser, S. and Scheuring, D. (2020) To lead or to follow: contribution of the plant vacuole to cell growth. *Front. Plant Sci.* 11, 553
23. Verbelen, J.-P. *et al.* (2006) The root apex of *Arabidopsis thaliana* consists of four distinct zones of growth activities: meristematic zone, transition zone, fast elongation zone, and growth terminating zone. *Plant Signal. Behav.* 1, 296–304
24. Baskin, T.I. *et al.* (2020) Positioning the root elongation zone is saltatory and receives input from the shoot. *iScience* 23, 101309
25. Monshausen, G.B. *et al.* (2011) Dynamics of auxin-dependent Ca^{2+} and pH signalling in root growth revealed by integrating high-resolution imaging with automated computer vision-based analysis. *Plant J.* 65, 309–318
26. Shih, H.-W. *et al.* (2015) The cyclic nucleotide-gated channel CNGC14 regulates root gravitropism in *Arabidopsis thaliana*. *Curr. Biol.* 25, 3119–3125
27. Arsuffi, G. and Braybrook, S.A. (2018) Acid growth: an ongoing trip. *J. Exp. Bot.* 137–146
28. Serre, N.B. *et al.* (2021) AFB1 controls rapid auxin signalling through membrane depolarization in *Arabidopsis thaliana* root. *Nat. Plants* 7, 1229–1238
29. Dindas, J. *et al.* (2018) AUX1-mediated root hair auxin influx governs $SCF^{TIR1/AFB}$-type Ca^{2+} signalling. *Nat. Commun.* 9, 1174
30. Spartz, A.K. *et al.* (2014) SAUR inhibition of PP2C-D phosphatases activates plasma membrane H^+-ATPases to promote cell expansion in Arabidopsis. *Plant Cell* 26, 2129–2142
31. Barbez, E. *et al.* (2017) Auxin steers root cell expansion via apoplastic pH regulation in *Arabidopsis thaliana*. *Proc. Natl. Acad. Sci. U. S. A.* 114, E4884–E4893
32. Ren, H. *et al.* (2018) A subset of plasma membrane-localized PP2C.D phosphatases negatively regulate SAUR-mediated cell expansion in Arabidopsis. *PLoS Genet.* 14, e1007455
33. Du, M. *et al.* (2020) Rapid auxin-mediated cell expansion. *Annu. Rev. Plant Biol.* 71, 379–402
34. Lin , W. *et al.* (2021) TMK-based cell surface auxin signalling activates cell-wall acidification. *Nature* 599, 278–282
35. Uchida, N. *et al.* (2018) Chemical hijacking of auxin signalling with an engineered auxin–TIR1 pair. *Nat. Chem. Biol.* 14, 299
36. Behera, S. *et al.* (2018) Cellular Ca^{2+} signals generate defined pH signatures in plants. *Plant Cell* 30, 2704–2719
37. Lavy, M. and Estelle, M. (2016) Mechanisms of auxin signalling. *Development* 143, 3226–3229
38. Leyser, O. (2018) Auxin signalling. *Plant Physiol.* 176, 465–479

39. Powers, S.K. and Strader, L.C. (2020) Regulation of auxin transcriptional responses. *Dev. Dyn.* 249, 483–495
40. Gallei, M. *et al.* (2020) Auxin signalling in growth: Schrödinger's cat out of the bag. *Curr. Opin. Plant Biol.* 53, 43–49
41. Prigge, M.J. *et al.* (2020) Genetic analysis of the Arabidopsis TIR1/AFB auxin receptors reveals both overlapping and specialized functions. *Elife* 9, e54740
42. Dai, N. *et al.* (2013) The TMK subfamily of receptor-like kinases in Arabidopsis display an essential role in growth and a reduced sensitivity to auxin. *PLoS One* 8, e60990
43. Gaillochet, C. *et al.* (2020) HY5 and phytochrome activity modulate shoot-to-root coordination during thermomorphogenesis in Arabidopsis. *Development* 147, dev192625
44. Cao, M. *et al.* (2019) TMK1-mediated auxin signalling regulates differential growth of the apical hook. *Nature* 568, 240–243
45. Xu, T. *et al.* (2014) Cell surface ABP1-TMK auxin-sensing complex activates ROP GTPase signalling. *Science* 343, 1025–1028
46. Xu, T. *et al.* (2010) Cell surface-and rho GTPase-based auxin signalling controls cellular interdigitation in Arabidopsis. *Cell* 143, 99–110
47. Pan, X.Fang, L.Liu, J.Senay-Aras, B.Lin, W.Zheng, S.Zhang, T. Guo, J.Manor, U.Van Norman, J.Chen, W. (2020) Auxin-induced signaling protein nanoclustering contributes to cell polarity formation. *Nat. Commun.* 11 (1), 1–4
48. Lin, D. *et al.* (2012) A ROP GTPase-dependent auxin signalling pathway regulates the subcellular distribution of PIN2 in Arabidopsis roots. *Curr. Biol.* 22, 1319–1325
49. Marques-Bueno, M.M. *et al.* (2021) Auxin-regulated reversible inhibition of TMK1 signalling by MAKR2 modulates the dynamics of root gravitropism. *Curr. Biol.* 31, 228–237.e210
50. Platre, Matthieu Pierre *et al.* (2019) Developmental control of plant Rho GTPase nano-organization by the lipid phosphatidylserine. *Science* 364, 57–62
51. Wang, Q.Qin, G.Cao, M.Chen, R.He, Y.Yang, L.Zeng, Z.Yu, Y. Gu, Y.Xing, W.Tao, W.A. (2020) A phosphorylation-based switch controls TAA1-mediated auxin biosynthesis in plants. *Nat. Commun.* 11 (1), 1
52. Woo, E.J. *et al.* (2002) Crystal structure of auxin-binding protein 1 in complex with auxin. *EMBO J.* 21, 2877–2885
53. Leblanc, N. *et al.* (1999) A novel immunological approach establishes that the auxin-binding protein, Nt-abp1, is an element involved in auxin signalling at the plasma membrane. *J. Biol. Chem.* 274, 28314–28320
54. Gao, Y. *et al.* (2015) Auxin binding protein 1 (ABP1) is not required for either auxin signalling or Arabidopsis development. *Proc. Natl. Acad. Sci. U. S. A.* 112, 2275–2280
55. Gelová, Z. *et al.* (2021) Developmental roles of auxin binding protein 1 in Arabidopsis Thaliana. *Plant Sci.* 303, 110750
56. Dunwell, J.M. *et al.* (2008) Germin and germin-like proteins: evolution, structure, and function. *Crit. Rev. Plant Sci.* 27, 342–375

Check for updates

Pinstatic Acid Promotes Auxin Transport by Inhibiting PIN Internalization[1][OPEN]

Akihiro Oochi,[a] Jakub Hajny,[b,h] Kosuke Fukui,[a] Yukio Nakao,[a] Michelle Gallei,[b] Mussa Quareshy,[c] Koji Takahashi,[d,e] Toshinori Kinoshita,[d,e] Sigurd Ramans Harborough,[f] Stefan Kepinski,[f] Hiroyuki Kasahara,[g,i] Richard Napier,[c] Jiří Friml,[b] and Ken-ichiro Hayashi[a,2,3]

[a]Department of Biochemistry, Okayama University of Science, Okayama 700-0005, Japan
[b]Institute of Science and Technology Austria, 3400 Klosterneuburg, Austria
[c]School of Life Sciences, University of Warwick, Coventry, CV4 7AL, United Kingdom
[d]Graduate School of Science, Nagoya University, Chikusa, Nagoya, 464-8602 Japan
[e]Institute of Transformative Bio-Molecules (WPI-ITbM), Nagoya University, Chikusa, Nagoya, 464-8601, Japan
[f]Centre for Plant Sciences, Faculty of Biological Sciences, University of Leeds, Leeds LS2 9JT, UK
[g]Institute of Global Innovation Research, Tokyo University of Agriculture and Technology, Fuchu-shi, Tokyo 183-8509, Japan
[h]Laboratory of Growth Regulators, The Czech Academy of Sciences, Institute of Experimental Botany & Palacký University, CZ-78371 Olomouc, Czech Republic
[i]RIKEN Center for Sustainable Resource Science, Yokohama, Kanagawa, 230-0045 Japan

ORCID IDs: 0000-0003-2140-7195 (J.H.); 0000-0001-8115-9803 (M.Q.); 0000-0001-5438-7624 (K.T.); 0000-0001-7621-1259 (T.K.); 0000-0002-0605-518X (R.N.); 0000-0002-8302-7596 (J.F.); 0000-0002-9812-2801 (K.H.).

Polar auxin transport plays a pivotal role in plant growth and development. PIN-FORMED (PIN) auxin efflux carriers regulate directional auxin movement by establishing local auxin maxima, minima, and gradients that drive multiple developmental processes and responses to environmental signals. Auxin has been proposed to modulate its own transport by regulating subcellular PIN trafficking via processes such as clathrin-mediated PIN endocytosis and constitutive recycling. Here, we further investigated the mechanisms by which auxin affects PIN trafficking by screening auxin analogs and identified pinstatic acid (PISA) as a positive modulator of polar auxin transport in Arabidopsis (*Arabidopsis thaliana*). PISA had an auxin-like effect on hypocotyl elongation and adventitious root formation via positive regulation of auxin transport. PISA did not activate $SCF^{TIR1/AFB}$ signaling and yet induced PIN accumulation at the cell surface by inhibiting PIN internalization from the plasma membrane. This work demonstrates PISA to be a promising chemical tool to dissect the regulatory mechanisms behind subcellular PIN trafficking and auxin transport.

The plant hormone auxin is a master regulator of plant growth and development. Indole 3-acetic acid (IAA), the predominant natural auxin, regulates numerous and diverse developmental processes such as establishment of embryo polarity, vascular differentiation, apical dominance, and tropic responses to light and gravity (Hayashi, 2012). The auxin responses regulating these diverse developmental events can be modulated at three major steps: auxin metabolism (Korasick et al., 2013; Kasahara, 2016), directional auxin transport (Adamowski and Friml, 2015), and signal transduction (Leyser, 2018).

Polar auxin transport plays a crucial role in auxin-regulated development by influencing local auxin maxima and gradients and is mediated principally by three families of membrane proteins, the Auxin1/Like Aux1 (AUX1/LAX) auxin influx carriers, the PIN-FORMED (PIN) auxin efflux facilitators, and several members of the ATP-binding cassette group B auxin transporters (Adamowski and Friml, 2015).

The polar subcellular localization of the auxin efflux machinery determines the directionality of auxin flow. The spatiotemporal regulation of auxin gradients also depends on the cell-specific expression

[1]This work was supported by the Ministry of Education, Culture, Sports, Science, and Technology (Grant-in-Aid for Scientific Research no. JP25114518 to K.H.), the Biotechnology and Biological Sciences Research Council (award no. BB/L009366/1 to R.N. and S.K.), and the European Union's Horizon2020 program (European Research Council grant agreement no. 742985 to J.F.).

[2]Author for contact: hayashi@dbc.ous.ac.jp.
[3]Senior author
The author responsible for distribution of materials integral to the findings presented in this article in accordance with the policy described in the Instructions for Authors (www.plantphysiol.org) is: Ken-ichiro Hayashi (hayashi@dbc.ous.ac.jp).

A.O., J.H., J.F., Y.N., and K.H. conceived this project and designed research and discussed the data; R.N., S.K., J.F., and K.H. wrote the paper; T.K. and K.T. performed rapid hypocotyl elongation assays; H.K. performed endogenous IAA analysis; M.Q. and R.N. performed surface plasmon resonance assays; S.R.H. and S.K. performed pull-down assays; A.O., J.H., M.G., F.K., J.F., Y.N., and K.H. performed all other experiments.
[OPEN]Articles can be viewed without a subscription.
www.plantphysiol.org/cgi/doi/10.1104/pp.19.00201

 © 2019 American Society of Plant Biologists. All Rights Reserved.

Downloaded from https://academic.oup.com/plphys/article/180/2/1152/6117699 by Institute of Science and Technology Austria user on 15 October 2021

and subcellular localization of plasma membrane (PM)-localized PIN proteins (PIN1–PIN4 and PIN7), the latter often being responsive to environmental and developmental cues (Adamowski and Friml, 2015). PIN proteins are often asymmetrically distributed within the cell and are constantly recycled between endosomal compartments and the PM. The dynamics of polar localization of PIN proteins regulates the rate and direction of cellular auxin export and this ultimately determines auxin gradients in the tissue. Therefore, the regulatory machinery of the polarity and abundance of PM-localized PIN proteins is crucial for diverse developmental processes and morphogenesis including embryogenesis, initiation of lateral organs, and tropic responses (Robert et al., 2013; Adamowski and Friml, 2015; Rakusová et al., 2015).

The exocytosis and endocytosis of PIN proteins at the PM can be modulated by ADP RIBOSYLATION FACTOR-GUANINE NUCLEOTIDE EXCHANGE FACTORS (ARF-GEFs) including GNOM (Naramoto et al., 2010). PIN proteins are internalized from the PM to the trans-Golgi network/early endosome compartments after which PINs can then proceed along the recycling route to the PM (Adamowski and Friml, 2015). An important tool for investigating exocytic protein sorting is Brefeldin A (BFA), which is a reversible inhibitor of ARF-GEFs including GNOM (Geldner et al., 2001, 2003). BFA treatment leads to accumulation of the endocytosed PINs in artificial intracellular aggregates called "BFA bodies," the formation of which can be reversed by washing out the BFA (Geldner et al., 2001).

Clathrin-mediated endocytosis is also involved in the internalization of PIN proteins from the PM (Kitakura et al., 2011; Adamowski et al., 2018) and is modulated by the Rho guanidine triphosphate hydrolases of plants (ROP) family of Rho-like GTPases and their associated ROP interactive CRIB motif-containing proteins (Lin et al., 2012; Nagawa et al., 2012). Genetic analysis has revealed that MACCHI-BOU4/ENHANCER OF PID/NAKED PINS IN YUCCA-like1 (MAB4/NPY1), a gene encoding NON-PHOTOTROPIC HYPOCOTYL3-like proteins and homologous MAB4/NPY1–like, regulates PIN abundance at the PM (Furutani et al., 2014). The internalization and trafficking of PIN proteins is dynamically regulated by developmental and environmental cues, such as plant hormones, gravity, and light (Ding et al., 2011; Rakusová et al., 2016). Short-term auxin treatments, in particular using synthetic auxin analogs, blocks clathrin-mediated internalization of PIN proteins from the PM and consequently enhances PIN abundance at the PM and increases auxin efflux (Paciorek et al., 2005; Robert et al., 2010). Auxin also induces PIN1 relocalization from basal to the inner lateral PM of root endodermal and pericycle cells (Prát et al., 2018). Similarly, auxin mediates PIN3 relocalization during gravitropic responses to terminate gravitropic bending (Rakusová et al., 2016). Prolonged auxin treatment induces PIN2 vacuolar targeting and degradation, and this is mediated by the $SCF^{TIR1/AFB}$ (SKP-Cullin-F box [SCF], TRANSPORT INHIBITOR RESISTANT1/AUXIN SIGNALING F-BOX [TIR1/AFB]) pathway (Abas et al., 2006; Baster et al., 2013), which presumably also explains the $SCF^{TIR1/AFBs}$-dependent auxin effect on PIN2-GFP accumulation in BFA bodies (Pan et al., 2009). In addition, auxin has been reported to reduce the abundance of photoconvertible PIN2-Dendra at the PM by repressing the translocation of newly synthesized PIN2 to the PM (Jásik et al., 2016). Besides an auxin effect on PIN trafficking, other hormones can influence different aspect of PIN trafficking, including cytokinin (Marhavý et al., 2011), salicylic acid (Du et al., 2013), and gibberellic acid (Salanenka et al., 2018), thus providing a possible entry point for crosstalk of these signaling pathways with the auxin distribution network.

Given these different and sometimes contradictory observations for different PINs resulting from investigations in different cells and using different approaches, the underlying cellular and molecular mechanisms for the targeting and recycling of PIN proteins, and in particular for their regulation by auxin, remain largely unknown.

To develop a useful chemical tool for dissecting the regulatory mechanism of PIN trafficking, we have screened phenylacetic acid (PAA) derivatives for selective modulation of PIN trafficking in Arabidopsis (*Arabidopsis thaliana*). We identified 4-ethoxyphenylacetic acid, which was designated as pinstatic acid (PISA) due to its activity on PIN-mediated polar auxin transport. PISA has an auxin-like effect on hypocotyl elongation and adventitious root formation by positively modulating auxin transport. Similar to conventional auxins, PISA blocks the internalization of PIN proteins from the PM and consequently induces PIN protein accumulation at the PM. PISA is notably different from other known auxin chemical tools, like auxin transport inhibitors 2,3,5-triiodobenzoic acid (TIBA) and N-1-naphthylphthalamic acid (NPA). Therefore, PISA represents a promising chemical tool for dissecting the complicated regulations of PIN trafficking by auxin.

RESULTS

Pinstatic Acid Is an Inactive PAA Analog on TIR1/AFB-Aux/IAA Coreceptor Complex

Auxins modulate the expression and degradation of PIN proteins via the $SCF^{TIR1/AFB}$ signaling pathway (Baster et al., 2013; Ren and Gray, 2015). On the other hand, clathrin-mediated endocytosis of PIN is inhibited by auxin via a nontranscriptional pathway (Robert et al., 2010). These positive and negative effects of auxin on PIN trafficking hinder access to the regulatory components in PIN trafficking using conventional genetic approaches. Therefore, we searched for an auxin

Downloaded from https://academic.oup.com/plphys/article/180/2/1152/6117699 by Institute of Science and Technology Austria user on 15 October 2021

transport modulator that would make PIN trafficking more amenable to experimentation. To this end, we initially screened PAA derivatives according to the following criteria: (1) The derivative should be inactive within the $SCF^{TIR1/AFB}$ pathway and (2) derivative treatment should induce auxin-related phenotypes that are different from the phenotypes typical of auxins or auxin transport inhibitors, such as TIBA and NPA.

In the course of screening, we found that 4-ethoxyphenylacetic acid (later denoted "PISA") promoted hypocotyl elongation but did not induce auxin-responsive *DR5*::*GUS* reporter gene expression, which is mediated by the $SCF^{TIR1/AFB}$ pathway (Figs. 1, A and C, and 2). Thus, PISA was selected as the most promising candidate from a series of 4-alkyloxy-PAA derivatives and further characterized in detail.

Auxin is biosynthesized by two enzymes, namely TAA1 and YUC in the indole 3-pyruvic acid pathway (Kasahara, 2016). The inhibition of this pathway by L-kynurenine, a TAA1 inhibitor, and yucasin DF, a YUC inhibitor, caused short and curled roots that are typical auxin-deficient phenotypes (Fig. 1B; He et al., 2011; Tsugafune et al., 2017). A quintuple *yuc 3 5 7 8 9* mutant showed a similar auxin-deficient root phenotype (Supplemental Fig. S1A; Chen et al., 2014). IAA and 1-naphthylacetic acid (NAA) at 50–100 nM recovered these auxin-deficient root defects in root elongation and gravitropism (Fig. 1B; Supplemental Fig. S1A). An analog of PISA, 3-Ethoxyphenylacetic acid (meta-substituted PISA: mPISA; Fig. 1A), that retains weak auxin activity in *DR5*::*GUS* expression (Fig. 1C) also rescued the auxin-deficient curled root phenotype (Fig. 1B). In contrast, PISA did not rescue these root defects caused by auxin deficiency, clearly indicating PISA does not directly act as a typical auxin like IAA or NAA in planta (Fig. 1B; Supplemental Fig. S1A).

The tobacco (*Nicotiana tabacum*) BY-2 cell suspension culture requires auxin for cell proliferation (Winicur et al., 1998). BY-2 cells proliferated in the presence of IAA and NAA (Supplemental Fig. S1B), but PISA failed to maintain this cell culture (Supplemental Fig. S1B). The cell morphology of the culture treated with PISA showed swollen cell shapes that are a hallmark of auxin-depletion (Supplemental Fig. S1C), further

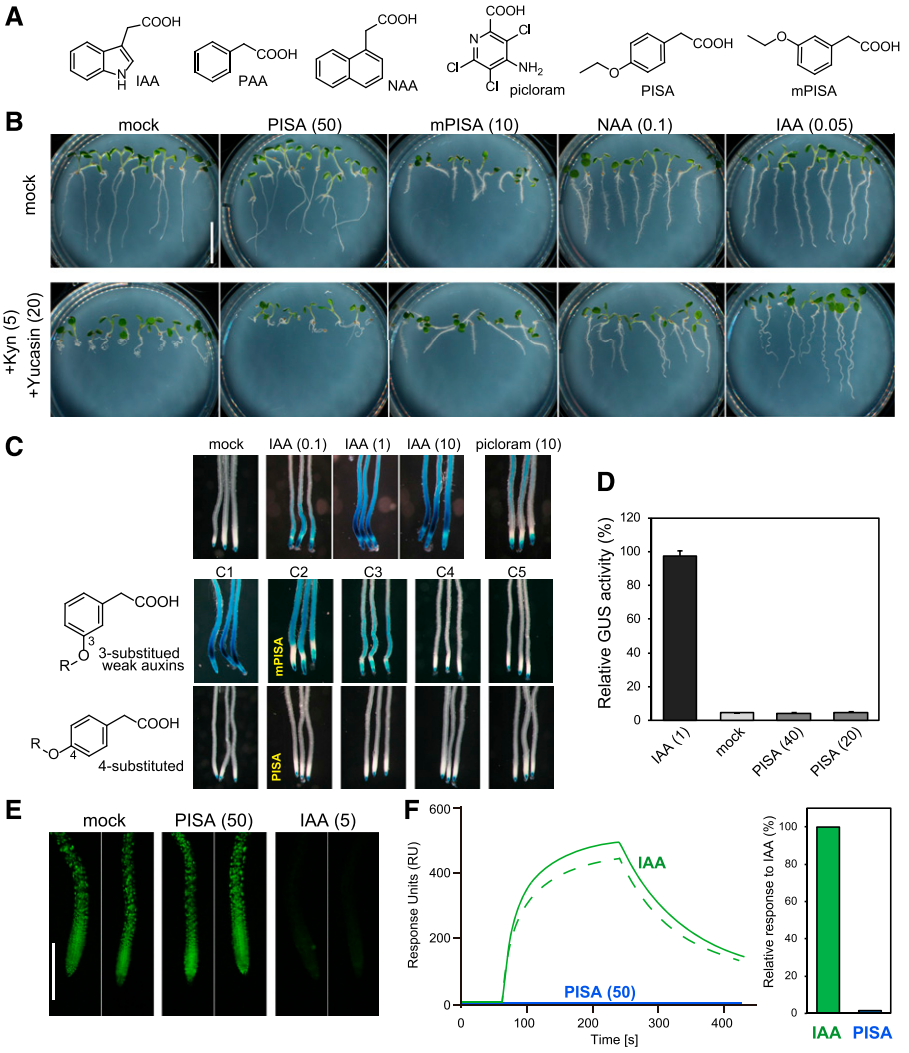

Figure 1. Evaluation of PISA for an auxin-like effect in the $SCF^{TIR1/AFB}$ pathway. A, The structures of auxins and PISA. B, Effects of PISA on auxin-deficient root phenotypes. Arabidopsis plants were cultured for 5 d on vertical agar plate containing chemicals with or without auxin biosynthesis inhibitors yucasin DF and L-kynurenine (Kyn). The values in parentheses represent the concentration of chemicals (micromolar). Bar = 5 mm. C, Effects of alkyloxy-PAA on auxin-responsive *DR5*::*GUS* expression. Five-d–old *DR5*::*GUS* seedlings were incubated with chemicals for 6 h. Methoxy (C1) to pentoxy (C5) PAA derivatives including mPISA and PISA were assessed at 50 μM. D, Quantitative analysis of GUS enzyme activity in the *DR5*::*GUS* line treated with IAA and PISA. Values are the means ± SD (n = 9). E, *DII-VENUS* seedlings were incubated with 10-μM yucasin DF for 3 h and then washed with medium. The seedling was incubated with PISA and IAA for another 60 min. Bar = 500 μm. F, SPR analysis of the auxin-induced interaction between TIR1 and IAA7 degron peptide. The sensorgram shows the effect of 50-μM IAA (green) and 50-μM PISA (blue) on TIR1-DII peptide association and dissociation. The bars show the relative response of PISA to IAA (100%).

Downloaded from https://academic.oup.com/plphys/article/180/2/1152/6117699 by Institute of Science and Technology Austria user on 15 October 2021

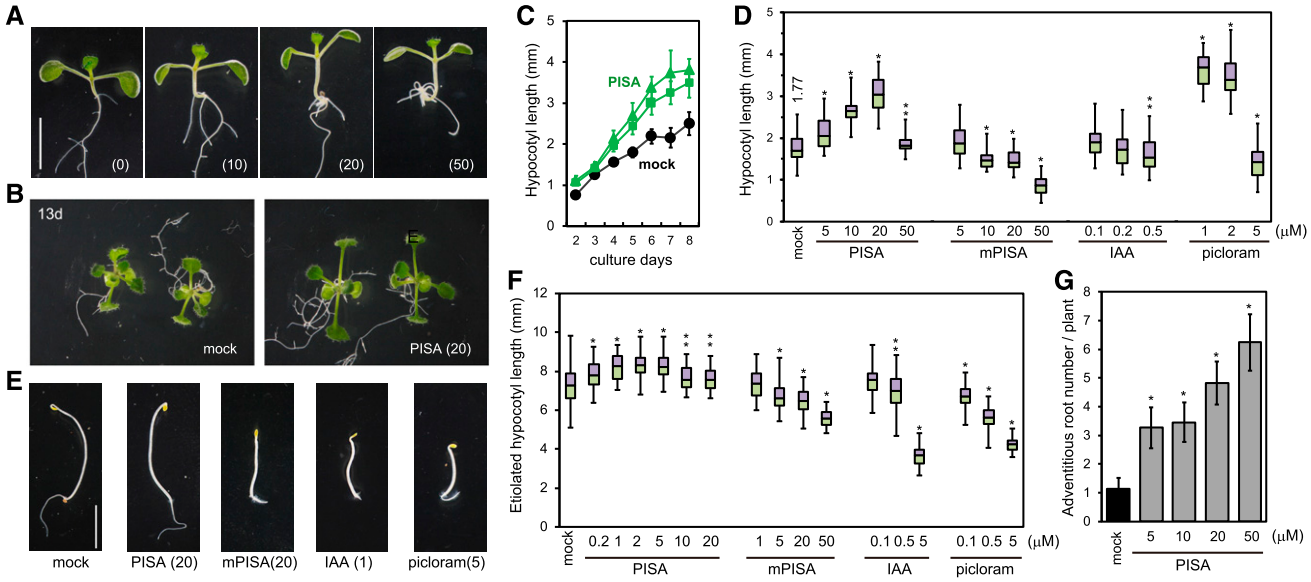

Figure 2. Effects of PISA on hypocotyl elongation and adventitious root formation. A, Arabidopsis seedlings cultured for 7 d with PISA. The values in parentheses represent the concentration of chemicals (micromolar). Bar = 5 mm. B, 13-d–old plants grown with PISA. C, Time course of hypocotyl length of seedlings cultured with PISA (solid square = 10 μM; solid triangle = 20 μM). Values are the means ± SD (n = 15–20). D, Hypocotyl lengths of seedlings cultured for 7 d with PISA and auxins. The hypocotyl length (millimeters) of the mock-treated seedlings is indicated. Box-and-whisker plots show a median (centerline), upper/lower quartiles (box limits), and maximum/minimum (whiskers; n = 30–38). Statistical significance assessed by Welch's two-sample t test. Asterisks indicate significant differences (**$P < 0.05$, *$P < 0.01$). E, Etiolated seedlings cultured for 5 d in dark with PISA and auxins. F, Hypocotyl lengths of etiolated seedling cultured for 3 d in dark with PISA and auxins. Statistical significance assessed by Welch's two-sample t test. Asterisks indicate significant differences (n = 50–72, **$P < 0.05$, *$P < 0.01$). G, Adventitious root production induced by PISA. Arabidopsis seedlings were cultured for 7 d with PISA and the adventitious root number at shoot and root junction was counted. Asterisks indicate significant differences (n = 30, **$P < 0.05$, *$P < 0.01$).

suggesting that PISA does not have the effect as an auxin on cell division (Winicur et al., 1998). Auxin-induced rapid cell elongation in etiolated hypocotyls was demonstrated to be mediated by TR1/AFB receptors (Fendrych et al., 2016). However, PISA failed to induce this rapid cell elongation (Supplemental Fig. S2), suggesting that PISA does not act as a conventional auxin to directly activate the TR1/AFB receptors in the hypocotyl.

IAA and the synthetic auxin picloram cause potent induction of auxin-responsive reporter genes such as *DR5* (Fig. 1C). In contrast, PISA did not induce any auxin-responsive *DR5*::*GUS* and *BA3*::*GUS* reporter expression, again suggesting that it is inactive as a ligand for the $SCF^{TIR1/AFB}$ pathway (Fig. 1, C and D; Supplemental Fig. S3A). DII-VENUS protein is a translational fusion of the TIR1-interacting domain of Aux/IAA proteins and the fluorescent reporter VENUS (Brunoud et al., 2012). IAA promotes the interaction between DII-VENUS and TIR1 receptor to induce the DII-VENUS degradation and loss of the VENUS signal (Fig. 1E). In contrast, PISA did not induce degradation of DII-VENUS, once again suggesting that PISA does not directly modulate TIR1/AFB-Aux/IAA auxin coreceptor complex formation. Additionally, PISA showed no activity in the yeast auxin-inducible degron system (Supplemental Fig. S3B; Nishimura et al., 2009). In this system, the minichromosome maintenance (MCM) complex is essential for DNA replication in yeast and lines in which MCM is deficient fail to grow (Nishimura et al., 2009). The auxins IAA and NAA, and analog mPISA, all repressed the growth of yeast expressing rice OsTIR1 and Aux/IAA-fused MCM4 protein by promoting the degradation of the fused MCM4 protein (Supplemental Fig. S3B; Nishimura et al., 2009). In contrast, PISA did not repress yeast growth in this auxin-inducible degron system, indicating again that PISA is not an active ligand for TIR1.

These findings were further supported by biochemical assays using Surface Plasmon Resonance (SPR) analysis (Fig. 1F) and a pull-down assay (Supplemental Fig. S3C; Lee et al., 2014). IAA promotes assembly of the coreceptor complex of TIR1 and Aux/IAA (domain II) in both assays. In contrast, PISA did not promote the interaction between TIR1 and Aux/IAA in either system (Fig. 1F; Supplemental Fig. S3C). Additionally, the SPR assay also showed that there was no binding of PISA with AFB5 (Supplemental Fig. S3C), and using the SPR assay to test for antiauxin activity by mixing 50-μM PISA with 5-μM IAA showed that PISA did not bind and block the TIR1 auxin-binding site (Supplemental Fig. S3E) whereas the known TIR1/AFB auxin receptor blocker auxinole (Hayashi et al., 2012) reduced the IAA signal dramatically. Thus, in these direct binding

Downloaded from https://academic.oup.com/plphys/article/180/2/1152/6117699 by Institute of Science and Technology Austria user on 15 October 2021

assays, PISA does not bind to TIR1/AFB coreceptors. In summary, PISA is completely inactive as a classical auxin that induces the Aux/IAA degradation via TIR1/AFB auxin receptors.

PISA Promotes Hypocotyl Elongation by Positively Modulating Polar Auxin Transport

PISA promotes hypocotyl elongation in a manner that is typical for auxin effects in Arabidopsis seedlings (Fig. 2A). Because PISA did not activate DR5-monitored auxin response, we carefully examined its effects on auxin-related phenotypes in planta to address possible modes of PISA action. In light-grown seedlings, PISA at 5–20-μM promoted hypocotyl elongation (Fig. 2, A–D). In contrast, IAA and mPISA inhibited growth at 0.5 and 20 μM, respectively, whereas the AFB5-selective synthetic auxin picloram strongly promoted hypocotyl elongation (Fig. 2D). In the dark, PISA at 2 μM slightly promoted the elongation of etiolated hypocotyls (Fig. 2, E and F), but did not inhibit their elongation at 20 μM. In contrast, exogenously applied IAA, picloram, and mPISA inhibited the elongation of etiolated hypocotyls (Fig. 2F).

Having explored a set of physiological responses, we made use of genetic and pharmacological tools to gain insight into the mechanism of PISA action. The auxin signaling mutants *axr1-3* and *tir1-1 afb2-1* showed high resistance to mPISA (Supplemental Fig. S4A), implying that mPISA targets auxin signaling in planta (Hayashi, 2012). In contrast, the hypocotyl of *axr1-3* elongated to a similar extent as that of the wild type when treated with PISA (Fig. 3A). Importantly, neither wild type nor *axr1-3* responded to PISA after the inhibition of SCF^{TIR1} auxin signaling by the auxin antagonist auxinole (Fig. 3A; Supplemental Fig. S4B). PISA also failed to promote hypocotyl elongation in the presence of the auxin biosynthesis inhibitor L-kynurenine (Fig. 3A; Supplemental Fig. S4C). These observations indicate that auxin-like effects of PISA on hypocotyl growth require the $SCF^{TIR1/AFB}$ auxin signaling to be activated by endogenous IAA.

To examine the effects of PISA on polar auxin transport, seedlings were cotreated with auxin efflux transport inhibitors and PISA. The promotion of elongation by PISA on hypocotyls was blocked by three auxin efflux transport inhibitors, TIBA, 2-(4-[diethylamino]-2-hydroxybenzoyl)benzoic acid (BUM), and NPA (Fig. 3, B and C; Supplemental Fig. S5A; Fukui and Hayashi, 2018). In addition, treatments with the synthetic auxin picloram and the auxin overproduction line *35S::YUC1* exhibited longer hypocotyls as a high auxin phenotype (Supplemental Fig. S5B), but in these lines TIBA and NPA did not suppress the elongation (Supplemental Fig. S5B). The data suggest that PISA could positively modulate polar auxin transport in hypocotyls. To examine further the effects of PISA on basipetal auxin transport, rootward movement of ^{3}H-IAA was analyzed (Fig. 3E). In this assay, NPA reduced the basipetal movement of ^{3}H-IAA in hypocotyls, whereas PISA enhanced it (Fig. 3E). These results collectively show that PISA positively modulates basipetal auxin transport in hypocotyls. Another possible target of PISA could be the regulation of endogenous auxin

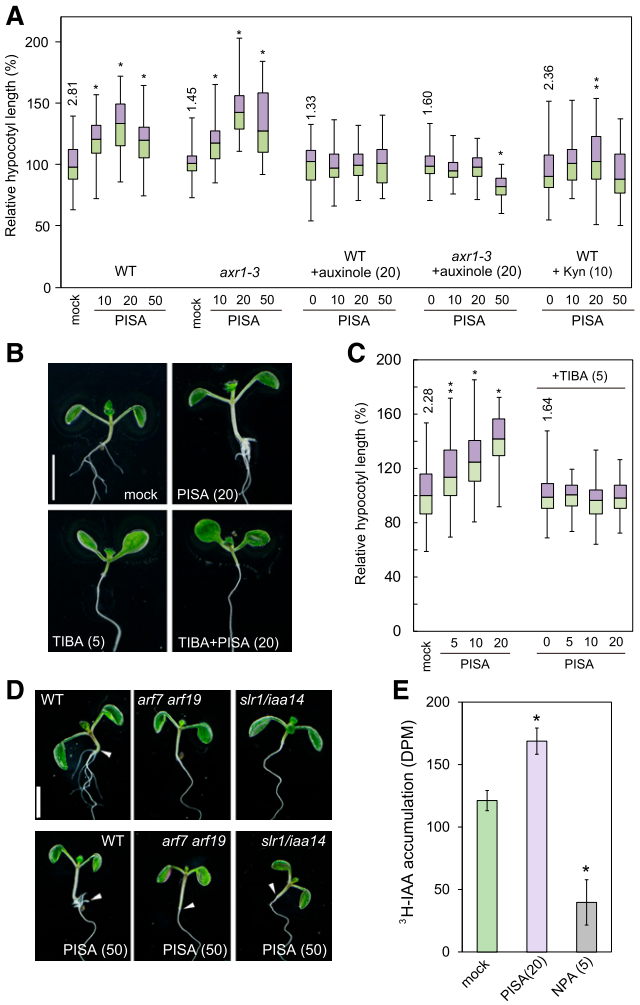

Figure 3. Auxin signaling and transport inhibitors repress PISA-induced hypocotyl phenotypes and PISA promotes basipetal auxin transport in the hypocotyl. A, The hypocotyl length of Arabidopsis wild-type and *axr1-3* mutant seedlings cultured for 7 d with chemicals. Relative hypocotyl length is shown as the percentage of that in mock-treated plants (100%). The actual length (millimeter) of mock-treated hypocotyls are indicated (n = 40–48). B, Seedlings cultured for 7 d with PISA and auxin transport inhibitor, TIBA. C, Hypocotyl length in seedlings cultured with or without TIBA and PISA. Relative hypocotyl length is shown as the percentage of that in mock-treated plants (100%). The actual length (millimeter) of mock-treated hypocotyls is indicated as box-and-whisker plots (n = 40–45). Statistical significance assessed by Welch's two-sample t test. Asterisks indicate significant differences (**$P < 0.05$, *$P < 0.01$). D, Seedlings of wild type, *arf7 arf19*, and *slr1/iaa14* mutants cultured for 7 d with or without PISA. The values in parentheses represents the concentration of chemicals (micromolar). Bar = 5 mm. E, Rootward transport of radiolabeled ^{3}H-IAA in decapitated hypocotyls. NPA, an auxin transport inhibitor, was used as the negative control. (*$P < 0.01$, n = 9).

Downloaded from https://academic.oup.com/plphys/article/180/2/1152/6117699 by Institute of Science and Technology Austria user on 15 October 2021

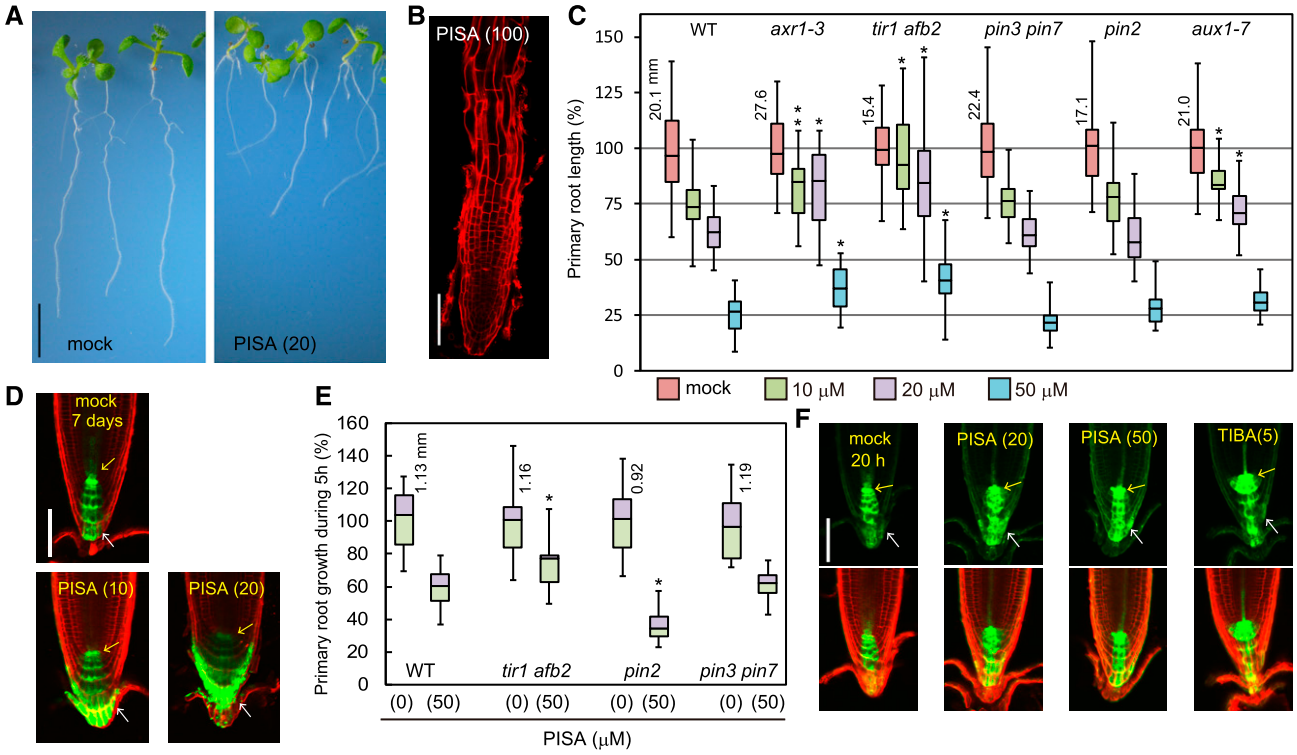

Figure 4. The effects of PISA on root elongation and auxin distribution in the root tip. A, Wild-type (WT) seedlings cultured for 7 d with PISA. Bar = 5 mm. B, Wild-type root cultured with 100-μM PISA . Root was counterstained with propidium iodide. Bar = 100 μm. C, The primary root length of Arabidopsis wild-type and auxin mutants (*axr1-3*, *tir1 afb2*, *pin3 pin7*, *pin2/eir1-1*, and *aux1-7*) cultured for 7 d on vertical plate containing PISA. Relative root length is shown as the percentage of that in mock-treated plants (100%). The actual length (millimeter) of mock-treated roots is indicated. Statistical significance was assessed by Welch's two-sample *t* test between wild type and mutants. Asterisks indicate significant differences ($n = 32–40$, $^{**}P < 0.05$, $^{*}P < 0.01$). D, The GFP expression of *DR5*::*GFP* in roots cultured vertically with PISA for 7 d. Arrows indicate QC (yellow) and lateral root cap (white). Bar = 100 μm. E, The primary root growth of Arabidopsis wild type and auxin mutants over 5 h on vertical plates containing PISA. The actual length (mm) of mock-treated roots is indicated, which was set to 100%. Asterisks indicate significant differences ($n = 14–17$, $^{*}P < 0.01$). F, The GFP expression of *DR5*::*GFP* cultured vertically with PISA and TIBA for 20 h. The values in parentheses represents the concentration of chemicals (micromolar). Bar = 100 μm.

concentrations, such as via auxin biosynthesis or catabolism. Analysis of endogenous IAA levels in Arabidopsis seedlings showed that they were not affected by PISA treatment (Supplemental Fig. S6). Together, these results indicate that PISA likely acts by affecting polar auxin transport.

PISA Inhibits Root Growth by Accumulating IAA at the Root Tip

PISA inhibited primary root growth in a manner that is similar to conventional auxins. The seedlings were cultured on vertical plates containing PISA for 7 d (Fig. 4, A–C). The auxin signaling mutants, *axr1-3* and *tir1 afb2*, were insensitive to PISA. Additionally, auxin influx transport mutant *aux1-7* was also less sensitive to PISA regarding root growth (Fig. 4C). Taken together with the effects of PISA on auxin transport in the hypocotyl, these results suggest that PISA inhibits primary root growth by modulating auxin transport to affect auxin distribution and maxima. Further, the roots treated with PISA at 100 μM showed severe defects in root cell morphology (Fig. 4B). To examine the effects of PISA on auxin distribution in roots, *DR5*::*GFP* seedlings were cultured with PISA for 7 d (Fig. 4D). PISA significantly induced GFP expression in the lateral root cap cell, indicating PISA accumulates IAA in the lateral root cap and root growth is inhibited as a consequence. In contrast to auxin signaling mutants, the sensitivity of *pin2* and *pin3 pin7* mutants was comparable to that of the wild type (Fig. 4C). To investigate the short-term effects of PISA, seedlings were treated with PISA for 5 h (Fig. 4E). PISA inhibited root elongation within this 5 h incubation. The *tir1 afb2* mutant was insensitive to PISA, but the *pin2* mutant was more sensitive than the wild type to PISA. Perhaps, in the *pin2* mutant, the accumulated IAA is not efficiently transported from the lateral root cap. Consistent with root elongation responses (Fig. 4E), PISA induced *DR5*::*GFP* expression in the lateral root cap after 20-h treatment suggesting enhanced accumulation of endogenous IAA (Fig. 4F). The

Downloaded from https://academic.oup.com/plphys/article/180/2/1152/6117699 by Institute of Science and Technology Austria user on 15 October 2021

auxin transport inhibitor TIBA blocks IAA efflux and inhibits root elongation by accumulating IAA (Supplemental Fig. S5). TIBA highly induced *DR5*::*GFP* expression near the quiescent center (QC) where IAA is biosynthesized (Fig. 4F; Brumos et al., 2018). Taken together, these results indicate that PISA promotes the auxin transport rate leading to accumulations of IAA at the lateral root cap, resulting in the inhibition of root elongation.

PISA Blocked Root Hair Formation by Positively Modulating Auxin Transport

PISA displayed auxin-like activity in its effects on hypocotyl elongation, primary root inhibition, and adventitious root formation (Fig. 2). Typical auxin efflux transport inhibitors commonly inhibit the elongation of both primary root and hypocotyl, supporting that PISA is not an inhibitor of auxin efflux transport. The effects of PISA on auxin-related phenotypes can be explained if it works by increasing auxin efflux. To further examine the effects of PISA on auxin efflux transport, the root hair phenotype was analyzed. This process involves the PIN2 proteins, which are localized at the apical side of root epidermal cells and mainly contribute to basipetal (shootward) auxin transport (Abas et al., 2006). The loss of function *pin2/eir1* mutant displays impaired root hair formation (Fig. 5, A and B). The ectopic overexpression of PIN1 in *35S*::*PIN1* roots also interferes with this shootward auxin transport, and, consequently, *35S*::*PIN1* seedlings also show defects in root hair formation (Fig. 5, A and B; Ganguly et al., 2010), suggesting shootward auxin flow is important for root hair formation (Rigas et al., 2013). In contrast, auxin efflux transport inhibitors TIBA and NPA promote root hair formation (Ganguly et al., 2010), probably by increasing the accumulation of endogenous IAA (Fig. 5C). Importantly, PISA inhibits root hair formation, implying PISA has an opposite effects to auxin efflux inhibitors.

PISA Affects Adventitious and Lateral Root Formation by Positively Modulating Auxin Transport

PISA induces adventitious root formation at the shoot/root junction as shown in Figure 2A. Importantly, auxin signaling mutants *slr/iaa14* and *arf7 arf19* show severe defects in lateral root formation (Fig. 3D; Table 1; Okushima et al., 2007). In these mutants, PISA did not promote adventitious root formation at the shoot/root junction and this is consistent with the auxin-like effects of PISA on hypocotyls (Fig. 3D; Table 1). This suggests that adventitious root formation in response to PISA treatment depends on auxin signaling downstream of $SCF^{TIR1/AFB}$. In such a situation, auxin efflux transport inhibitors BUM, NPA, and TIBA would reduce polar auxin transport in hypocotyls, resulting in the inhibition of the adventitious root formation and this is indeed what we observed, as shown in Table 1

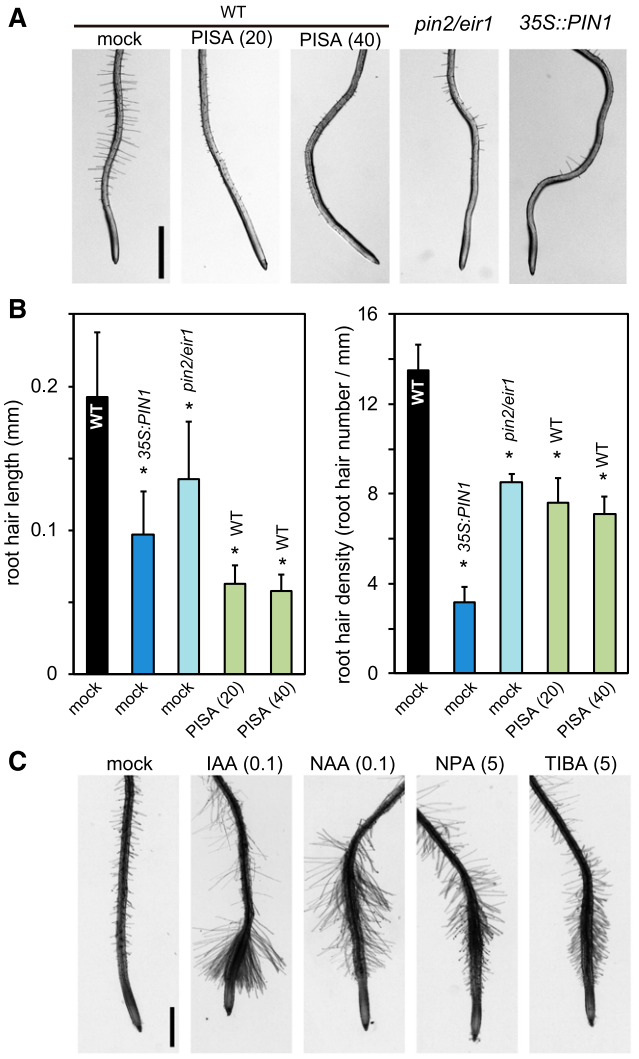

Figure 5. PISA inhibits root hair formation. A, Root hairs of *pin2/eir1*, *35S*::*PIN1*, and wild-type (WT) plants treated with PISA. Five-d–old seedlings were cultured for 2 d on vertical agar plates with or without PISA. The values in parentheses represent the concentration of chemicals (micromolar). B, The root hair length and density of *pin2/eir1*, *35S*::*PIN1*, and wild-type plants treated with PISA. The length and density of root hairs within the 2–4-mm region from root tip were measured. Values are the means ± SD. Asterisks indicate significant differences (n = 8–11, $^*P < 0.01$). C, The root hair formation of wild-type seedlings grown with auxins and auxin transport inhibitors. The values in parentheses represent the concentration of chemicals (micromolar). Bar = 1 mm.

and Supplemental Figure S5A. Taken together, these results suggest that PISA positively modulates the polar auxin transport system, thereby leading to the accumulation of auxin at the shoot/root junction and promoting adventitious root formation.

In contrast to the promotion of adventitious roots at the shoot/root junction (Fig. 2A; Table 1), PISA alone repressed lateral root formation in primary roots (Fig. 6A). In contrast, PISA strongly promoted lateral root numbers when coincubated with exogenous IAA (Fig. 6, B and C; Supplemental Fig. S7A). TIBA and

Downloaded from https://academic.oup.com/plphys/article/180/2/1152/6117699 by Institute of Science and Technology Austria user on 15 October 2021

Table 1. *Effect of PISA on adventitious root formation at shoot/root junction*

Modulator	Wild Tpe (Col)	*arf7 arf19*	*slr/iaa14*	TIBA (5 μM)	NPA (5 μM)
Mock	1.57 ± 0.65[a]	0	0	0	0
PISA (20 μM)	3.21 ± 0.70	0	0	0	0
PISA (50 μM)	5.07 ± 1.03	0	0	0	0

[a]Adventitious root number at shoot/root junction for each of the 6-d–old seedlings.

NPA did not affect the lateral root number induced by exogenous IAA (Supplemental Fig. S8A), suggesting that inhibition of auxin efflux does not enhance IAA-induced lateral root formation. This was further investigated using the cell cycle reporter *CYCB1;1*::*GUS*, which is induced strongly by IAA and NAA in initiating lateral roots. In this assay, PISA enhanced *CYCB1;1*::*GUS* expression when in the presence of auxins, IAA and NAA (Supplemental Fig. S7B). Similarly, auxin-induced *DR5*::*GUS* expression was dramatically enhanced by pretreatments with PISA (12 h; Fig. 6D). In this experiment, IAA treatment for 6 h at 100 and 500 nM induced *DR5*::*GUS* expression in elongation zones only (Fig. 6D). This expression pattern was extended along the entire root by the coincubation of IAA and PISA (Supplemental Fig. S8B). In contrast, cotreatment with IAA and auxin transport inhibitors (NPA, TIBA, 5-benzykoxy IAA, and BUM; Fukui and Hayashi, 2018) activated *DR5*::*GUS* expression only at the root tips (Fig. 6D). To examine the effects of PISA on basipetal auxin transport, shootward movement of IAA from the root tip was evaluated by *DR5*::*GUS* assay

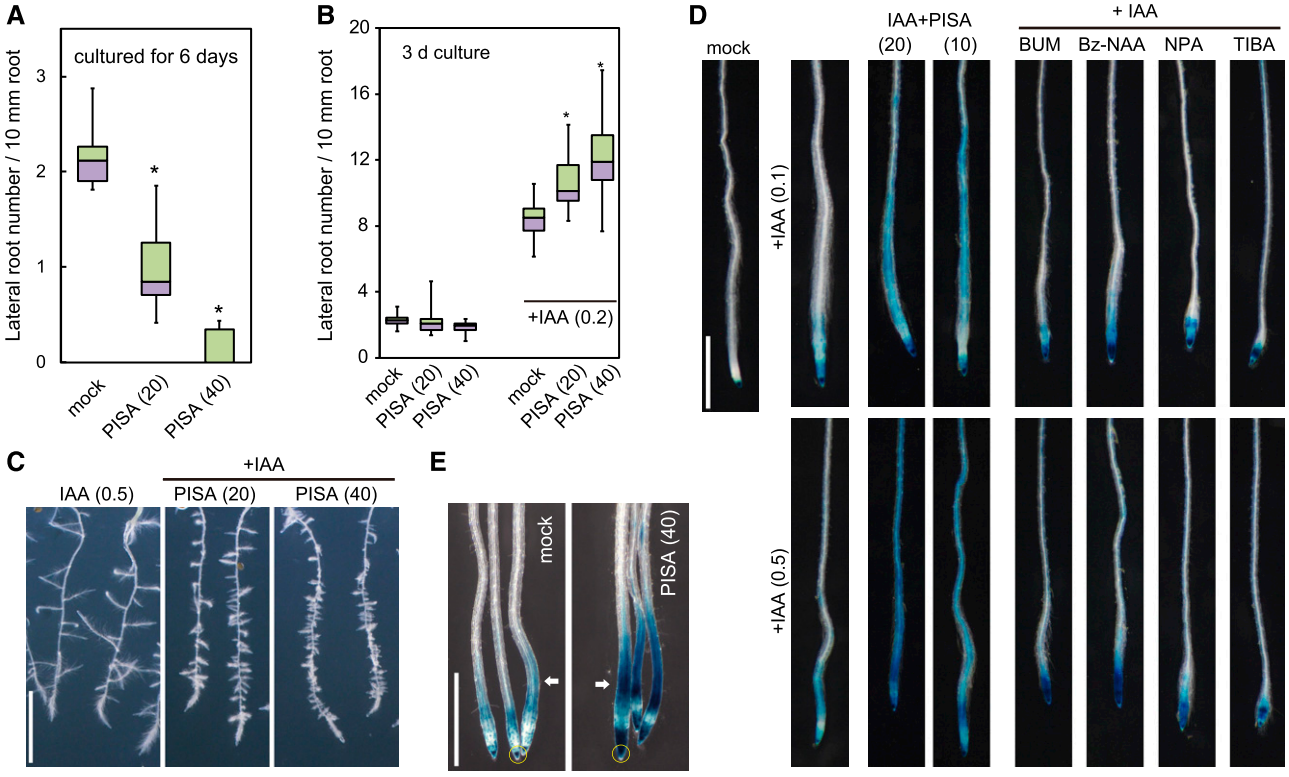

Figure 6. Effects of PISA on IAA-induced lateral root formation and shootward IAA transport. A, Effects of PISA on the lateral root formation. Arabidopsis seedlings were cultured for 6 d with PISA. The number of lateral roots were counted and the density of lateral roots are shown as box-and-whisker plots (n = 14–16). B and C, Effects of PISA on IAA-induced lateral root formation. Five-d–old seedlings were cultured for additional 3 d with PISA in the presence of IAA. The density of lateral roots are shown as box-and-whisker plots (B, n = 14–16) and representative images are shown (C). Bar = 5 mm. D, Effects of PISA on IAA-induced *DR5*::*GUS* expression. Five-d–old *DR5*::*GUS* seedlings were incubated for 12 h in liquid GM medium with or without PISA or auxin transport inhibitors. IAA was added to the GM medium and the seedlings were further incubated for additional 6 h. The IAA-induced GUS activity was visualized by X-Gluc. Bar = 1 mm. E, Effects of PISA on shootward IAA transport. An agar block containing IAA was applied to *DR5*::*GUS* root tips (yellow ring) and the seedlings were incubated on vertical plates containing 40-μM PISA for 10 h. Arrows show the IAA-induced GUS activity. Bar = 1 mm. Statistical significance assessed by Welch's two-sample t test. Asterisks in (A) and (B) indicate significant differences (*$P < 0.01$). The values in parentheses represent the concentration of chemicals (micromolar).

Downloaded from https://academic.oup.com/plphys/article/180/2/1152/6117699 by Institute of Science and Technology Austria user on 15 October 2021

(Fig. 6E; Buer and Muday, 2004; Lewis and Muday, 2009). In this shootward auxin transport assay, the *DR5*::*GUS* seedlings were placed on vertical plates containing PISA and then an agar block containing IAA was placed onto the root tips. The seedlings were then incubated for 10 h. PISA promoted *DR5*::*GUS* induction derived from root tip IAA (Fig. 6E), suggesting that PISA enhances shootward auxin transport from the root tip. Taken together, these results indicate that PISA increases the net flow of auxin in the roots by positively modulating auxin transport.

Other possible targets for PISA are the AUX1/LAX auxin influx transporters. PISA might promote IAA-induced lateral root formation by increasing the uptake of exogenous IAA. To test the effects of PISA on IAA influx transport, seedlings were cotreated with PISA and the membrane-permeable IAA prodrugs, IAA methyl ester and IAA octyl ester (Supplemental Fig. S9). These lipophilic IAA esters and NAA (Supplemental Fig. S7B) can be incorporated into cells by passive diffusion, but not by the AUX1/LAX transporters. PISA enhanced lateral root formation to the same extent with the two IAA esters, NAA and IAA (Supplemental Fig. S7B and S9), indicating that IAA influx transport is not required for the activity of PISA on lateral root promotion.

PISA Perturbed Asymmetric Auxin Distribution and Gravitropism in Root

Gravistimulation rapidly induces asymmetric auxin distributions in roots and thereby changes the *DR5* reporter expression pattern (Fig. 7A). This gravistimulated asymmetric auxin distribution is driven by PIN- mediated shootward auxin movement in the root epidermis (Wisniewska et al., 2006; Baster et al., 2013). After 4-h gravistimulation, the *DR5*::*GFP* signal increased at the lower side of gravistimulated roots. PISA treatment completely diminished this asymmetric expression of *DR5*::*GFP* (Fig. 7, A and B) and concomitantly blocked root gravitropic responses (Fig. 7C). These observations show that PISA not only modulates polar auxin transport but specifically affects PIN-mediated asymmetric auxin distribution in gravistimulated roots.

PISA Blocked the Internalization of PIN Proteins and Promoted Their Accumulation at the PM

All the phenotypic effects of PISA can be explained by the positive modulation of auxin transport by PISA. PISA treatment did not affect the expression profiles of *proPIN1*::*GFP*, *proPIN2*::*GUS* and *proPIN7*::*GUS* (Supplemental Fig. S10), indicating that the primary target of PISA in auxin transport is not the regulation of PIN transcription. To address the mechanism of positive effects of PISA on auxin efflux, we examined the effects of PISA on the recycling of PIN proteins in roots. BFA induces the formation of BFA bodies that

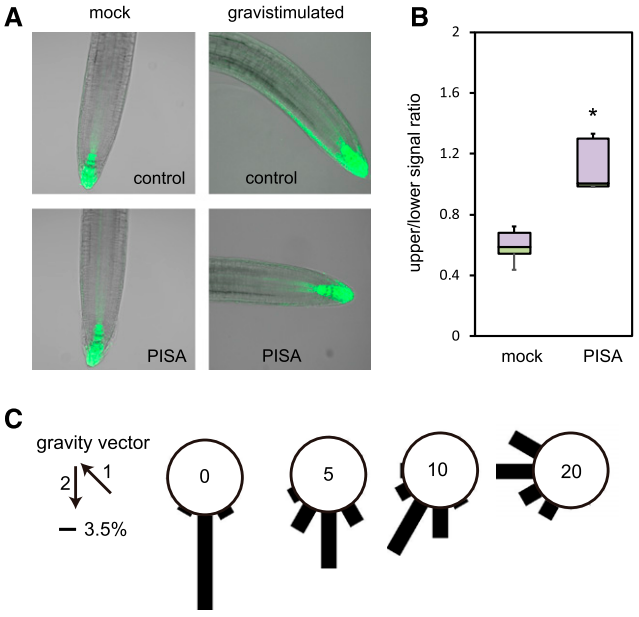

Figure 7. PISA inhibits auxin distribution and root gravitropism. A, Effect of PISA on auxin asymmetric distribution. Four-d–old *DR5*::*GFP* seedlings were transferred to 20-μM PISA and control medium for 1 h. After 1 h, seedlings were gravistimulated for 4 h and imaged. PISA pretreatment abolished auxin asymmetric distribution and seedlings did not respond to gravity stimuli. B, Quantitative evaluation of (A), showing a mean ratio of the signal intensity of the upper-/lower-half of the root. (*$P < 0.01$). C, Effect of PISA on root gravitropic response. Five-d–old wild-type seedlings were placed on vertical GM agar plates containing PISA and then cultured for 3 h in the dark. The plates were further incubated for 16 h after rotating plates at 135° angle against vertical direction. The arrows indicate the vector of gravity before (1) and after (2) the initiation of gravistimulation. The angles were grouped into 30° classes and plotted as circular histograms.

incorporate PIN2-GFP protein in *proPIN2*::*PIN2-GFP* line (Geldner et al., 2003). Auxin (NAA) was shown to inhibit BFA body formation by blocking the endocytosis of PIN2 protein (Fig. 8A; Paciorek et al., 2005). The negative control compound benzoic acid (BA) did not affect BFA body formation (Fig. 8A), but PISA inhibited BFA body formation to the same extent as NAA (Fig. 8, A and B). Additionally, BFA body formation with both PIN1-GFP fusion and PIN1 native protein was also blocked by NAA and PISA (Supplemental Fig. S11). These observations suggest that PISA interferes with PIN recycling or vacuolar targeting, and as a consequence promotes the accumulation of PIN proteins at the PM. Because constitutive PIN recycling has been linked to maintenance of its asymmetric, polar distribution, we tested PISA effect on PIN polarity. Indeed, PISA treatment diminished PIN2 polarity at the PM. PIN2 showed pronounced accumulation at the lateral cell sides (Fig. 8, C and D; Supplemental Fig. S12) and PIN1 showed almost no polarity after treatment with PISA (Supplemental Fig. S13). Furthermore, PISA at 100 μM disrupted the root architectures and PIN2 polar localization (Supplemental Fig. S14).

Downloaded from https://academic.oup.com/plphys/article/180/2/1152/6117699 by Institute of Science and Technology Austria user on 15 October 2021

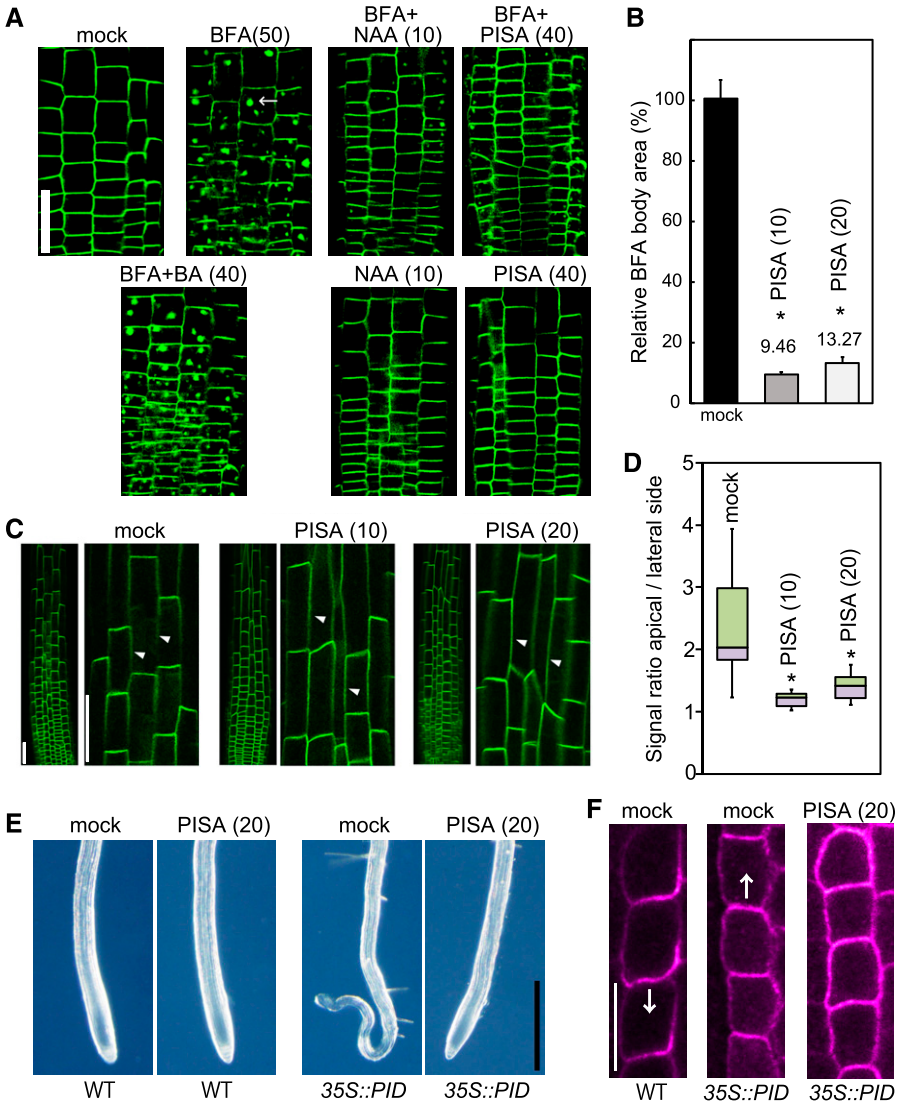

Figure 8. Effects of PISA on PIN internalization from the PM. A and B, Effect of PISA on the BFA body formation of PIN2-GFP. Five-d–old *proPIN2*::*PIN2-GFP* seedlings were incubated for 30 min in liquid GM medium containing PISA, benzoic acid (BA) and NAA, and then BFA was added to the medium. Seedlings were then incubated for additional 60 min. BFA induced PIN2-GFP-marked BFA bodies. The area of BFA body was measured and the area in BFA-treated seedlings (n = 25–40, $*P < 0.01$) was adjusted to 100%. The value of the area is shown the means ± SD in (B). Bar = 50 μm. C and D, Effect of PISA on the internalization of PIN2-GFP. Five-d–old *proPIN2*::*PIN2-GFP* seedlings were incubated for 12 h with PISA. The fluorescence intensity of the apical and lateral sides of cells in the root (n = 18–20, $*P < 0.01$) were quantified and the fluorescent signal rate (apical side/lateral side) is shown as the means ± SD in (D). The values in parentheses represent the concentration of chemicals (micromolar). Bar = 50 μm. Arrowheads show lateral cell side. E, Effects of PISA on a collapse of the primary root meristem. Five-d–old root tips of wild-type (WT) and *35S*::*PID* plants grown vertically on agar plates containing PISA. Bar = 500 μm. F, Effects of PISA on PIN1 localization in the endodermis of wild-type and *35S*::*PID* roots. Immunolocalization of PIN1 after treatment with PISA for 4 h. Bar = 10 μm. Arrows indicate the direction of IAA transport by PIN1.

This change in the localization of PIN proteins was further investigated using PINOID (PID), a Ser Thr kinase of the AGC kinase family that is known to regulate PIN localization on the cellular membranes (Adamowski and Friml, 2015). Overexpression of PID triggers a basal to apical shift in PIN1 localization, thereby perturbing the auxin gradient in the root tip, depleting auxin from the root tip maxima and leading to meristem collapse (Benjamins et al., 2001; Friml et al., 2004). Consistently, PIN1 was localized at apical side in the endodermis of *35S*::*PID* roots (Fig. 8F). Intriguingly, PISA rescued collapsed root meristems in *35S*::*PID* roots (Fig. 8E) and the apical polarity of PIN1 in *35S*::*PID* was lost and switched to an apolar pattern in endodermal cells (Fig. 8F). Thus, PISA appears to repress IAA depletion from the *35S*::*PID* apical meristem by diminishing shootward IAA transport. This is fully consistent with the PISA effect on the polar localization of PIN proteins.

To gain further insight into the mechanism by which PISA induces PIN accumulation at the PM, the effects of PISA on PIN2-GFP accumulation were examined in a *tir1 afb1 afb2 afb3* quadruple mutant line (Supplemental Fig. S15). As in wild-type roots, PIN2-GFP protein was found to be predominantly located at the apical cell sides and not at lateral cell sides despite the severe growth defects in these roots. PISA promoted the accumulation of PIN2-GFP at lateral cell sides in the quadruple mutant, the same as in the wild-type root. This observation strongly suggests that PISA leads to increases in PIN protein accumulation at the PM without activating the $SCF^{TIR1/AFB}$ pathway.

DISCUSSION

Pinstatic Acid Is an Inert Molecule for the TIR1/AFB-Aux/IAA Coreceptor Complex

In the screening for the auxin transport modulators from the PAA analogs, PISA was found to be the most

Downloaded from https://academic.oup.com/plphys/article/180/2/1152/6117699 by Institute of Science and Technology Austria user on 15 October 2021

promising candidate. PISA does not bind to the $SCF^{TIR1/AFB}$ complex. The classical structure activity relationships of monosubstituted PAAs demonstrated that 4-substituted PAA is less or inactive as an auxin (Muir et al., 1967). Consistent with these early structure activity relationship studies of PAA derivatives, our results clearly demonstrated that PISA is not a classical auxin directly modulating the $SCF^{TIR1/AFB}$ machinery (Fig. 1). Consistent with this, a docking study using the auxin binding cavity of TIR1 showed that the 4-ethoxy chain in PISA would prevent stable binding of this compound (Supplemental Fig. S16).

In analogy to PISA, the introduction of alkyloxy chains into IAA and NAA at the 5- or 6-positions diminished their TIR1 binding activity (Tsuda et al., 2011). However, it appears that these alkoxy-IAA and -NAAs are still recognized by PIN efflux proteins to inhibit polar IAA transport in competition with endogenous IAA (Tsuda et al., 2011), suggesting alkoxy-IAAs and alkoxy-NAAs could act as auxin transport inhibitors. On the other hand, PAA is not actively and directionally transported in response to gravitropic stimuli and the distribution of PAA is not inhibited by NPA, suggesting that PAA is distributed by passive diffusion (Sugawara et al., 2015). As for PAA, it seems unlikely that PISA itself would be recognized by PINs in planta.

PISA Positively Modulates Polar Auxin Transport to Induce Auxin-Like Activity

PISA showed characteristic auxin-like activity on primary root and shoot responses. PISA inhibited primary root elongation and induced adventitious root formation at the shoot/root junction (Fig. 2). The auxin signaling mutants *axr1-3*, *tir1 afb2*, *slr1-1*, and *arf7 arf19* were resistant to PISA in primary root inhibition and adventitious root formation, suggesting that some PISA-induced responses might be mediated by the $SCF^{TIR1/AFB}$ signaling pathway. However, these responses can also be well explained by the accumulation of endogenous IAA at root tip and the shoot/root junction after elevated IAA efflux (Fig. 4D). Auxin efflux inhibitors completely repressed adventitious root formation induced by PISA (Table 1), suggesting that IAA movement is required for PISA activity on adventitious root formation. In the primary root, IAA is biosynthesized near the QC, where TAA1 is strongly expressed (Brumos et al., 2018). Auxin efflux inhibitors TIBA and NPA are considered to have repressed IAA efflux, leading to induction of *DR5*::*GFP* expression near the QC (Fig. 4D) and then results in the inhibition of root elongation (Brumos et al., 2018). In contrast, PISA would promote auxin efflux from the QC to lateral root cap, thereby *DR5*::*GFP* signal was induced at that place (Fig. 4D). Thus, PISA inhibits root elongation by distinct mechanism of auxin efflux inhibitors.

Furthermore, PISA promoted hypocotyl elongation. Auxin efflux transport inhibitors, TIBA, NPA, and BUM completely suppressed hypocotyl elongation (Figs. 3, B and C; Supplemental Fig. S5A). Hypocotyl elongation by synthetic auxin picloram or YUC1 overexpression could not be cancelled by auxin efflux transport inhibitors (Supplemental Fig. S5B). These evidences suggest that PISA positively modulated auxin transport to show auxin-like activity in the hypocotyl. This was further confirmed by ^{3}H-IAA transport assays in hypocotyl segments (Fig. 3E). Importantly, no auxin analog has been reported to be positive modulator of auxin transport.

PISA Affects Root Auxin Responses by Positively Modulating Shootward Auxin Transport

In contrast to auxin-like effects on primary root growth and shoot elongation, PISA-treated roots showed typical auxin-repressed phenotypes: reduced root hair formation, fewer lateral roots, and reduced gravitropic response. Auxin transport inhibitors promoted root hair formation (Fig. 5B) by accumulating endogenous IAA, but blocked lateral root formation and gravitropic responses by perturbing auxin distribution. The impaired root phenotypes by PISA resemble the root defects in PIN1 overexpressing roots (Rigas et al., 2013), supporting the hypothesis that PISA represses auxin-regulated phenotypes by enhancing auxin efflux. Intriguingly, PISA dramatically enhanced IAA-induced lateral root formation and PISA also promoted IAA-induced *DR5*::*GUS* expression in entire roots when auxin transport inhibitors did not (Fig. 6, B–D). Additionally, PISA enhanced shootward auxin movement from the root tip in basipetal auxin transport assays (Fig. 6E). PISA did not increase the endogenous IAA (Supplemental Fig. S6). Thus, it is unlikely that PISA would elevate endogenous IAA in the shoot by upregulating *TAA1* and *YUC* expression in the IAA biosynthesis pathway or by inhibiting the IAA inactivation pathway involving GH3 and DAO1 (Korasick et al., 2013). These observations suggest that PISA positively modulates shootward IAA transport in the root.

PISA Blocks PIN Internalization to Accumulate PIN at the PM in Arabidopsis

The localization and trafficking of PIN1 and PIN2 proteins have been extensively investigated by Adamowski and Friml (2015) and Rakusová et al. (2015). ROP GTPases-RIC signaling have been shown to inhibit the PIN internalization (Lin et al., 2012; Nagawa et al., 2012), PID kinase and D6 Protein Kinase could directly phosphorylate PIN at the PM to regulate the PIN trafficking in a GNOM-dependent manner (Adamowski and Friml, 2015). However, the molecular mechanism for the regulation of PIN trafficking, especially PIN internalization, by auxin has been unclear. Our results show that PISA inhibited the formation of

Downloaded from https://academic.oup.com/plphys/article/180/2/1152/6117699 by Institute of Science and Technology Austria user on 15 October 2021

BFA bodies containing PIN1 and PIN2 proteins (Fig. 8; Supplemental Fig. S11). Furthermore, PISA promoted the accumulation of PIN1 and PIN2 proteins at the lateral side of cells. These observations, together with phenotypic data, clearly indicate that by inhibiting PIN internalization PISA would increase PM-localized PIN content, leading to characteristic phenotypes caused by enhanced auxin efflux.

The target of PISA remains an open and intriguing question. PISA is completely inert for transcriptional auxin signaling modulated by SCF $^{TIR1/AFB}$–Aux/IAA machinery. PISA enhanced PIN2 accumulation at the PM in *tir1 afb1 afb2 afb3* quadruple mutant (Supplemental Fig. S15; Pan et al., 2009), implying TIR1/AFB receptors are not a prerequisite for the inhibition of PIN2 internalization by PISA. Modulation of PIN localization and trafficking are influenced by many regulatory steps (Adamowski and Friml, 2015) and it is likely that auxin could coordinately modulate pathways involving recycling rate, biosynthesis, and degradation of PINs in response to environmental and hormonal stimuli.

Many questions still remain as to the mode of action of PISA. It has been reported that auxin reduced formation of BFA bodies by inhibiting delivery of newly synthesized protein rather than by inhibition of PIN internalization (Jásik et al., 2016). On the other hand, PISA inhibited BFA body formation of PIN2-GFP, but enhanced amounts of PIN2-GFP on the PM, suggesting that delivery is not impaired and internalization is reduced. Given this, we have no reason to believe that PISA would target the regulatory component of PIN internalization to which endogenous auxin would bind. We anticipate that PISA will become a very useful chemical tool to dissect the regulatory mechanism of auxin transport.

MATERIALS AND METHODS

Plant Materials and Growth Conditions

Arabidopsis (*Arabidopsis thaliana*) ecotype Columbia (Col-0) was used for all experiments. The following transgenic and mutant lines were in the Col-0 ecotype: *axr1-3* [CS3075], *tir1-1 afb2-3* [CS69691], *iaa14/slr1-1* (Okushima et al., 2007; Chae et al., 2012; Spartz et al., 2012), *arf7 arf19* (Okushima et al., 2007), *DII-VENUS* (Brunoud et al., 2012), *yuc3 5 7 8 9* (Chen et al., 2014), *proPIN1::PIN1-GFP* (Vieten et al., 2005), *proPIN2::PIN2-GFP* (Vieten et al., 2005), *pin2/eir1-1* [CS16706], *35S::PIN1* [CS9375], *35S::PID* (Benjamins et al., 2001), and *pPIN2::PIN2-GFP / tir1 afb1 afb2 afb3* (Pan et al., 2009). Seeds were surface-sterilized and grown on germination medium (GM; one-half strength Murashige and Skoog salts [Gibco-BRL], 12 g/L of Suc, 1× B5 vitamins, and 0.2 g/L of MES containing 4 g/L of agar for a horizontal agar plate or 14 g/L of agar for a vertical agar plate, at pH 5.8) containing the indicated hormone and/or chemicals. The length of hypocotyl and lateral root number was measured using the software ImageJ (National Institutes of Health; http://rsb.info.nih.gov/ij).

Chemicals

PISA, and mPISA were synthesized from 4-hydroxyphenylacetic acid methyl ester and 3-hydroxyphenylacetic acid methyl ester, respectively. PISA is commercially available from some chemical suppliers (CAS Registry Number: 4919-33-9, Alfa Aesar, Santa Cruz Biotechnology, and Acros Organics).

Histochemical and Quantitative GUS Measurements

For GUS histochemical analysis, the seedlings were washed with a GUS-staining buffer (100 mM of sodium P at pH 7.0, 10 mM of EDTA, 0.5 mM of $K_4Fe[CN]_6$, 0.5 mM of $K_3Fep[CN]_6$, and 0.1% [w/v] Triton X-100) and transferred to the GUS-staining buffer containing 1 mM of 5-bromo-4-chloro-3-indolyl-β-d-glucuronide (X-Gluc), the substrate for histochemical staining, and incubated at 37°C until sufficient staining developed. For quantitative measurement, seedlings or the excised roots (n = 15–20) were homogenized in an extraction buffer as described in Hayashi et al. (2012). After centrifugation to remove cell debris, GUS activity was measured with 1 mM of 4-methyl umbelliferyl-β-D-glucuronide as a fluorogenic substrate at 37°C. The protein concentration was determined by Bradford protein assay (Bio-Rad). The experiments were repeated at least three times with four replications.

DII-VENUS Assay

Six-d–old *DII-VENUS* seedlings (Brunoud et al., 2012) were incubated in GM liquid medium containing 10-μM yucasin DF for 3 h at 24°C. The *DII-VENUS* seedlings were washed out well with fresh medium and incubated in fresh GM liquid medium for 5 min. Exogenous IAA and PISA was added to this medium and fluorescent images of roots were recorded after 60 min.

SPR Assay

SPR assays were performed as described in Quareshy et al. (2017). A quantity of 50-μM IAA or PISA was used to assay for the formation of the auxin-induced TIR1-IAA7 coreceptor complex, or AFB5-IAA7 complex. For the antiauxin assay, 5-μM IAA and 50-μM PISA (or control compound) were mixed and the sensorgram assessed for a reduced signal to the IAA.

Exogenous IAA-Induced Lateral Root Promotion

For lateral root growth, Arabidopsis seedlings were grown vertically for 5 d in continuous light on a GM agar plate. The seedlings were transferred to liquid GM medium containing the indicated concentration of IAA and PISA. The seedlings were cultivated under continuous light for another 3 d at 24°C and then the lateral root numbers were recorded. Three independent experiments were performed.

Gravitropic Response Assay

Six-d–old seedlings were grown vertically on GM agar plates under continuous light at 24°C. The seedlings were then transferred to agar plates containing chemicals and cultured vertically for 2 h. The plates were rotated 135° in the vertical plane, followed by incubation for 16 h in the dark. Photographs of the roots were recorded with a digital camera.

Auxin Transport Assay

For shoot basipetal transport, 6-d–old Col-0 etiolated seedlings grown on GM agar plates were decapitated to avoid endogenous auxin biosynthesis in cotyledons and a droplet of GM agar (12 g/L agar) with ^{3}H-IAA was applied to apical part of the hypocotyls. The seedlings were preincubated with 20-μM PISA for 1 h on an agar plate containing PISA. After 6 h, all roots were removed, hypocotyls were collected, homogenized using grinder and liquid N, and incubated overnight in Opti-Fluor scintillation solution (Perkin Elmer). The amount of ^{3}H-IAA was measured in a scintillation counter (300SL; Hidex) for 300 s with three technical repetitions. The decapitated seedlings were placed on a GM agar plate containing 5-μM NPA to inhibit auxin transport, and then a ^{3}H-IAA agar droplet was applied to each apical part. The negative control (diffusion) was estimated with seedlings transferred to GM agar containing 5-μM NPA during the ^{3}H-IAA droplets incubation (6 h) to inhibit auxin transport.

The root basipetal transport assay was carried out with slight modifications according to the method of Lewis and Muday (2009). A narrow strip of aluminum foil was vertically embedded in GM agar plate (20 g/L agar) containing 40-μM PISA. Five-d–old *DR5::GUS* seedlings were placed on the GM agar so that the root tip stepped over the edge of the foil strip. An agar block (10-μM IAA and 40-μM PISA) was placed on the root tip. The aluminum strip blocks the diffusion of IAA into the GM agar plate. The plate was incubated vertically for 10 h and GUS activity was visualized histochemically with X-Gluc.

Downloaded from https://academic.oup.com/plphys/article/180/2/1152/6117699 by Institute of Science and Technology Austria user on 15 October 2021

Asymmetric Auxin Distribution Measurement and PIN Immunolocalization Analysis

All measurements were performed using the software ImageJ. Quantification of auxin asymmetry was performed on maximal intensity projection of Z-scans of root tip by measuring the ratio of signal intensity of upper/lower half of the root. *DR5rev-GFP* reporter line was imaged before and after gravistimulation. PIN immunolocalizations of primary roots were carried out as described in Sauer et al. (2006) and Robert et al. (2010). The antibodies used in this study were anti-PIN1, 1:1,000; and anti-PIN2, 1:1,000.

Imaging and Image Analysis

Fluorescence images were recorded with a fluorescence microscope (BX-50; Olympus) and a laser scanning confocal microscope (FV-3000; Olympus). Typically, the seedlings were incubated with GM medium containing chemicals for the indicated time at 24°C and fluorescence images were then immediately recorded. For quantification of the fluorescent signal in epidermal cell in *pro-PIN2*::*PIN2-GFP* and *proPIN1*::*PIN1-GFP*. The same image acquisition parameters were used for all signal measurements. The regions of the visible BFA bodies in the same number and area of root cell were selected and the BFA body signal area (the area of BFA body/the constant root cell area containing same cell number) were calculated by the software ImageJ. To measure signal intensity of PM-localized PIN2-GFP, the mean pixel intensities were obtained from the apical and lateral sides of the individual cells by ImageJ. The PM-accumulation of PIN2-GFP was shown as the ratio of intensity (the apical side/the lateral side), 50–60 cells were analyzed for 5–7 seedlings in three independent treatments.

Statistical Analysis

Statistically significant differences in the results (**$P < 0.05$ or *$P < 0.01$) are based on Welch's two-sample *t* test by SigmaPlot (v.14; Systat). The values of mock-treated and PISA-treated samples (Figs. 2, 3, and 5–8) and the values of wild-type and mutant samples treated with PISA at the same concentration (Fig. 4) were statistically tested. Data are means ± SD of independent replicates. Box-and-whisker plots show a median (centerline), upper/lower quartiles (box limits), and maximum/minimum (whiskers).

Accession Numbers

Sequence data from this article can be found in the GenBank/EMBL data libraries under accession numbers: *TIR1* (At3g62980), *AFB2* (At3g26810), *AXR1* (At1g05180), *PIN1* (At1g73590), *PIN2* (At5g57090), *PIN3* (At1g70940), *IAA14* (At4g14550), *AUX1* (At2g38120), and *PID* (At2g34650).

Supplemental Data

The following supplemental materials are available.

Supplemental Figure S1. Auxin activity in an auxin-deficient Arabidopsis mutant and BY2 tobacco cell culture.

Supplemental Figure S2. Effects of PISA on rapid cell expansion in hypocotyl.

Supplemental Figure S3. Effects of PISA on SCF^{TIR1} signaling.

Supplemental Figure S4. Effects of mPISA and PISA on the phenotype related to $SCF^{TIR1/AFB}$ pathway.

Supplemental Figure S5. Auxin transport inhibitors blocked PISA-induced high-auxin phenotype, but did not inhibit the high-auxin phenotypes by picloram and YUC1 overexpression.

Supplemental Figure S6. Effects of PISA on endogenous IAA level.

Supplemental Figure S7. Phenotype of Arabidopsis seedlings cocultured with PISA and auxins.

Supplemental Figure S8. Effects of PISA and auxin transport inhibitors on auxin response in root.

Supplemental Figure S9. PISA promoted the lateral root formation induced by membrane-permeable IAA precursors.

Supplemental Figure S10. PISA did not affect the expression of *PIN1*::*GUS*, *PIN2*::*GUS* and *PIN7*::*GUS* reporter expression.

Supplemental Figure S11. Effect of PISA on the BFA body formation of PIN1.

Supplemental Figure S12. Effect of PISA on the internalization of PIN2-GFP.

Supplemental Figure S13. Effect of PISA on the internalization of PIN1.

Supplemental Figure S14. Effect of PISA on the internalization of PIN2 at high concentration.

Supplemental Figure S15. Effects of PISA on PIN2 membrane localization in *tir1 afb 1 afb 2 afb3* mutant.

Supplemental Figure S16. Molecular docking study of PAA, mPISA, and PISA with TIR1.

Supplemental Methods. Tobacco BY2 cell culture, pull-down assay, rapid cell elongation assay and the endogenous IAA measurement.

ACKNOWLEDGMENTS

We thank Dr. H. Fukaki (University of Kobe), Dr. R. Offringa (Leiden University), Dr. Jianwei Pan (Zhejiang Normal University), and Dr. M. Estelle (University of California at San Diego) for providing mutants and transgenic line seeds.

Received February 20, 2019; accepted March 21, 2019; published April 1, 2019.

LITERATURE CITED

Abas L, Benjamins R, Malenica N, Paciorek T, Wiśniewska J, Moulinier-Anzola JC, Sieberer T, Friml J, Luschnig C (2006) Intracellular trafficking and proteolysis of the Arabidopsis auxin-efflux facilitator PIN2 are involved in root gravitropism. Nat Cell Biol **8:** 249–256

Adamowski M, Friml J (2015) PIN-dependent auxin transport: Action, regulation, and evolution. Plant Cell **27:** 20–32

Adamowski M, Narasimhan M, Kania U, Glanc M, De Jaeger G, Friml J (2018) A functional study of AUXILIN-LIKE1 and 2, two putative clathrin uncoating factors in Arabidopsis. Plant Cell **30:** 700–716

Baster P, Robert S, Kleine-Vehn J, Vanneste S, Kania U, Grunewald W, De Rybel B, Beeckman T, Friml J (2013) SCF(TIR1/AFB)-auxin signalling regulates PIN vacuolar trafficking and auxin fluxes during root gravitropism. EMBO J **32:** 260–274

Benjamins R, Quint A, Weijers D, Hooykaas P, Offringa R (2001) The PINOID protein kinase regulates organ development in Arabidopsis by enhancing polar auxin transport. Development **128:** 4057–4067

Brumos J, Robles LM, Yun J, Vu TC, Jackson S, Alonso JM, Stepanova AN (2018) Local auxin biosynthesis is a key regulator of plant development. Dev Cell **47:** 306–318 e305

Brunoud G, Wells DM, Oliva M, Larrieu A, Mirabet V, Burrow AH, Beeckman T, Kepinski S, Traas J, Bennett MJ, et al (2012) A novel sensor to map auxin response and distribution at high spatio-temporal resolution. Nature **482:** 103–106

Buer CS, Muday GK (2004) The transparent testa4 mutation prevents flavonoid synthesis and alters auxin transport and the response of Arabidopsis roots to gravity and light. Plant Cell **16:** 1191–1205

Chae K, Isaacs CG, Reeves PH, Maloney GS, Muday GK, Nagpal P, Reed JW (2012) Arabidopsis SMALL AUXIN UP RNA63 promotes hypocotyl and stamen filament elongation. Plant J **71:** 684–697

Chen Q, Dai X, De-Paoli H, Cheng Y, Takebayashi Y, Kasahara H, Kamiya Y, Zhao Y (2014) Auxin overproduction in shoots cannot rescue auxin deficiencies in Arabidopsis roots. Plant Cell Physiol **55:** 1072–1079

Ding Z, Galván-Ampudia CS, Demarsy E, Łangowski Ł, Kleine-Vehn J, Fan Y, Morita MT, Tasaka M, Fankhauser C, Offringa R, et al (2011) Light-mediated polarization of the PIN3 auxin transporter for the phototropic response in Arabidopsis. Nat Cell Biol **13:** 447–452

Du Y, Tejos R, Beck M, Himschoot E, Li H, Robatzek S, Vanneste S, Friml J (2013) Salicylic acid interferes with clathrin-mediated endocytic protein trafficking. Proc Natl Acad Sci USA **110:** 7946–7951

Downloaded from https://academic.oup.com/plphys/article/180/2/1152/6117699 by Institute of Science and Technology Austria user on 15 October 2021

Fendrych M, Leung J, Friml J (2016) TIR1/AFB-Aux/IAA auxin perception mediates rapid cell wall acidification and growth of Arabidopsis hypocotyls. eLife **5:** 5

Friml J, Yang X, Michniewicz M, Weijers D, Quint A, Tietz O, Benjamins R, Ouwerkerk PB, Ljung K, Sandberg G, et al (2004) A PINOID-dependent binary switch in apical-basal PIN polar targeting directs auxin efflux. Science **306:** 862–865

Fukui K, Hayashi KI (2018) Manipulation and sensing of auxin metabolism, transport and signaling. Plant Cell Physiol **59:** 1500–1510

Furutani M, Nakano Y, Tasaka M (2014) MAB4-induced auxin sink generates local auxin gradients in Arabidopsis organ formation. Proc Natl Acad Sci USA **111:** 1198–1203

Ganguly A, Lee SH, Cho M, Lee OR, Yoo H, Cho HT (2010) Differential auxin-transporting activities of PIN-FORMED proteins in Arabidopsis root hair cells. Plant Physiol **153:** 1046–1061

Geldner N, Friml J, Stierhof YD, Jürgens G, Palme K (2001) Auxin transport inhibitors block PIN1 cycling and vesicle trafficking. Nature **413:** 425–428

Geldner N, Anders N, Wolters H, Keicher J, Kornberger W, Muller P, Delbarre A, Ueda T, Nakano A, Jürgens G (2003) The Arabidopsis GNOM ARF-GEF mediates endosomal recycling, auxin transport, and auxin-dependent plant growth. Cell **112:** 219–230

Hayashi K (2012) The interaction and integration of auxin signaling components. Plant Cell Physiol **53:** 965–975

Hayashi K, Neve J, Hirose M, Kuboki A, Shimada Y, Kepinski S, Nozaki H (2012) Rational design of an auxin antagonist of the SCF(TIR1) auxin receptor complex. ACS Chem Biol **7:** 590–598

He W, Brumos J, Li H, Ji Y, Ke M, Gong X, Zeng Q, Li W, Zhang X, An F, et al (2011) A small-molecule screen identifies L-kynurenine as a competitive inhibitor of TAA1/TAR activity in ethylene-directed auxin biosynthesis and root growth in Arabidopsis. Plant Cell **23:** 3944–3960

Jásik J, Bokor B, Stuchlík S, Mičieta K, Turňa J, Schmelzer E (2016) Effects of auxins on PIN-FORMED2 (PIN2) dynamics are not mediated by inhibiting PIN2 endocytosis. Plant Physiol **172:** 1019–1031

Kasahara H (2016) Current aspects of auxin biosynthesis in plants. Biosci Biotechnol Biochem **80:** 34–42

Kitakura S, Vanneste S, Robert S, Löfke C, Teichmann T, Tanaka H, Friml J (2011) Clathrin mediates endocytosis and polar distribution of PIN auxin transporters in Arabidopsis. Plant Cell **23:** 1920–1931

Korasick DA, Enders TA, Strader LC (2013) Auxin biosynthesis and storage forms. J Exp Bot **64:** 2541–2555

Lee S, Sundaram S, Armitage L, Evans JP, Hawkes T, Kepinski S, Ferro N, Napier RM (2014) Defining binding efficiency and specificity of auxins for SCF(TIR1/AFB)-Aux/IAA co-receptor complex formation. ACS Chem Biol **9:** 673–682

Lewis DR, Muday GK (2009) Measurement of auxin transport in *Arabidopsis thaliana*. Nat Protoc **4:** 437–451

Leyser O (2018) Auxin signaling. Plant Physiol **176:** 465–479

Lin D, Nagawa S, Chen J, Cao L, Chen X, Xu T, Li H, Dhonukshe P, Yamamuro C, Friml J, et al (2012) A ROP GTPase-dependent auxin signaling pathway regulates the subcellular distribution of PIN2 in Arabidopsis roots. Curr Biol **22:** 1319–1325

Marhavý P, Bielach A, Abas L, Abuzeineh A, Duclercq J, Tanaka H, Pařezová M, Petrášek J, Friml J, Kleine-Vehn J, et al (2011) Cytokinin modulates endocytic trafficking of PIN1 auxin efflux carrier to control plant organogenesis. Dev Cell **21:** 796–804

Muir RM, Fujita T, Hansch C (1967) Structure-activity relationship in the auxin activity of mono-substituted phenylacetic acids. Plant Physiol **42:** 1519–1526

Nagawa S, Xu T, Lin D, Dhonukshe P, Zhang X, Friml J, Scheres B, Fu Y, Yang Z (2012) ROP GTPase-dependent actin microfilaments promote PIN1 polarization by localized inhibition of clathrin-dependent endocytosis. PLoS Biol **10:** e1001299

Naramoto S, Kleine-Vehn J, Robert S, Fujimoto M, Dainobu T, Paciorek T, Ueda T, Nakano A, Van Montagu MC, Fukuda H, et al (2010) ADP-ribosylation factor machinery mediates endocytosis in plant cells. Proc Natl Acad Sci USA **107:** 21890–21895

Nishimura K, Fukagawa T, Takisawa H, Kakimoto T, Kanemaki M (2009) An auxin-based degron system for the rapid depletion of proteins in nonplant cells. Nat Methods **6:** 917–922

Okushima Y, Fukaki H, Onoda M, Theologis A, Tasaka M (2007) ARF7 and ARF19 regulate lateral root formation via direct activation of LBD/ASL genes in Arabidopsis. Plant Cell **19:** 118–130

Paciorek T, Zazímalová E, Ruthardt N, Petrásek J, Stierhof YD, Kleine-Vehn J, Morris DA, Emans N, Jürgens G, Geldner N, et al (2005) Auxin inhibits endocytosis and promotes its own efflux from cells. Nature **435:** 1251–1256

Pan J, Fujioka S, Peng J, Chen J, Li G, Chen R (2009) The E3 ubiquitin ligase SCFTIR1/AFB and membrane sterols play key roles in auxin regulation of endocytosis, recycling, and plasma membrane accumulation of the auxin efflux transporter PIN2 in *Arabidopsis thaliana*. Plant Cell **21:** 568–580

Prát T, Hajný J, Grunewald W, Vasileva M, Molnár G, Tejos R, Schmid M, Sauer M, Friml J (2018) WRKY23 is a component of the transcriptional network mediating auxin feedback on PIN polarity. PLoS Genet **14:** e1007177

Quareshy M, Uzunova V, Prusinska JM, Napier RM (2017) Assaying auxin receptor activity using SPR assays with F-Box proteins and Aux/IAA degrons. Methods Mol Biol **1497:** 159–191

Rakusová H, Fendrych M, Friml J (2015) Intracellular trafficking and PIN-mediated cell polarity during tropic responses in plants. Curr Opin Plant Biol **23:** 116–123

Rakusová H, Abbas M, Han H, Song S, Robert HS, Friml J (2016) Termination of shoot gravitropic responses by auxin feedback on PIN3 polarity. Curr Biol **26:** 3026–3032

Ren H, Gray WM (2015) SAUR proteins as effectors of hormonal and environmental signals in plant growth. Mol Plant **8:** 1153–1164

Rigas S, Ditengou FA, Ljung K, Daras G, Tietz O, Palme K, Hatzopoulos P (2013) Root gravitropism and root hair development constitute coupled developmental responses regulated by auxin homeostasis in the Arabidopsis root apex. New Phytol **197:** 1130–1141

Robert HS, Grones P, Stepanova AN, Robles LM, Lokerse AS, Alonso JM, Weijers D, Friml J (2013) Local auxin sources orient the apical-basal axis in Arabidopsis embryos. Curr Biol **23:** 2506–2512

Robert S, Kleine-Vehn J, Barbez E, Sauer M, Paciorek T, Baster P, Vanneste S, Zhang J, Simon S, Čovanová M, et al (2010) ABP1 mediates auxin inhibition of clathrin-dependent endocytosis in Arabidopsis. Cell **143:** 111–121

Salanenka Y, Verstraeten I, Löfke C, Tabata K, Naramoto S, Glanc M, Friml J (2018) Gibberellin DELLA signaling targets the retromer complex to redirect protein trafficking to the plasma membrane. Proc Natl Acad Sci USA **115:** 3716–3721

Sauer M, Paciorek T, Benková E, Friml J (2006) Immunocytochemical techniques for whole-mount in situ protein localization in plants. Nat Protoc **1:** 98–103

Spartz AK, Lee SH, Wenger JP, Gonzalez N, Itoh H, Inzé D, Peer WA, Murphy AS, Overvoorde PJ, Gray WM (2012) The SAUR19 subfamily of SMALL AUXIN UP RNA genes promote cell expansion. Plant J **70:** 978–990

Sugawara S, Mashiguchi K, Tanaka K, Hishiyama S, Sakai T, Hanada K, Kinoshita-Tsujimura K, Yu H, Dai X, Takebayashi Y, et al (2015) Distinct characteristics of indole-3-acetic acid and phenylacetic acid, two common auxins in plants. Plant Cell Physiol **56:** 1641–1654

Tsuda E, Yang H, Nishimura T, Uehara Y, Sakai T, Furutani M, Koshiba T, Hirose M, Nozaki H, Murphy AS, et al (2011) Alkoxy-auxins are selective inhibitors of auxin transport mediated by PIN, ABCB, and AUX1 transporters. J Biol Chem **286:** 2354–2364

Tsugafune S, Mashiguchi K, Fukui K, Takebayashi Y, Nishimura T, Sakai T, Shimada Y, Kasahara H, Koshiba T, Hayashi KI (2017) Yucasin DF, a potent and persistent inhibitor of auxin biosynthesis in plants. Sci Rep **7:** 13992

Vieten A, Vanneste S, Wisniewska J, Benková E, Benjamins R, Beeckman T, Luschnig C, Friml J (2005) Functional redundancy of PIN proteins is accompanied by auxin-dependent cross-regulation of PIN expression. Development **132:** 4521–4531

Winicur ZM, Zhang GF, Staehelin LA (1998) Auxin deprivation induces synchronous Golgi differentiation in suspension-cultured tobacco BY-2 cells. Plant Physiol **117:** 501–513

Wisniewska J, Xu J, Seifertová D, Brewer PB, Ruzicka K, Blilou I, Rouquié D, Benková E, Scheres B, Friml J (2006) Polar PIN localization directs auxin flow in plants. Science **312:** 883

Downloaded from https://academic.oup.com/plphys/article/180/2/1152/6117699 by Institute of Science and Technology Austria user on 15 October 2021

Plant Science 303 (2021) 110750

Contents lists available at ScienceDirect

Plant Science

journal homepage: www.elsevier.com/locate/plantsci

Developmental roles of Auxin Binding Protein 1 in *Arabidopsis thaliana*

Zuzana Gelová [a], Michelle Gallei [a], Markéta Pernisová [b,c], Géraldine Brunoud [b], Xixi Zhang [a,d], Matouš Glanc [a,e], Lanxin Li [a], Jaroslav Michalko [a], Zlata Pavlovičová [a], Inge Verstraeten [a], Huibin Han [a], Jakub Hajný [a,f], Robert Hauschild [a], Milada Čovanová [g], Marta Zwiewka [h], Lukas Hoermayer [a], Matyáš Fendrych [a], Tongda Xu [i], Teva Vernoux [b], Jiří Friml [a,*]

[a] *Institute of Science and Technology (IST), Am Campus 1, 3400 Klosterneuburg, Austria*
[b] *Laboratoire Reproduction et Développement des Plantes, Univ Lyon, ENS de Lyon, UCB Lyon 1, CNRS, INRA, 69342 Lyon, France*
[c] *Functional Genomics and Proteomics, National Centre for Biomolecular Research, Faculty of Science, Masaryk University, Kamenice 5, 62500 Brno, Czech Republic*
[d] *Department of Applied Genetics and Cell Biology, University of Natural Resources and Life Sciences (BOKU), Muthgasse 18, 1190 Vienna, Austria*
[e] *Department of Experimental Plant Biology, Faculty of Science, Charles University, Viničná 5, 12844 Prague, Czech Republic*
[f] *Laboratory of Growth Regulators, The Czech Academy of Sciences, Institute of Experimental Botany & Palacký University, Šlechtitelů 27, 78371 Olomouc, Czech Republic*
[g] *The Czech Academy of Sciences, Institute of Experimental Botany, Rozvojová 263, 165 02 Praha 6, Czech Republic*
[h] *Mendel Centre for Plant Genomics and Proteomics, Central European Institute of Technology (CEITEC), Masaryk University, Kamenice 5, 625 00 Brno, Czech Republic*
[i] *FAFU-Joint Centre, Horticulture and Metabolic Biology Centre, Haixia Institute of Science and Technology, Fujian Agriculture and Forestry University, Fuzhou, 350002 Fujian, People's Republic of China*

ARTICLE INFO

Keywords:
AUXIN BINDING PROTEIN 1 (ABP1)
Auxin
Plant development
Auxin signaling

ABSTRACT

Auxin is a major plant growth regulator, but current models on auxin perception and signaling cannot explain the whole plethora of auxin effects, in particular those associated with rapid responses. A possible candidate for a component of additional auxin perception mechanisms is the *AUXIN BINDING PROTEIN 1 (ABP1)*, whose function *in planta* remains unclear.

Here we combined expression analysis with gain- and loss-of-function approaches to analyze the role of *ABP1* in plant development. *ABP1* shows a broad expression largely overlapping with, but not regulated by, transcriptional auxin response activity. Furthermore, *ABP1* activity is not essential for the transcriptional auxin signaling. Genetic *in planta* analysis revealed that *abp1* loss-of-function mutants show largely normal development with minor defects in bolting. On the other hand, *ABP1* gain-of-function alleles show a broad range of growth and developmental defects, including root and hypocotyl growth and bending, lateral root and leaf development, bolting, as well as response to heat stress. At the cellular level, *ABP1* gain-of-function leads to impaired auxin effect on PIN polar distribution and affects BFA-sensitive PIN intracellular aggregation.

The gain-of-function analysis suggests a broad, but still mechanistically unclear involvement of *ABP1* in plant development, possibly masked in *abp1* loss-of-function mutants by a functional redundancy.

1. Introduction

The phytohormone auxin is a major coordinator of plant growth that governs a multitude of developmental processes. Its versatility is related to its differential distribution within plant tissues and the ability of cellular auxin concentrations determine various cell fate decisions. The establishment of these morphogenic auxin gradients and local auxin maxima is achieved by a combination of local auxin biosynthesis [1] and synergetic, directional cell-to-cell polar auxin transport [2].

Auxin concentration affects cellular processes, mainly through a modulation of transcription. A broad range of auxin-responsive transcriptional regulators remodel the transcriptome of cells through tissue specific expression and thus trigger complex developmental changes [3]. On this transcriptional level, auxin controls processes such as embryogenesis, vascular tissues formation and organogenesis of the shoot apex or maintenance of the root apical meristem [4].

Nevertheless, some cellular auxin effects occur too fast to be a result of transcriptome remodeling and/or they were shown not to require

* Corresponding author.
E-mail address: jiri.friml@ist.ac.at (J. Friml).

https://doi.org/10.1016/j.plantsci.2020.110750
Received 1 September 2020; Accepted 5 November 2020
Available online 13 November 2020
0168-9452/© 2020 The Author(s). Published by Elsevier B.V. This is an open access article under the CC BY license (http://creativecommons.org/licenses/by/4.0/).

functional transcription or *de novo* protein synthesis. Auxin triggers rapid hyperpolarization of the plasma membrane leading to protoplast swelling [5,6], induces calcium ion and proton fluxes across the plasma membrane and therefore alkalizes the apoplast [7,8], and inhibits clathrin-mediated endocytic trafficking processes [9,10].

The auxin signal is transduced via several mechanisms [11,12]. The canonical pathway is mediated by a nuclear-localized co-receptor complex comprising the TRANSPORT INHIBITOR RESISTANT1/AUXIN SIGNALING F-BOX (TIR1/AFB) F-box proteins and the AUXIN/INDOLE-3-ACETIC ACID (Aux/IAA) transcriptional repressors. Here, auxin promotes the interaction of TIR1/AFBs with Aux/IAAs that results in ubiquitin-dependent degradation of the Aux/IAA proteins. Aux/IAA proteins act as transcriptional repressors of AUXIN RESPONSE FACTORs (ARFs) transcription factors and thus their degradation activates auxin-responsive transcription [13].

Notably, recent findings suggest that TIR1/AFB signaling mediates both rapid transcriptional as well as even faster non-transcriptional auxin effects on growth. In shoots, auxin via the TIR1/AFB pathway induces fast apoplast acidification and growth promotion by a rapid transcriptional regulation of *SMALL AUXIN UPREGULATED (SAUR)* genes [14,15]. In contrast, auxin-mediated growth inhibition in roots occurs within 30 s and does not require *de novo* protein synthesis but is still strictly dependent on the TIR1/AFB pathway [16]. Furthermore, the auxin-mediated fast depolarization of the plasma membrane and Ca^{2+} uptake were demonstrably linked with the TIR1/AFB signaling pathway [17].

Recently, two additional non-canonical auxin-sensing mechanisms were described. Auxin has been shown to bind directly to the atypical ARF ARF3/ETTIN to modulate chromatin states and interaction with other transcriptional regulators during gynoecium development [18,19]. The other mechanism involves TRANSMEMBRANE KINASE 1 (TMK1), a member of the plasma membrane-localized TMK receptor-like kinase family [20]. It was shown that auxin triggers cleavage of TMK1's intracellular kinase domain and its consequent translocation to the nucleus. There, the TMK1 kinase domain binds, phosphorylates and thus stabilizes two non-canonical Aux/IAAs, IAA32 and IAA34. Via this alternative transcriptional pathway, auxin regulates apical hook development [21]. TMK1 also regulates lateral root organogenesis and auxin biosynthesis by other cellular mechanisms [22,23]. Importantly, while the canonical TIR1/AFB receptors sense auxin predominantly in the nucleus, the TMKs located in the plasma membrane may perceive auxin from the apoplast by an unknown perception mechanism.

The accumulating developmental roles of TMKs in conjunction with their plasma membrane localization stir up a decades-lasting debate on the existence of a cell-surface auxin receptor. In the past, the best candidate appeared to be AUXIN BINDING PROTEIN 1 (ABP1). This evolutionally conserved 22-kDa glycoprotein [24,25] has been shown to bind auxin at apoplastic pH 5.5 [26–28] and although it predominantly localizes to the endoplasmic reticulum (ER), a small fraction has been proposed to reside in the apoplast [29]. ABP1 has been proposed to be mainly associated with rapid non-transcriptional auxin-mediated processes, but the genetic analysis has been hampered by the lack of viable loss-of-function mutants. It has also remained unclear how apoplastic ABP1 could transduce the auxin signal into the cell and therefore the requirement of a plasma membrane-localized docking partner was hypothesized. Later, ABP1 was found to interact with TMK1 in an auxin-dependent manner. It was proposed that ABP1 and TMK1 form an auxin-sensing complex at the plasma membrane that activates downstream cellular processes via small GTPases ROP2 and ROP6 and their effector proteins RIC1 and RIC4 [30–32]. Based on the phenotypes of *ABP1* gain-of-function mutants, the weak *abp1-5* allele and conditional *abp1* knock-down lines [33] *ABP1* was proposed to play a role in clathrin-mediated endocytosis [10,34,35], growth-correlating microtubule re-orientation [36], cell wall remodeling [37] or interdigitated growth of leaf pavement cells [30,36]. All these proposed roles were called into question by the failure to complement the alleged embryo lethal *abp1* phenotypes, by the coding sequence of *ABP1* [35] and by the identification of new *abp1* knock-out alleles with no obvious morphological phenotypes [38]. These discrepancies were clarified by proofs that the original *abp1* embryo lethal phenotypes were caused by disruption of a neighboring gene rather than *ABP1* itself [39,40]. Furthermore, the *abp1-5* line carries many additional mutations [41] and the conditional knock-down lines, despite independently targeting either ABP1 mRNA or protein [33], also have other targets [42]. Thus, with much of the previously used genetic material called into question and with only superficial phenotype analysis of the more recent, verified knock-out lines [38], the developmental and physiological roles of ABP1 still remain largely unclear.

Here we used the verified gain- and loss-of-function mutant lines in Arabidopsis to (re)evaluate the role of ABP1 in cellular processes, physiological responses and plant development.

2. Materials and methods

2.1. Plant material

Wild-type Col-0 (NASC, The Nottingham Arabidopsis Stock Centre; http://www.arabidopsis.info, N1092) was used as a control line. Previously published *Arabidopsis thaliana* lines were used in this study: *ABP1*$_{i1,2}$*::GUS* [43]; *abp1-C1*, *abp1-TD1* and background Col-0 used for generating *abp1-C1* by CRISPR (in text mentioned as WT for *abp1-C1*) [38]; *DR5rev::GFP* [44]; *35S::ABP1-GFP* [10]. The following *Arabidopsis thaliana* lines were generated in this study: *DR5rev::GFP;abp1-C1* and *DR5rev::GFP;abp1-TD1*. *DR5rev::GFP* was introduced into both *abp1* mutant backgrounds by genetic crossing. The *ABP1::ABP1;abp1-TD1* line was generated by introducing the *ABP1::ABP1* construct into the *abp1-TD1* background and the *ABP1::GFP-ABP1;abp1-C1* line was generated by introducing the *ABP1::GFP-ABP1* construct into the *abp1-C1* background using Agrobacterium-mediated transformation [45]. All transgenic lines and mutants used in this study are listed in Supplemental Table 1. All primers used for genotyping are listed in Supplemental Table 2.

2.2. Vector construction

All plasmids were constructed by the Gateway cloning technology (www.invitrogen.com). Previously generated constructs pDONR221-ABP1cDNA and pDONR221-ABP1cDNA-M2X containing cDNA sequence of *ABP1* [35] were used to construct the final plasmids *35S::ABP1* and *35S::ABP1-M2X* by recombination into the p2GW7 destination vector. *ABP1::ABP1* was constructed as follows: the 3.0 kb promoter, genomic coding region and 0.6 kb of 3' untranslated region for *ABP1* was amplified and inserted into a pDONR-Zeo vector, then inserted into the pGWB401 destination vector. *ABP1::GFP-ABP1* was constructed using a 1585 bp promoter fragment [43] and a N-terminal GFP fusion directly after the N-terminal signal peptide. The GFP insertion was flanked at the 5' end by a PKAPA linker (tested for cleavage using the SignalP-5.0 server) and at the 3' end by a PKPAPKPA linker. The *ABP1* fragments were amplified from genomic DNA using primer pairs 1 and 2 (promoter, signal peptide and 5' linker), 3 and 4 (GFP and 3' linker) and 5 and 6 (gABP1 gene body including 3' UTR). All three fragments were fused in a single overlap PCR reaction and cloned into the pDONR221 entry vector. The resulting construct was cloned into the pKGW,0 destination vector and sequenced. All primers used in this study are listed in Supplemental Table 2. All plasmids used in this study are listed in Supplemental Table 3.

2.3. Growth conditions

Seeds were chlorine gas sterilized or sterilized with 70 % EtOH, sown on plates with ½ Murashige and Skoog (MS) medium supplemented with

1 % (w/v) sucrose and 0.8 % (w/v) Phytoagar (pH 5.9) and stratified for 2 days at 4 °C. For experiments using Arabidopsis seedlings, the seedlings were grown on plates at 21 °C under a long-day photoperiod (16 h light/8 h dark) for the required time period. For experiments performed in soil, *in vitro* grown seedlings were transferred to soil and grown under a long-day photoperiod (16 h light/8 h dark) at 21 °C and 40 % relative humidity for the required time period. The light sources used were Philips GreenPower light emitting diode production modules in a deep red, far red, blue combination with a photon density of 140.4 µmol/m^2/s ± 3 %. For phyllotaxis measurement experiment, plants in soil were cultivated in growth chambers at 22 °C and 40 % relative humidity. Plants were kept under short day conditions (8 h light/16 h dark) for 28 days and then transferred to long day conditions (16 h light/8 h dark). Plants were always grown together within the growth chamber and with randomized positions within each tray in order to minimize the effect of environmental fluctuations. For etiolated growth, the plated and stratified seeds were exposed to light for 8 h and further covered with aluminum foil to cultivate them in the dark at 21 °C for 4 days (the shoot gravity response experiment) or in the dark chamber at 24 °C for 5 days (the etiolated growth experiment).

2.4. Histochemical GUS staining

6-d-old light-grown seedlings or 3-d-old etiolated seedlings of *ABP1$_{i1,2}$::GUS* were stained in 0.1 M sodium phosphate buffer (pH 7.0) containing 0.1 % X-GlcA sodium salt (Duchefa, 7240-90-6), 2 mM K_3[Fe(CN)$_6$], 2 mM K_4[Fe(CN)$_6$] and 0.05 % Triton X-100 for 2 h (light-grown seedlings) or 1 h (etiolated seedlings) at 37 °C. Further, samples were incubated overnight in 80 % (v/v) ethanol at room temperature. Tissue clearing was conducted as previously described [46]. DIC microscopy for analysis of GUS staining was performed using an Olympus BX53 microscope equipped with 10x and 20x air objectives and a DP26 CCD camera. For treatment, 5-d-old seedlings of *ABP1$_{i1,2}$::GUS* were transferred to ½ MS media supplemented with DMSO (mock) for 3.5 h, 25 µM L-Kynurenine (Sigma-Aldrich, 2922-83-0) for 3.5 h and 25 µM L-Kynurenine for 2 h followed by 300 nM IAA (Duchefa, 87-51-4) for 1.5 h. Subsequently, GUS staining and DIC microscopy were performed as described above.

2.5. Quantitative real-time PCR

After treatment with 100 nM IAA, seedlings were sampled in 4 biological replicates at different times (t0, 5 min, 30 min, 1 h, 2 h and 4 h). Total RNA was prepared from max100 mg of shoots/roots of 5-d-old seedlings with the RNeasy Plant Mini Kit (Qiagen, 74904) according to the manufacturers's instructions. cDNA was synthesized from 2 µg of total RNA using the QuantiNova Reverse Transcription Kit (Qiagen, 205410). For the mutant expression analyses, 3 biological replicates of full seedlings were used. All samples were pipetted in 3 technical replicates in a 384 well plate using an automated JANUS Workstation (PerkinElmer). According to the manufacturer's instructions, 5 µL reaction volume contained 2.5 µL Luna® Universal qPCR mastermix (NEB, M3003S). RT-qPCR analyses were performed using the Real-time PCR Roche Lightcycler 480 and the expression of PP2AA3 (At1G13320) or EF1a (At5G60390) was used as a reference [47]. For *ABP1*, 5 different primer pairs were evaluated and one representative graph is included in the manuscript. The primers used for the presented analysis are listed in Supplemental Table 2.

2.6. Confocal laser scanning microscopy and image analysis

Confocal laser scanning microscopy for analysis of fluorescence intensity was performed on a Zeiss LSM800 microscope assisted with Zeiss Zen 2011 software. Images were acquired with 20x/0.8 NA air (DR5 evaluation) or 40x/1.2 NA water immersion objectives (immunostaining).

2.7. DR5-GFP intensity measurement

5-d-old seedlings were transferred from solid ½ MS media to plates supplemented with either DMSO or 1 µM IAA for 3 h and imaged using confocal microscopy. The fluorescence intensity of GFP (excitation wavelength: 488 nm) was measured in ImageJ.

2.8. Microfluidic vRootchip

A microfluidic chip, vRootchip was used to analyze root tip growth in real-time. The manufacturing of the chip, sample preparation procedure, and data analysis of root tip growth was performed as described previously [16] and according to Li and Verstraeten *et* al. (unpublished). vRoot-chip was used with 10 nM IAA treatment in ¼ MS and 0.1 % sucrose. For imaging, the vertical confocal microscopy setup was used as described previously [16,48] and according to Li and Verstraeten et al. (unpublished). The 10 nM IAA solution was supplemented with the cell-impermeable fluorescent dye Tetramethylrhodamine isothiocyanate–Dextran [16].

2.9. Protoplast assay

Protoplasts from 3-d-old Arabidopsis root suspension culture were isolated and transformed as previously described [49]. Plasmids were prepared with an E.Z.N.A. Plasmid Maxi Kit I (Omega Bio-Tek, D6922-02). Protoplasts were co-transfected with 6 µg of *35S::ABP1* or *35S::ABP1-M2X*, 2.5 µg of *DR5::LUC* [50] and 2.5 µg of *35S::Renilla* [51]. As a control, protoplasts co-transfected with *DR5::LUC* and *35S::Renilla* were used. The protoplasts were incubated with either 100 nM NAA (Sigma-Aldrich, 86-87-3) for 16 h or without treatment for 12 h followed by 100 nM NAA for 4 h in the dark at room temperature. The corresponding amount of DMSO was used as mock treatment. Chemiluminescence measurement was performed with the Dual-Luciferase Reporter Assay System kit (Promega, E1910) using a Spectrophotometer BioTek SynergyH1 plate reader and Gen 5 software (both BioTek).

2.10. Root length analysis

Plates with 4- and 7-d-old seedlings were scanned using an Epson Perfection V370 Photo flatbed scanner and the root length was measured using ImageJ.

2.11. Root gravitropic assay

For measurements of root gravitropic curvature kinetics, 4-d-old seedlings were placed on plates with ½ MS and rotated 90° and roots were imaged using a vertically placed flatbed scanner (Epson Perfection V370 Photo). Multiple plates were held in place on the scanner by a custom-made holder. Max. 12 ROIs of the seedlings were automatically imaged with a resolution of 1200 dpi in 10 min time intervals using an AutoIt script for 8 h. In ImageJ, the time-lapse movies of the seedlings were manually cropped and registered (stabilized) using the Fiji plugin "StackReg" in "Rigid body" mode.

2.12. Root growth (RG)-tracker

We developed a custom MATLAB application named RG-tracker (https://research-explorer.app.ist.ac.at/librecat/record/8294) with a graphical user interface that allows entirely automated root growth analysis and tracking of the root tips. Root tips were segmented based on the pixel classification workflow of Ilastik [52], which only requires manual retraining in case the imaging conditions change drastically. For each point in time, the positions of the root tips were determined by segmenting the tip-probability output, performing particle size filtering and calculating the center of mass. The root tips were then tracked over time by solving the linear assignment problem using the Hungarian

algorithm (Munkres). The tracking algorithm can deal with gaps in the root tip detection and both the gap closing and the maximum linking distance can be specified in the GUI. Completed tracks are filtered by minimum track length, duration and maximum growth speed to remove miss-detections and then presented to the user as an overlay of raw data, tip segmentation and tip tracks. At this point the user can exclude additional tracks from further analysis and export the overlay of the tracks and the root time-lapse. The x/y coordinates of each root tip, growth speed, direction of growth, growth angle and root length are then calculated for each point in time and exported for further analysis. All experiment specific parameters such as the segmentation threshold, particle size, and track filters can be saved and together with the segmentation project file form the complete data set to clearly recapitulate the data analysis.

2.13. Lateral root analysis

For the analysis of lateral root primordia, samples of 6-d-old seedling were collected and the tissue was cleared as previously described [46]. To visualize the lateral root primordia DIC microscopy was performed using an Olympus BX53 microscope equipped with a 20x air objective. The lateral root primordia were staged according to Malam and Benfey (1997) [46]. For analysis of emerged lateral roots, 4-d-old seedlings were transferred from ½ MS plates to plates supplemented with 500 nM NAA or DMSO. After 3 days, the plates were scanned using an Epson Perfection V370 Photo flatbed scanner and the pictures were analyzed using ImageJ.

2.14. Etiolated hypocotyl growth

To analyze the growth of etiolated hypocotyls, the seedlings were recorded at 12 h intervals for 120 h in a dark chamber equipped with an infrared light source (880 nm LED; Velleman, Belgium) and a spectrum-enhanced camera (EOS035 Canon Rebel Xti, 400DH) with built-in clear wideband-multicoated filter and standard accessories (Canon) and operated by the EOS utility software. The hypocotyl length was measured using ImageJ.

2.15. Etiolated hypocotyl bending

To determine hypocotyl gravitropism, the 3-d-old dark grown seedlings were rotated 90°. The plates were scanned using an Epson Perfection V370 Photo flatbed scanner and the hypocotyl bending angle was measured after gravity stimulation in 6 h intervals for 24 h using ImageJ.

2.16. Rosette size analysis

Seeds were germinated and grown on horizontally placed plates for 12 days, scanned using an Epson Perfection V370 Photo flatbed scanner and the rosette size was measured manually in ImageJ.

2.17. Vasculature development analysis

10-d-old cotyledons were collected and the tissue was cleared as follows: 2 days incubation in 70 % ethanol with a subsequent incubation in 4 % HCl, 20 % methanol solution at 65 °C for maximum 15 min, followed by an incubation in 7 % NaOH, 60 % ethanol solution at RT for another 15 min. The cotyledons were then re-hydrated in a series of decreasing ethanol concentrations (60 %, 40 %, 20 % and 10 %) for 1 h in each concentration at RT. Before mounting the cotyledons in 50 % glycerol onto microscopy slides they were incubated for 1 h in 25 % glycerol, 5 % ethanol solution at RT. Imaging was done using an Olympus BX53 microscope equipped with a 4x air objective.

2.18. Hypocotyl growth under high temperature

Seeds were germinated and grown on ½ MS plates with or without 10 g/L sucrose under 28 °C, continuous light for 7 days. The plates were scanned using an Epson Perfection V370 Photo flatbed scanner and the hypocotyl length was measured using ImageJ.

2.19. Hyperosmotic stress assay

4-d-old seedlings were transferred on media supplemented with either 200 mM mannitol or 100 mM NaCl for 4 days. The plates were scanned using an Epson Perfection V370 Photo flatbed scanner and the root extension was measured using ImageJ.

2.20. UV laser ablation and periclinal division analysis

3-d-old seedlings were transferred from solid ½ MS medium to plates containing 10 μM propidium iodide (Sigma-Aldrich, 25535-16-4) supplemented with 1 μM NAA or DMSO. The subsequent sample preparation, UV laser ablation, imaging and periclinal cell division analysis was performed as described previously [53].

2.21. Bolting time, leaf number and branch number analysis

Seeds were suspended in 0.1 % agarose and spread out in soil. The number of plants, bolted and with the primary inflorescence stem grown 1 cm, was recorded every day. The number of rosette and cauline leaves was counted when the first flower of each plant bloomed. The rosette branch was referred to the branch directly attached to the rosette, while the cauline branch was defined as the branch on the primary stem. The number of cauline branches and rosette branches were counted 21 days after sowing.

2.22. Phyllotaxis and internode length measurement

Analyses of 25 plants per genotype were performed when the last flowers had appeared. Angles and internode lengths between two subsequent siliques were measured starting from the lowest one. For each individual of each genotype, the variance of the divergence angles was computed, and individual variances of divergence angles were compared between genotypes using a non-parametric Kruskal–Wallis test in R (version 3.5.1, r-project.org), since their values were not normally distributed.

2.23. Immunostaining

Immunostaining was performed with 3 to 4-d–old seedlings as previously described [54]. The primary antibodies used were rabbit anti-PIN1 [9] diluted 1:1000 (v/v) and rabbit anti-PIN2 [55] diluted 1:1000 (v/v). The secondary antibody used was sheep anti-rabbit conjugated with Cy3 (Sigma-Aldrich, C2306) diluted 1:600 (v/v).

2.24. PIN lateralization

3to 4-d-old seedlings were treated either with 10 μM NAA or DMSO as a control for 4 h in liquid ½ MS medium. Subsequently, immunostaining using PIN1 and PIN2 antibodies was performed. Samples were imaged using confocal microscopy. The fluorescence intensity of Cy3 (excitation wavelength: 548 nm) was measured using ImageJ.

2.25. BFA treatment

4-d–old seedlings were incubated in liquid ½ MS medium at a final concentration of 25 μM BFA (Sigma-Aldrich, 20350-15-6) for 1 h. For BFA/NAA treatment the seedlings were pre-treated with 5 μM NAA for 30 min followed by co-treatment with 25 μM BFA and 5 μM NAA for 1 h.

As control, seedlings were incubated in liquid ½ MS medium supplemented with DMSO substituting NAA. Subsequently, immunostaining using PIN1 and PIN2 antibodies was performed. Samples were imaged using confocal microscopy and the fluorescence signal of Cy3 (excitation wavelength: 548 nm) was detected. BFA body formation was scored from 0 (no BFA body formation) to 3 (maximal BFA body formation) for each image, reflecting both the number of cells with BFA bodies as well as size and number of BFA bodies per cell. To avoid cognitive bias, all images were encoded prior to analysis.

2.26. Global transcriptome data analysis

Tissue-specific expression pattern and expression following different perturbations were obtained using Genevestigator (www.genevestigator.com) and were based on the 'AT_AFFY_ATH1-0' dataset.

2.27. Statistical analysis

If not mentioned differently, all data were analyzed using Student's t tests with p-value (*, $P < 0.05$; ** $P < 0.01$; *** $P < 0.001$) in the software Prism v8.3.0 (GraphPad).

2.28. Accession numbers

Sequences data from this article can be found in the GenBank/EMBL libraries under the following accession numbers: ABP1 (AT4G02980); PP2AA3 (At1G13320); EF1a (At5G60390).

3. Results

3.1. ABP1 expression and regulation by auxin

To obtain indications regarding the developmental processes and conditions in which ABP1 might play a role, we analyzed the *ABP1* expression pattern. The analysis of publicly available global transcriptome data in GENEVESTIGATOR® [56] suggested that *ABP1* is expressed constitutively in different tissues during development. *ABP1* transcription appears to be the highest in rosette leaves and roots, whilst lowest in pollen (Fig. S1A-B). In seedlings, *ABP1* is expressed in cotyledons, hypocotyls and root tips as well as in lateral roots. Global transcriptomics data following different perturbations suggested that *ABP1* expression is elevated in response to heat and slightly decreased following biotic stress (Fig. S1C).

To obtain more detailed insight into the *ABP1* expression pattern and confirm the global transcriptome analysis-based notions, we used an *ABP1::GUS* line to report *ABP1* promoter activity *in vivo*. GUS staining of

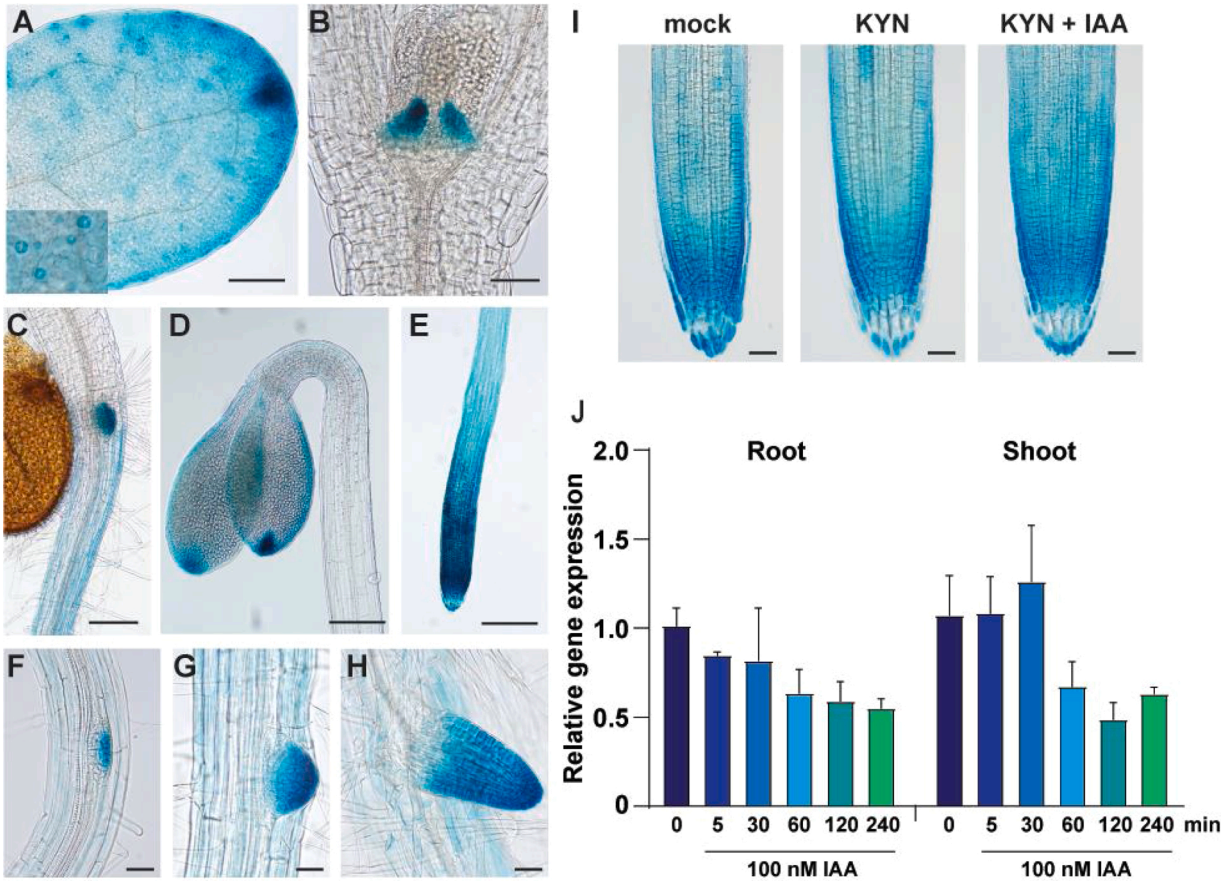

Fig. 1. *ABP1* expression and regulation by auxin.
(A–H) *ABP1::GUS* expression pattern. (A) 6-d-old cotyledon with inset detail of stomata, scale bar =100 μm. (B) shoot with hydathods of 6-d-old seedling, scale bar =50 μm. (C) shoot-root junction of 6-d-old seedling, scale bar =50 μm. (D) apical hook of 3-d-old etiolated seedling, scale bar =100 μm. (E) root tip of 6-d-old seedling, scale bar =100 μm. (F–H) lateral root primordia of 6-d-old seedling in IV, V and emerged stage respectively, scale bar =20 μm.
(I) Representative pictures of *ABP1::GUS* expression pattern in 5-d-old seedlings after treatment with DMSO (mock) for 3.5 h, 25 μM L-Kynurenine for 3.5 h and 25 μM L-Kynurenine for 2 h followed by 300 nM IAA for 1.5 h. For each treatment, at least 15 seedlings were evaluated. The experiment was repeated 2 times with similar results. Scale bar =20 μm.
(J) Quantitative Real-time PCR of *ABP1* expression in roots and shoots of 5-d-old Col-0 seedlings after DMSO (mock), and 5 min, 60 min, 120 min and 240 min of 100 nM IAA treatments. Expression of *ABP1* is normalized on expression of *PP2A* housekeeping gene. Experiment was repeated 3 times with similar result.

6-d-old seedlings confirmed the *ABP1* expression in cotyledons in which we detected stronger *ABP1* promoter activity in hydathodes and stomata (Fig. 1A-B). In both light- and dark-grown hypocotyls, the *ABP1* promoter activity was very low (Fig. 1C–D). Further, we confirmed *ABP1* expression in the primary root, particularly in the root tip (Fig. 1E) and during different stages of lateral root development (Fig. 1F–H). We observed that *ABP1* expression pattern in hydathodes, root tip and lateral roots largely overlaps with that of *DR5* reporters for transcriptional auxin response [43,44,50,57–59].

Therefore, we tested whether auxin regulates *ABP1* promoter activity and transcription. We employed L-Kynurenine, an inhibitor of auxin biosynthesis [60], to decrease auxin levels in the *ABP1::GUS* seedlings. We tested both, the effect of L-Kynurenine treatment alone or with subsequent auxin treatment, to study the effect of exogenously applied auxin. Overall, we detected no obvious changes in GUS reporter activity either after L-Kynurenine or after L-Kynurenine followed by auxin treatments (Fig. 1I).

To additionally verify these observations, we examined the auxin effect on *ABP1* transcription using real-time quantitative PCR (RT-qPCR). We performed RT-qPCR with roots and shoots of 5-d-old wild-type seedlings after auxin treatment. Consistent to what we observed with the *ABP1::GUS* transgenic line, auxin treatment did not strongly affect *ABP1* transcription (Fig. 1J).

These results show that *ABP1* expression overlaps with auxin

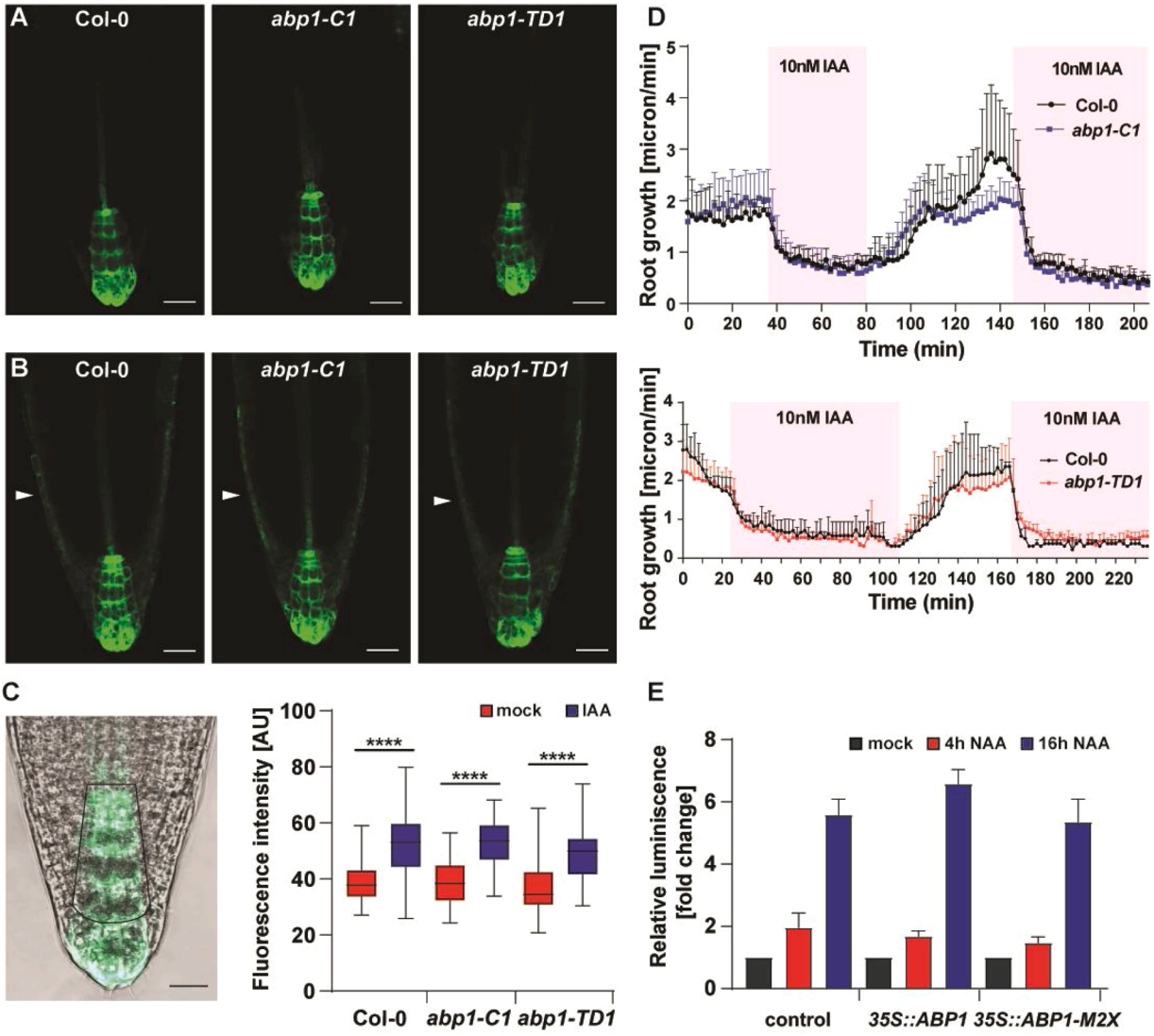

Fig. 2. Involvement of ABP1 in TIR1/AFB-mediated auxin responses.

(A–B) *DR5rev::GFP* expression pattern in 5-d-old seedlings of wild-type Col-0, *abp1-C1* and *abp1-TD1* mutants with DMSO (A) or with 1 μM IAA (B) treatment for 3 h. Arrowheads point to DR5 signal expanded to lateral root cap. Scale bar =30 μm.

(C) Representative picture of *DR5rev::GFP* expression in Col-0 with highlighted region that was quantified. Scale bar =50 μm. Quantification of *DR5rev::GFP* signal in root tips of 5-d-old Col-0, *abp1-C1* and *abp1-TD1* seedlings with DMSO (A) or with 1 μM IAA (B) treatment for 3 h. For each genotype per treatment, at least 15 seedlings were measured. The pooled result of 2 independent experiments is presented. For box plot, box defines the first and third quartiles, and the central lines in the box represent the median. Whiskers, from minimum to maximum. Asterisks indicate significant differences according to Student's t-tests (****, $P < 0.0001$).

(D) Root growth rate of *abp1-C1* (upper graph) and *abp1-TD1* (lower graph) compared to Col-0 measured in the vRootchip with repetitive 10 nM IAA treatment (magenta). n = 5, 6 for Col-0 and *abp1-C1*, respectively. n = 5 for *abp1-TD1*; n = 3,2 for Col-0 from 0−102 min and 102−236 min, respectively. Error bars denote standard deviation. The experiment was repeated 2 times with similar results.

(E) Activity of *DR5::LUC* reporter in response to *ABP1* and *ABP1-M2X* overexpression after mock (DMSO) and 100 nM IAA treatment in protoplasts. The values presented were calculated as a ratio between *DR5::LUC* enzymatic activity and internal control *Renilla::LUC* enzymatic activity and were further normalized on mock treatment values. Error bars denote standard error. The statistical difference was tested by Student's t-test. The experiment was repeated 2 times with similar results.

response maxima during seedling development, but that *ABP1* promoter activity and *ABP1* transcription are not significantly regulated by auxin.

3.2. Involvement of ABP1 in TIR1/AFB-mediated auxin responses

Considering that *ABP1::GUS* expression pattern largely overlaps with that of DR5 reporters for transcriptional auxin response [43,44,50,57–59], we investigated whether *ABP1* function is in any way linked to the transcriptional auxin signaling downstream of TIR1/AFB receptors [12,61]. First, we introduced *DR5rev::GFP* reporter into *abp1* loss-of-function mutants (*abp1-C1* and *abp1-TD1*). In the *abp1* mutant backgrounds, *DR5rev::GFP* expression pattern in the root tip was not visibly altered and showed the typical maximum in the columella cells and quiescent center [57,58,62] (Fig. 2A). After auxin treatment, the *DR5rev::GFP* signals in *abp1* mutants expanded to the lateral root cap and stele to the same extent as in the control (Fig. 2B). Quantification of the DR5 signal without and with auxin treatment in the root tips did not reveal any differences between the control and *abp1* mutants (Fig. 2C). Taken together, these results show that the DR5 auxin response reporter's readout does not depend on a functional *ABP1*.

Recently it was demonstrated, that the TIR1/AFB pathway is required for a rapid non-transcriptional auxin response [16]. We used this experimental system to investigate TIR1/AFB-mediated non--transcriptional auxin effects on root growth in the mutant lines. Evaluation of root growth on the vertical imaging set-up with high spatio-temporal resolution [16,48] revealed a comparable auxin sensitivity of the *abp1-C1* and *abp1-TD1* mutants and the control line in terms of rapid inhibition of root growth (Fig. 2D) suggesting that *abp1* loss-of-function does not affect the TIR1/AFB-mediated non-transcriptional response.

Next, we tested the effect of *ABP1* gain-of-function on TIR1/AFB-mediated transcriptional auxin signaling by performing a transient expression assay in Arabidopsis protoplasts. We derived protoplasts from root cell culture, co-transfected them with *DR5::LUC* reporter together with either *35S::ABP1* or *35S::ABP1-M2X* carrying a mutation in the auxin-binding site [35] and measured the *DR5::LUC* signal with and without auxin. The DR5-driven luciferase activity increased after both short (4 h) and long (16 h) term auxin treatment, however neither *ABP1* nor *ABP1-M2X* overexpression had any significant influence on this induction (Fig. 2E).

These results do not support a strict requirement of *ABP1* function in the canonical, TIR1/AFB-mediated auxin signaling pathway.

3.3. Role of ABP1 in primary root growth and root gravity response

Since *ABP1* is expressed in the primary root and root tip (Fig. 1C, E) and auxin is a major regulator of root growth [16,63–65], we analyzed whether *abp1* loss-of-function or the overexpression influences primary root growth. We used two independent loss-of function mutant lines, *abp1-C1* and *abp1-TD1* and a line expressing *ABP1-GFP* under the control of the ubiquitous 35S promoter (*ABP1-GFP^{OE}*) (Fig. S2). Visually, roots of all tested lines developed normally (Fig. 3A). We measured the root length of 4- and 7-d-old seedlings and found that the root growth of *abp1* mutants was comparable to WT, while roots of *ABP1-GFP^{OE}* were shorter

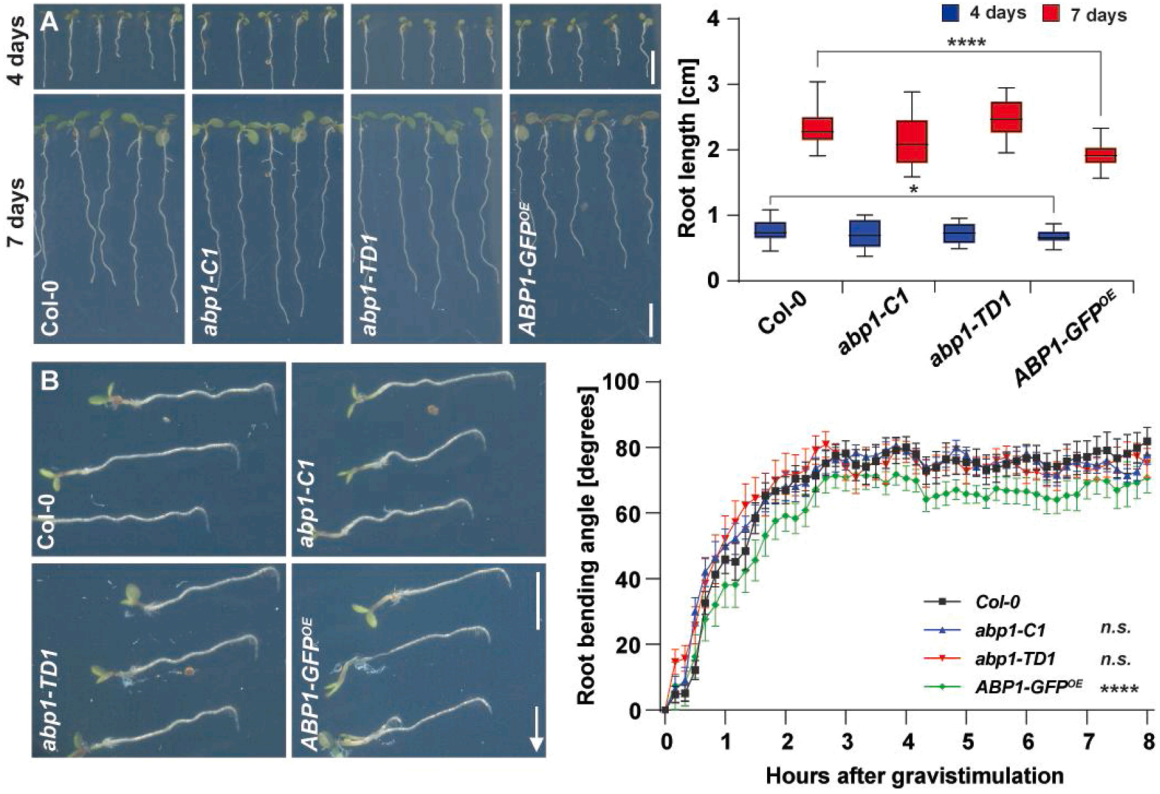

Fig. 3. Role of ABP1 in primary root growth and root gravity response.
(A) Representative images of 4- (upper panel) and 7-d-old (lower panel) Col-0, *abp1-C1*, *abp1-TD1*, and *ABP1-GFP^{OE}* seedlings. Scale bar =5 mm. The boxplot shows the root length of 4- and 7-d-old Col-0, *abp1-C1*, *abp1-TD1*, and *ABP1-GFP^{OE}* seedlings. For each genotype, at least 15 roots were measured. For box plot, box defines the first and third quartiles, and the central lines in the box represent the median. Whiskers, from minimum to maximum. Asterisks indicate significant differences according to Student's t tests (*, $P < 0.05$; ****, $P < 0.0001$). The experiment was repeated 2 times with similar results.
(B) Representative images of 4-d-old Col-0, *abp1-C1*, *abp1-TD1*, and *ABP1-GFP^{OE}* seedlings after 8 h gravistimulation by 90° reorientation. Scale bar =1 cm. Arrow indicates gravity direction. Kinetics of root bending during 8 h of gravity stimulus for Col-0, *abp1-C1*, *abp1-TD1*, and *ABP1-GFP^{OE}*. For each line at least 15 roots were measured. Error bars denote standard deviation. Asterisks indicate significant differences according to Student's t tests (****, $P < 0.0001$). The experiment was repeated 2 times with similar results.

(Fig. 3A).

Asymmetric auxin distribution is involved in gravitropism, an important plant adaptive process manifested by shoot and root bending [66–69]. In order to describe a role of *ABP1* during root bending, we gravistimulated (90° reorientation) roots of 4-d-old *abp1* and *ABP1-GFP*^{OE} seedlings for 8 h and measured the root bending kinetics. We observed that *abp1* mutants showed a normal root gravitropic response while the roots of *ABP1-GFP*^{OE} bent significantly slower (Fig. 3B).

In summary, the *abp1* loss-of-function mutants do not have any impact on either root growth or root bending, whereas gain-of-function leads to slower root growth and root bending.

3.4. Role of ABP1 during lateral root development

As *ABP1* is expressed during lateral root development (Fig. 1F–H), and auxin promotes lateral root initiation and formation [59], we analyzed lateral root development in 6-d-old *abp1* and *ABP1-GFP*^{OE} seedlings. We counted and scored all lateral root primordia stages. The analysis revealed that both *abp1* mutants and *ABP1-GFP*^{OE} developed a comparable number of lateral root primordia (Fig. 4A). In addition, we could not find any differences in the frequency of individual primordial stages (Fig. 4B).

To test the auxin effect on lateral root emergence, we transferred 4-d-old seedlings to media supplemented with auxin and 3 days later we counted the density of emerged lateral roots. We observed that the density of emerged lateral roots was comparable between *abp1* mutants and WT, while *ABP1-GFP*^{OE} developed less lateral roots (Fig. 4C).

Together, the results presented above demonstrate that both *abp1* loss-of-function mutants do not have any impact on lateral root development, but that *ABP1* overexpression leads to impaired auxin-induced lateral root development.

3.5. Role of ABP1 in etiolated growth and shoot gravity response

Auxin is required for a sustained rapid hypocotyl-elongation of

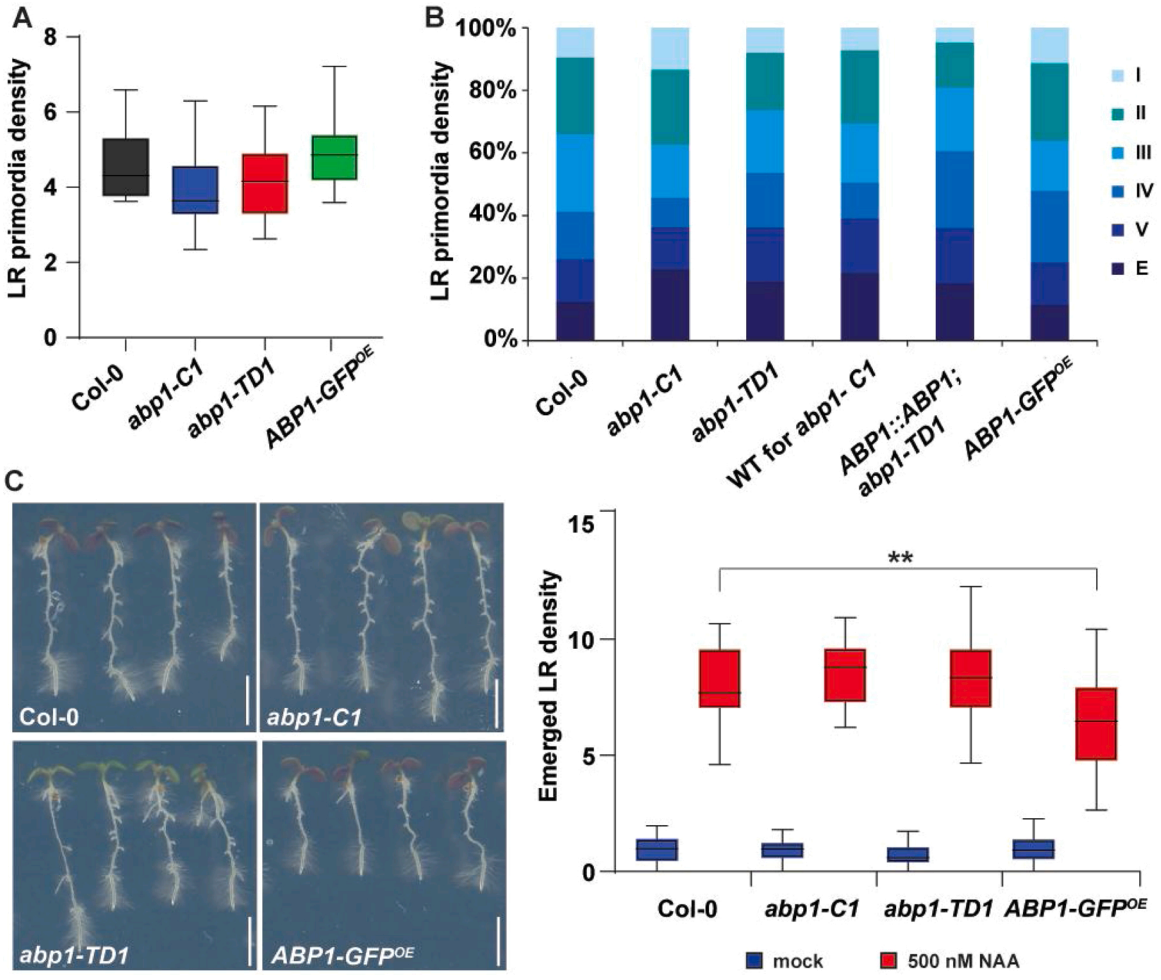

Fig. 4. Role of ABP1 during lateral root development.

(A) Density of lateral root (LR) primordia in 6-d-old Col-0, *abp1-C1*, *abp1-TD1*, and *ABP1-GFP*^{OE} seedlings. For each line, primordia of at least 15 roots were counted. For box plot, box defines the first and third quartiles, and the central lines in the box represent the median. Whiskers, from minimum to maximum. The statistical difference was tested by Student's t-test. The experiment was repeated 2 times with similar results.

(B) Density of individual lateral root primordia stages in 6-d-old Col-0, *abp1-C1*, *abp1-TD1*, WT for *abp1-C1* as control for *abp1-C1*, complemented *abp1-TD1* mutant (*ABP1::ABP1;abp1-TD1*) as control for *abp1-TD1*, and *ABP1-GFP*^{OE} seedlings expressed as percentage. For each line, primordia of at least 15 roots were scored. The experiment was repeated 2 times with the similar results.

(C) Representative pictures of Col-0, *abp1-C1*, *abp1-TD1*, and *ABP1-GFP*^{OE} roots 3 days after 500 nM NAA treatment. Scale bar =5 mm. The box plot shows emerged lateral root density. For each line at least 15 roots were scored. For box plot, box defines the first and third quartiles, and the central lines in the box represent the median. Whiskers, from minimum to maximum. Asterisks indicate significant differences according to Student's t tests (** $P < 0.01$). The experiment was repeated 2 times with similar results.

plants grown in darkness [70–72]. The auxin-induced growth of etiolated hypocotyl segments is not altered in *abp1* loss-of-function mutants [15]. To complement these observations in intact plants, we analyzed growth of etiolated hypocotyls for both *abp1* loss- and gain-of-function lines and measured the hypocotyl length of the dark-grown seedlings every twelve hours (Fig. 5A). Initially, the hypocotyls of all tested lines elongated at the same speed. Later, starting 36 h after germination, etiolated hypocotyls of *ABP1-GFP*^{OE} elongated faster and they were significantly longer than the control 120 h after germination. On the other hand, etiolated hypocotyls of both *abp1* mutant alleles elongated comparably to the controls.

The gravitropic response of the hypocotyl is also regulated by auxin [67–69]. To investigate a possible function of *ABP1* in hypocotyl gravitropism, we gravistimulated 3-d-old etiolated hypocotyls and measured the bending angle after 6, 18 and 24 h. The analysis revealed that the *ABP1-GFP*^{OE} hypocotyls bend significantly less than WT (Fig. 5B). The difference was noticeable already 6 h after gravistimulation. Notably, both *abp1* mutants showed a similar tendency towards slower bending, albeit not significant.

In summary, these observations unveiled that *abp1* loss-of-function alleles do not show defects in etiolated hypocotyl growth and gravitropic responses, whereas gain-of-function of *ABP1* leads to increased elongation and defective gravity-mediated hypocotyl bending.

3.6. Role of ABP1 in leaf development and vasculature formation

In cotyledons, auxin and its directional transport act as a positional cue for vasculature vein formation [73,74] and also regulate leave shape and serration [75]. We analyzed whether ABP1 plays a role in the young rosette growth and development as well as in cotyledon vasculature formation. Macroscopically, neither *abp1* mutants nor *ABP1-GFP*^{OE} showed any defects in cotyledon development (Fig. 6A). We measured the size of young rosettes consisting of both cotyledons and primary leaves. We found that *ABP1-GFP*^{OE} had slightly bigger rosettes (Fig. 6A).

The vasculature of cotyledons typically consists of four formed closed loops (Fig. 6B). We scored the number and the completeness of these loops in *abp1* mutants and *ABP1-GFP*^{OE}. We observed a normal vasculature pattern in both *abp1* mutants, but *ABP1-GFP*^{OE} showed irregularities at higher frequency than WT (Fig. 6B). The most striking difference in *ABP1-GFP*^{OE} were fewer loops (22 % in WT and 46 % in *ABP1-GFP*^{OE}) and loops that were opened at their upper end, which is almost never seen in WT (2 % in WT and 6.5 % in *ABP1-GFP*^{OE}).

The results show that, whilts *abp1* loss-of-function has no impact on leaves growth and venation, *ABP1* gain-of-function affects vasculature formation.

3.7. Role of ABP1 during stress

Abiotic stresses, such as salinity and osmotic stress, induce changes in turgor pressure and in polar auxin transport [76–78] and thus lead to root growth inhibition. On the other hand, an increase of auxin biosynthesis results in higher salt tolerance [79,80]. The regulation of *ABP1* transcription by various stresses such as heat (Fig. S1) prompted us to test the requirement of *ABP1* to adapt to stress.

We challenged *abp1* mutants with osmotic stress using mannitol or sodium chloride treatments to assess the involvement of *ABP1* in stress

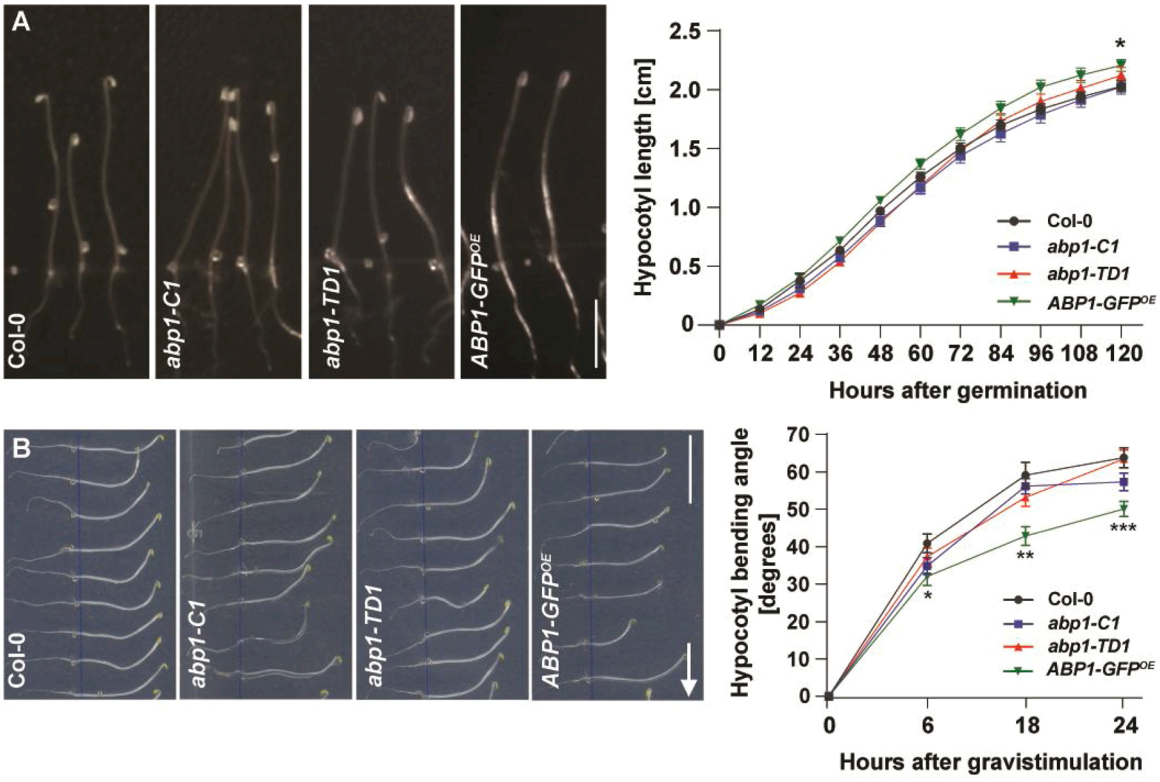

Fig. 5. Role of ABP1 in etiolated growth and shoot gravity response.
(A) Representative images of 3-d-old etiolated hypocotyls of Col-0, *abp1-C1*, *abp1-TD1*, and *ABP1-GFP*^{OE}. Scale bar =1 cm. Elongation rate of Col-0, *abp1-C1*, *abp1-TD1*, and *ABP1-GFP*^{OE} etiolated hypocotyls. For each line at least 10 hypocotyls were measured. Error bars denote standard error. The experiment was repeated for 2 times with similar results. Asterisks indicate significant differences according to Student's t tests (*, $P < 0.05$).
(B) Representative images of 24 h gravity stimulated etiolated hypocotyls of Col-0, *abp1-C1*, *abp1-TD1*, and *ABP1-GFP*^{OE}. Scale bar =1 cm. Arrow indicates gravity direction. Kinetics of hypocotyl bending of Col-0, *abp1-C1*, *abp1-TD1* and *ABP1-GFP*^{OE} during 24 h of gravity stimulation. For each line at least 10 hypocotyls were measured. Error bars denote standard error. Asterisks indicate significant differences according to Student's t tests (*, $P < 0.05$; ** $P < 0.01$; *** $P < 0.001$). The experiment was repeated 3 times with similar results.

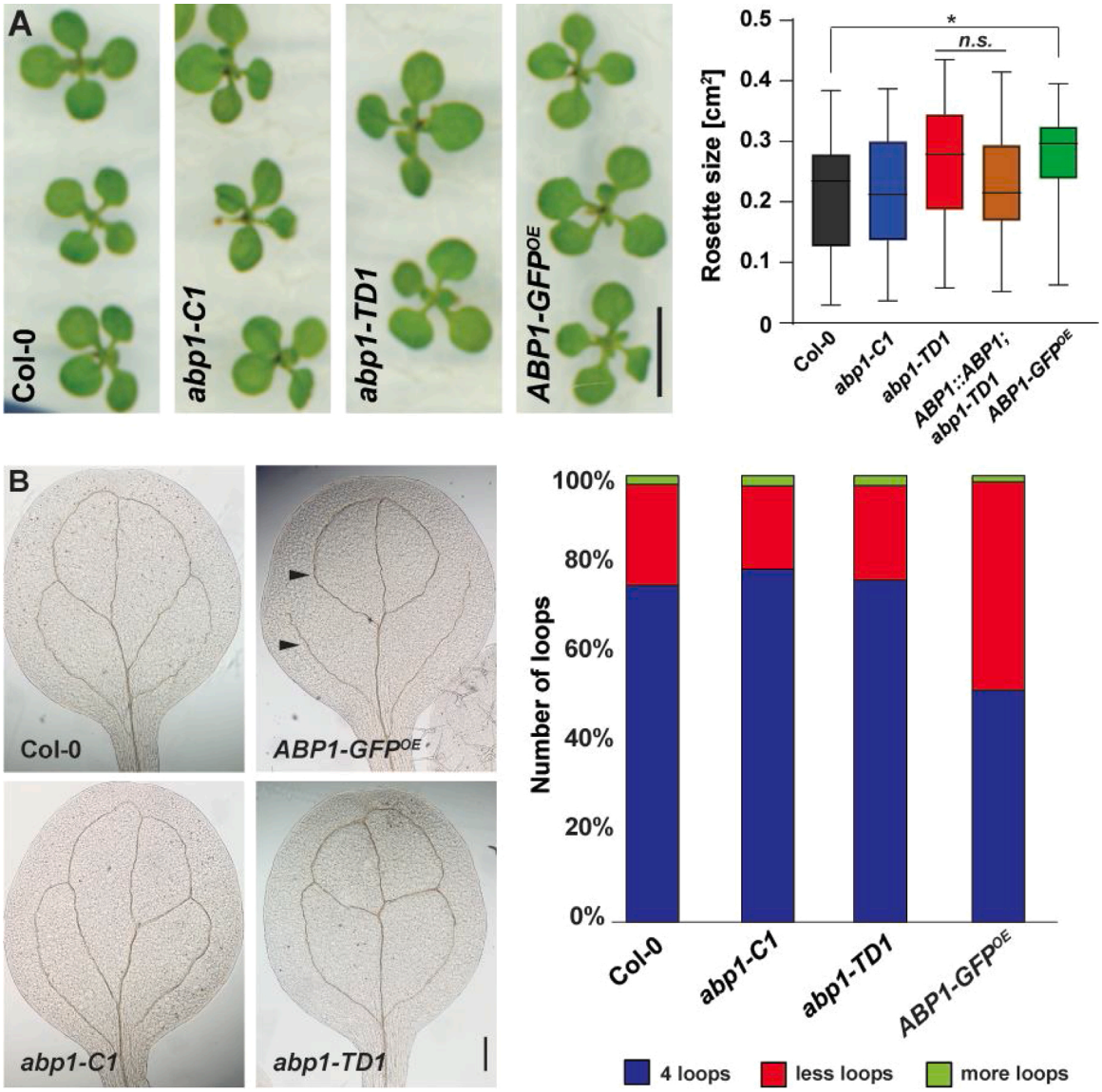

Fig. 6. Role of ABP1 in leaf development and vasculature formation.

(A) Representative images of the rosettes of 12-d-old of Col-0, *abp1-C1*, *abp1-TD1* and *ABP1-GFP^{OE}* seedlings. Scale bar =5 mm. The boxplot shows the size of the rosettes for Col-0, *abp1-C1*, *abp1-TD1*, complemented *abp1-TD1* mutant (*ABP1::ABP1;abp1-TD1*) as control for *abp1-TD1*, and *ABP1-GFP^{OE}*. For each genotype and experiment, more than 19 rosettes from 12-d-old seedlings were measured. For box plot, box defines the first and third quartiles, and the central lines in the box represent the median. Whiskers, from minimum to maximum. Asterisks indicate significant differences according to Student's *t*-tests (*, $P < 0.05$). The experiment was repeated 2 times with the similar result.

(B) Representative pictures of cotyledons venation pattern of 10-d-old Col-0, *abp1-C1*, *abp1-TD1* and *ABP1-GFP^{OE}* seedlings. Scale bar =200 μm. Arrowheads point to typical vasculature defects in *ABP1-GFP^{OE}*. Quantification of number of loops in 10-d-old cotyledons of Col-0, *abp1-C1*, *abp1-TD1* and *ABP1-GFP^{OE}* is presented as percentage. For each line at least 20 cotyledon leaves were scored. The experiment was repeated 2 times with similar results.

responses. Overall, following the treatments, root growth and lateral root formation of WT and *abp1* mutants were inhibited (Fig. 7A–C). In addition, no obvious differences in root growth inhibition were observed after mannitol or sodium chloride treatment between the tested lines (Fig. 7B–C).

High temperature promotes auxin biosynthesis, thereby leading to rapid hypocotyl growth [70]. To address a potential role of *ABP1* in auxin-mediated rapid hypocotyl growth in response to high temperature and the presence of sugar, we characterized hypocotyl elongation of *abp1* and *ABP1-GFP^{OE}* seedlings grown under high temperature (28 °C), on media supplemented with or without sucrose. When grown in high temperature (28 °C) on the medium with sucrose, *ABP1-GFP^{OE}* exhibited longer hypocotyls compared to WT, whereas the hypocotyl length of *abp1* mutants was comparable to that of WT plants (Fig. 7D). At high temperature (28 °C), but in absence, of sucrose the hypocotyl elongation of *ABP1-GFP^{OE}* line was less inhibited than in WT (Fig. 7E).

To test whether *ABP1* plays a role in wound healing responses, we performed a targeted cell ablation in the root tips of *abp1-TD1* and *ABP1-GFP^{OE}* lines [53,81]. After cell ablation, the numbers of initiating periclinal cell divisions in *abp1-TD1* and *ABP1-GFP^{OE}* were similar to that in WT (Fig. S3).

Taken together, the results show that the root growth of *abp1* loss-of-function mutants is not influenced differently by salt stress and high temperature. *ABP1* gain-of-function seedlings show increased hypocotyl growth when grown at high temperature.

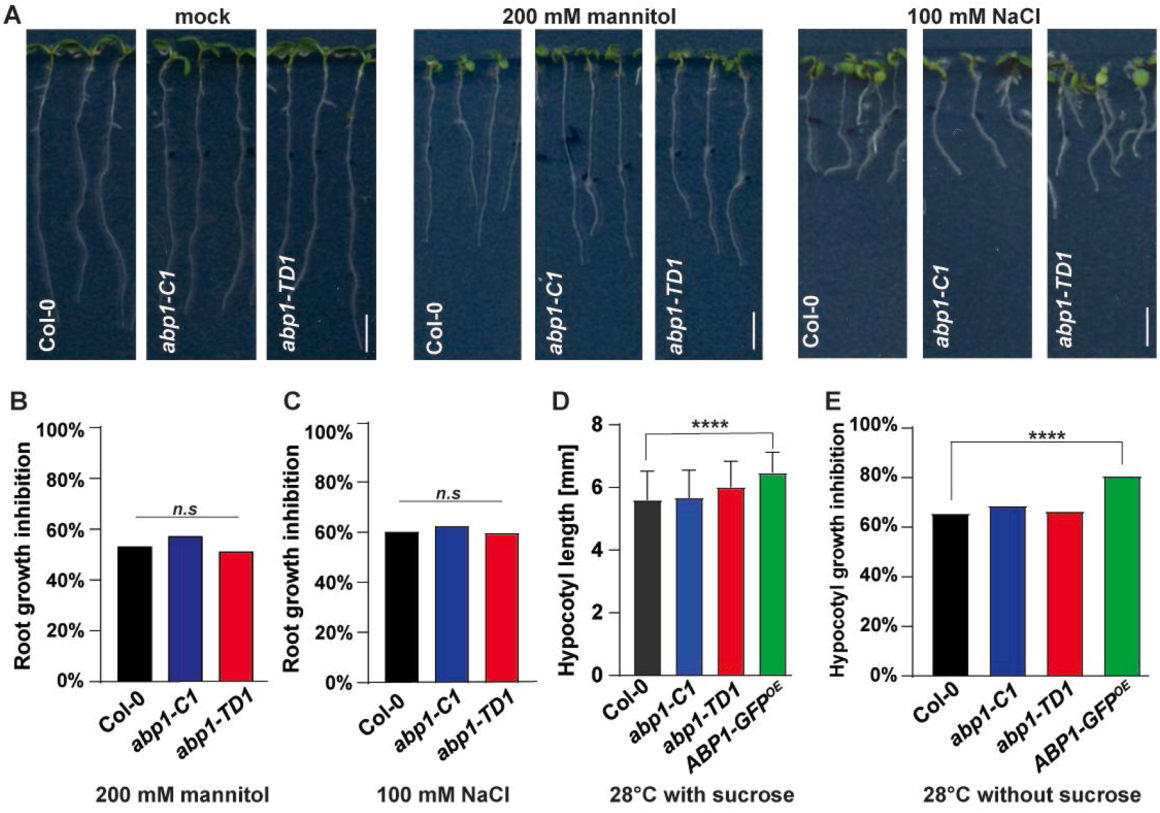

Fig. 7. Role of ABP1 during stress.

(A) Representative images of 8-d-old Col-0, *abp1-C1, abp1-TD1* and *ABP1-GFP*^{OE} seedlings grown for 4 days on control media or on media supplemented with either 200 mM mannitol or 100 mM NaCl. Scale bar =5 mm.

(B–C) Quantification of the root growth inhibition of Col-0, *abp1-C1* and *abp1-TD1* seedlings after treatment with 200 mM mannitol (B) or 100 mM NaCl (C). For each genotype, at least 10 roots were measured per experiment. The experiment was repeated 3 times with the similar results and the pooled values are presented. The statistical significance was tested by Wilcoxon test.

(D) Quantification of the hypocotyl length of 7-d-old Col-0, *abp1-C1, abp1-TD1* and *ABP1-GFP*^{OE} seedlings grown under continuous light, higher temperature (28 °C). For each genotype and experiment, at least 25 hypocotyls were analyzed. Error bars denote standard error. Asterisks indicate significant differences according to Student's t tests (****, $P < 0.0001$). The experiment was repeated 3 times with the similar results.

(E) Quantification of the hypocotyl growth inhibition sucrose of Col-0, *abp1-C1, abp1-TD1* and *ABP1-GFP*^{OE} seedlings grown under continuous light, higher temperature (28 °C) and in absence of sucrose. For each genotype, at least 10 roots were measured per experiment. Asterisks indicate significant differences according to Student's t tests (****, $P < 0.0001$). The experiment was repeated 3 times with the similar results and the pooled values are presented.

3.8. Role of ABP1 in rosette leaves and inflorescence development

The establishment of auxin maxima in the shoot apical meristem (SAM) and directed basipetal polar auxin transport are crucial for overall shoot development [59,82–86]. *ABP1* is expressed in both SAM and rosette leaves (Fig. S1B), therefore we investigated its possible function in shoot development.

First, we characterized leaf development. Visually, the size and shape of rosette leaves in *abp1* mutants and *ABP1-GFP*^{OE} plants were comparable to that of WT plants. We quantified the rosette leaves number at the stage when the first flower of each individual plant bloomed. We observed that the *apb1-TD1* mutant developed slightly more, whereas the *ABP1-GFP*^{OE} line developed significantly less rosette leaves in comparison to WT (Fig. 8A). However, the results for the *abp1-TD1* mutant line were variable between the experimental repetitions. We found no difference in the number of cauline leaves for any of the analyzed lines (Fig. S4A).

Further, we studied the function of *ABP1* during bolting. We measured the length of the first internode of *abp1* mutants and *ABP1-GFP*^{OE} and we recorded the timing to reach 1 cm. Compared to WT, both *abp1* mutants and *ABP1-GFP*^{OE} line bolt earlier, at 21st and 22nd day after sowing versus 23rd day in WT (Fig. 8B).

To determine whether *ABP1* is involved in phyllotaxis establishment, we measured the sequence of divergence angles between siliques in *abp1* mutants. Visually, *abp1* mutants developed normal inflorescence stems (Fig. 8C). WT plants typically exhibit a spiral phyllotaxis that leads to a distribution of the consecutive organs on the stem with a divergence angle close to 137.5° [87]. Our analysis revealed that the distribution of divergence angles in *abp1* mutants was not altered (Fig. 8D–F). We also analyzed the internode length between the siliques and counted the number of rosette and cauline branches of *abp1* mutant and *ABP1-GFP*^{OE} plants. However, we did not detect any differences (Fig. S4B-D).

The results show that overexpression of *ABP1* affects the number of rosette leaves and that both *ABP1* loss- and gain-of-function accelerate bolting.

3.9. Role of ABP1 in auxin-mediated PIN polarization and BFA-visualized PIN trafficking

The formation of organized vasculature requires coordinated cell polarization. The canalization hypothesis proposes that auxin acts as a polarizing cue in this process [88] and that auxin feed-back on PIN polarity, together with constitutive PIN endocytic trafficking are important features in this process [54,89,90]. Since overexpression of *ABP1* results in defects in vascular tissue formation (Fig. 6B), we tested whether *abp1* loss- or gain-of-function alleles show defects in these

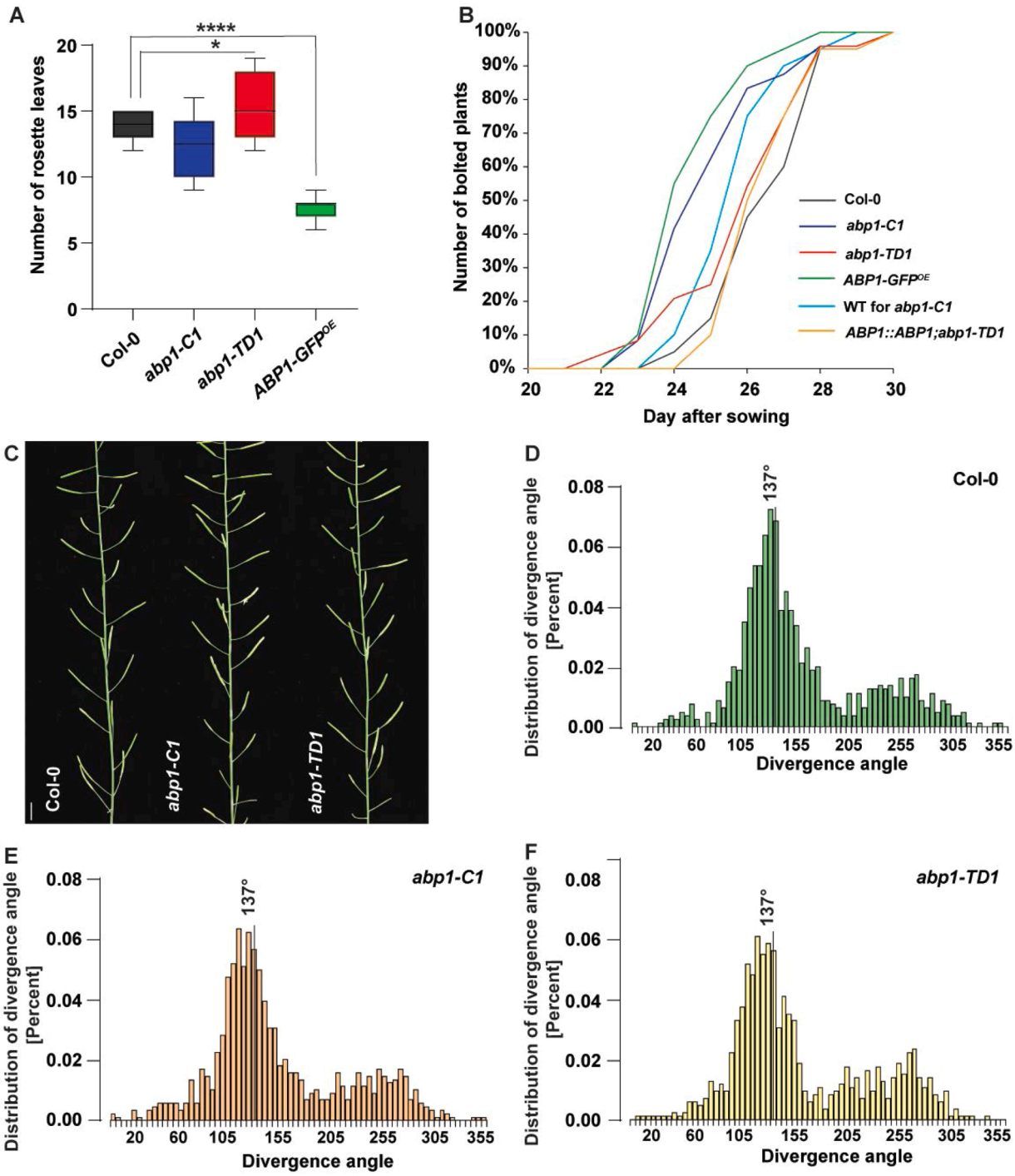

Fig. 8. Role of ABP1 in rosette leaves and inflorescence development.

(A) Boxplot showing the number of rosette leaves of Col-0, *abp1-C1*, *abp1-TD1* and *ABP1-GFP*^{OE} plants. For each genotype per experiment, at least 10 rosettes were scored when the first flower bloomed on each single plant. For box plot, box defines the first and third quartiles, and the central lines in the box represent the median. Whiskers, from minimum to maximum. Asterisks indicate significant differences according to Student's t tests (*, $P < 0.05$; ****, $P < 0.0001$). The experiment was repeated 3 times with the similar result.

(B) Quantification of bolting time of Col-0, *abp1-C1*, *abp1-TD1*, *ABP1-GFP*^{OE}, WT for *abp1-C1*, and *ABP1::ABP1;abp1-TD1*. The graph shows number of plants with inflorescence stem $\geq$ 1 cm for the given day in percentage. For each genotype per experiment, at least 20 plants were scored. The experiment was at this given setup repeated 2 times with the similar result, and additionally 2 times for Col-0, *abp1-C1*, *abp1-TD1*, *ABP1-GFP*^{OE} with the similar result.

(C) Representative pictures of the inflorescence stem of Col-0, *abp1-C1*, and *abp1-TD1*. Scale bar =1 cm.

(D–F) Distribution of divergence angles between the siliques in Col-0, *abp1-C1*, and *abp1-TD1*. For each genotype divergence angles of 25 individual plants were measured.

processes. To evaluate the effect of auxin on PIN polarity, we analyzed the repolarization of PIN1 from the basal to the inner lateral side in root endodermis cells and the repolarization of PIN2 from the basal to the outer lateral side in root cortex cells [54] following auxin treatment in *abp1* mutants and *ABP1-GFP*^{OE}. Anti-PIN1 and anti-PIN2 immunolocalization revealed that PIN1 and PIN2 repolarization was not altered in *abp1* mutants, while overexpression of ABP1 led to reduced or no repolarization of PIN1 and PIN2 respectively (Fig. 9A–B).

Further, we used the trafficking inhibitor Brefeldin A (BFA) to indirectly visualize PIN intracellular trafficking [91]. BFA treatment results in PIN internal aggregation manifested as BFA-body formation and this effect is decreased when BFA is used together with auxin [9]. The anti-PIN1 immunostaining in roots after BFA treatment showed that the intracellular aggregation of PIN1 was similar to that of WT in both *abp1* mutants (Fig. 9C) and [92]. In *ABP1-GFP*^{OE} we observed repeatedly that BFA affected PIN1 intracellular aggregation more severely (BFA bodies were more pronounced) (Fig. 9C). Anti-PIN1 immunostaining after auxin and BFA co-treatment confirmed that auxin inhibited BFA-body formation. Comparison of the *abp1* mutants with the corresponding complemented lines did not reveal any consistent changes in the auxin effect on BFA-induced PIN1 aggregation, whereas *ABP1-GFP*^{OE} showed again slightly more BFA-induced PIN1 aggregation even in presence of auxin (Fig. 9C). The analysis of the BFA effect on PIN2 intracellular aggregation revealed no consistent and reproducible differences in BFA-body formation between WT, *abp1* mutants and *ABP1-GFP*^{OE} (Fig. 9D). Accordingly, auxin and BFA co-treatment led to a comparable and variable decrease of PIN2 intracellular aggregation in WT, *abp1* mutants and *ABP1-GFP*^{OE} (Fig. 9D).

Taken together, the *ABP1* overexpression interferes with auxin-induced PIN repolarization and slightly affects BFA-induced, constitutive PIN1 but not PIN2 trafficking, while mutation in *ABP1* does not show altered auxin feed-back on PIN polarity or constitutive PIN recycling.

4. Discussion

ABP1 has been identified in maize decades ago based on its potential ability to bind auxin [93,94]. Nonetheless, the developmental roles and cellular functions of ABP1 remain unclear due to problems with some of the genetic material [35,39,40,42] and due to the lack of obvious developmental defects after superficial analyzes of the verified knock-out lines [38].

Here, we assessed the function of ABP1 in various developmental processes and (re)evaluated its role in cellular processes related to trafficking and polar distribution of PIN auxin transporters.

4.1. ABP1 is not essential for or regulated by TIR1/AFB-mediated auxin responses

ABP1 promoter activity has been reported to overlap, to some extent, with that of the transcriptional DR5 auxin reporter during early seedling development [43]. Our analysis revealed a similar overlap in hydathodes, root tips and lateral root primordia as well as in older seedlings. The activity of the *ABP1* promoter at places with high auxin response suggested either that auxin might regulate the transcription of *ABP1* or that ABP1 is somehow linked to TIR1/AFB-mediated transcriptional auxin signaling.

Indeed, *ABP1* was previously identified among early auxin-regulated genes. *ABP1* transcription was upregulated by auxin in a dose dependent manner within 30 min in 19-d-old WT seedlings [95]. Our observations in 5-d-old WT roots and shoots did not reveal any changes in *ABP1* expression following auxin treatment. These contradictory findings suggest that a potential auxin effect on *ABP1* transcription could be tissue- and/or developmental stage-dependent.

Also, the connection between *ABP1* and TIR1/AFB-mediated auxin signaling was previously investigated. Downregulation of the *ABP1* activity was shown to affect transcription of auxin-responsive genes [33,95,96], to regulate Aux/IAA homeostasis and thus negatively impact on the SCF$^{TIR1/AFB}$ pathway [97]. However, these observations are inconclusive due to the potential off-targets in the conditional knock-down lines [42] and the inactivation of *ABP1* did not have any significant effects on the DR5 auxin response reporter activity [33]. In the verified *abp1* knock-out lines it was reported that auxin-regulated gene expression is unchanged [38] and our analysis in these lines and following *ABP1* overexpression in protoplasts did also not reveal any changes in DR5 reporter activity. Furthermore, *abp1* knock-out lines also showed normal TIR1/AFB-mediated non-transcriptional auxin effect on root growth. Overall, these observations suggest that *ABP1* is not directly involved in the TIR1/AFB-mediated auxin response.

4.2. ABP1 loss-of-function mutants show minor defects in development

The initial analysis of CRISPR and T-DNA insertion *abp1* knock-out mutants did not reveal any obvious defects during development under normal conditions leading to a conclusion that *ABP1* is not required for Arabidopsis development [38]. We analyzed different auxin-related phenotypes of the corresponding *abp1* knock-out mutants in more detail. We observed that both *abp1* alleles exhibited normal root growth, etiolated hypocotyl, root and shoot gravitropic responses, lateral root and leaf development, including venation and phyllotaxis. Notably, both *abp1* mutant alleles bolted earlier compared to the control lines. Accelerated bolting in *abp1* mutants might be caused by changes in auxin levels caused by either impaired biosynthesis, auxin transport or eventually a change in auxin sensitivity. Nonetheless, it is unclear why such changes are not reflected also in other developmental processes regulated by auxin.

4.3. ABP1 gain-of-function lines show a plethora of auxin-related phenotypes

ABP1 overexpression has been shown previously to cause several postembryonic developmental defects [5,10,35,98,99]. Similarly, our analysis of a stable line expressing *35S::ABP1-GFP* revealed that *ABP1* gain-of-function leads to developmental changes. Seedlings overexpressing *ABP1* have reduced root length, impaired auxin-induced lateral root development, enhanced elongation of both high temperature- and dark-grown hypocotyls, reduced root and shoot gravitropic response, defective vasculature development, increased size of young rosettes but decreased number of rosettes leaves. Additionally, similar to the *abp1* mutants, *ABP1* overexpressors also bolted earlier. At the cellular level, we confirmed the previous observations [10,35] that the *ABP1* gain-of-function affects the BFA-sensitive PIN endocytic trafficking and newly showed that they also impair auxin effects on PIN polar distribution in root cells.

All aforementioned processes, which were found defective in *ABP1* gain-of-function mutants are linked to auxin regulation. It is therefore conceivable that, in line with the importance of the auxin binding pocket for the *ABP1* function [35], *ABP1* plays so far a mechanistically unclear role in auxin perception and signaling.

4.4. Potential role and functional mechanism of Arabidopsis ABP1

Arabidopsis *ABP1* was identified based on the orthology with *ABP1* previously found in maize [98,100]. Auxin-binding properties of maize ABP1 are well characterized. Several biochemical studies along with the structural analysis of the ABP1-auxin co-crystal revealed that maize ABP1 binds auxin with the highest affinity at apoplastic pH 5.5, while binding at pH 7.2 corresponding to the ER lumen where the majority of protein is localized, is much lower [26–29,94,101]. In contrast, the auxin-binding properties of Arabidopsis ABP1 have not been characterized yet. Based on the high homology with the maize protein, it is assumed that Arabidopsis ABP1 binds auxin in a similar manner. This

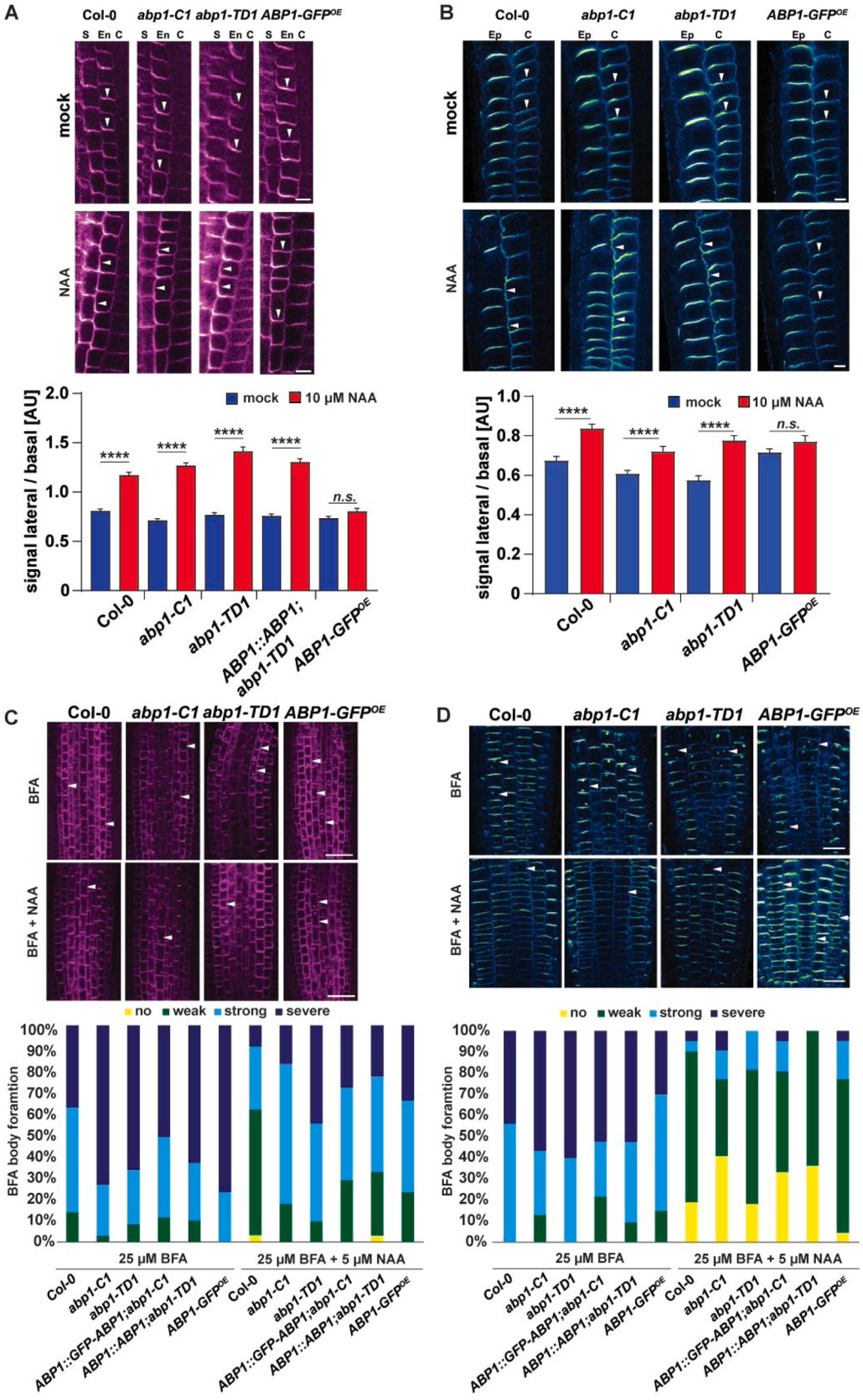

Fig. 9. Role of ABP1 in auxin-mediated PIN polarization and BFA-visualized PIN trafficking.

(A) Representative pictures of PIN1 immunolocalization in root meristem of 4-d-old Col-0, *abp1-C1*, *abp1-TD1* and *ABP1-GFP*^{OE} after mock (upper panel) and 4 h 10μM NAA treatment (lower panel). Scale bar =5 μm. The letters indicate an appropriate cell file - S (stele), En (endodermis), C (cortex). Arrow heads point to basal/lateral PIN1 localization in endodermis. The quantitative evaluation shows mean ratio of PIN1 lateral-to-basal signal intensity ratio in endodermis cells of Col-0, *abp1-C1*, *abp1-TD1*, *ABP1::ABP1;abp1-TD1* and *ABP1-GFP*^{OE}. Error bars denote standard error. Asterisks indicate significant differences according to Student's t tests (****, $P < 0.0001$). The experiment was repeated 3 times, one representative experiment is presented.

(B) Representative pictures of PIN2 immunolocalization in root meristem of 4-d-old Col-0, *abp1-C1*, *abp1-TD1* and *ABP1-GFP*^{OE} after mock (upper panel) and 4 h 10μM NAA treatment (lower panel). Scale bar =5 μm. The letters indicate an appropriate cell file – Ep (epidermis), C (cortex). Arrow heads point to basal/lateral PIN2 localization in cortex. The quantitative evaluation shows mean ratio of PIN2 lateral-to-basal signal intensity ratio in cortex cells of Col-0, *abp1-C1*, *abp1-TD1* and *ABP1-GFP*^{OE}. Error bars denote standard error. Asterisks indicate significant differences according to Student's t tests (****, $P < 0.0001$). The experiment was repeated 3 times, one representative experiment is presented.

(C) Representative pictures of PIN1 immunolocalization in primary root stele of 4-d-old Col-0, *abp1-C1*, *abp1-TD1* and *ABP1-GFP*^{OE} after 1 h 25 μM BFA treatment (upper panel) and after 30 min 5 μM NAA pre-treatment followed by 1 h 25 μM BFA and 5 μM NAA co-treatment (lower panel). Arrow heads point to affected cells. Scale bar =20 μm. The quantitative evaluation shows the scoring of an overall count of formed BFA bodies in Col-0, *abp1-C1*, *abp1-TD1*, *ABP1::GFP-ABP1;abp1-C1*, *ABP1::ABP1;abp1-TD1* and *ABP1-GFP*^{OE}. At least 8 roots were scored for each genotype and experiment. The pooled result of 3 independent experiments is presented.

(D) Representative pictures of PIN2 immunolocalization in primary root epidermis of 4-d-old Col-0, *abp1-C1*, *abp1-TD1* and *ABP1-GFP*^{OE} after 1 h 25 μM BFA treatment (upper panel) and after 30 min 5 μM NAA pre-treatment followed by 1 h 25 μM BFA and 5 μM NAA co-treatment (lower panel). Arrow heads point to affected cells. Scale bar =20 μm. The quantitative evaluation shows the scoring of an overall count of formed BFA bodies in Col-0, *abp1-C1*,

abp1-TD1, *ABP1::GFP-ABP1;abp1-C1*, *ABP1::ABP1;abp1-TD1* and *ABP1-GFP*^{OE}. At least 8 roots were scored for each genotype and experiment. The pooled result of 3 independent experiments is presented.

statement is supported by the finding that the auxin-binding pocket of Arabidopsis ABP1 is important for its gain-of-function cellular and developmental roles [35].

The ABP1 binding optimum at pH 5.5 would imply that ABP1 is functional in the apoplast, further supported by auxin-dependent interaction between ABP1 and the plasma membrane-localized receptor-like kinase TMK1 [30,31]. TMK1 belongs to a four-member TMK receptor-like kinase family, that function redundantly and multiple mutants show severe reduction in organ size and substantial growth retardation [20]. Both TMK1 and TMK4 play roles in auxin-mediated developmental processes and in the control of local auxin biosynthesis [22,23,30]. Importantly, TMK1 mediates auxin signaling that regulates differential growth of the apical hook [21]. However, the mechanism of how TMK1 perceives auxin remains elusive.

The function of ABP1 as a part of the auxin perception machinery contributing towards TMK-based downstream signaling, is a tempting hypothesis consistent with a rather broad spectrum of auxin-related growth defects. But it is not supported by the rather mild phenotypic defects in the *abp1* loss-of-function mutants, especially considering that *ABP1* is a single copy gene in Arabidopsis [100]. On the other hand, *ABP1* is evolutionary conserved and ubiquitous in vascular plants [102], suggesting that it has an important and conserved function. Structurally ABP1 belongs to an ancient group of germin and germin-like proteins that have a highly conserved tertiary structure despite low similarity in primary sequence among the members [28,103]. Therefore, it is possible that some other proteins from the germin family are functionally redundant with ABP1, thus masking the effect of the *abp1* mutation. Nonetheless, to identify and characterize functional homologues within this large family will be a challenging task. An alternative explanation for the weak developmental defects in *abp1* loss-of-function mutants is that *ABP1* plays an important role in specific processes that provide competitive advantage in nature but are not easily manifested under laboratory conditions.

5. Conclusions

In conclusion, our detailed phenotypic analysis of both *ABP1* gain- and loss-of-function lines provides new insights into the developmental role of *ABP1*. Despite the overlap of *ABP1* expression pattern with auxin response maxima during seedling development, none of our observations supports a direct involvement of *ABP1* in the TIR1/AFB-mediated transcriptional auxin response. *abp1* knock-out mutants show only mild phenotypic defects, whereas *ABP1* overexpression generates a broad range of potentially auxin-related phenotypes. The previously described strong and related defects in conditional *abp1* knock-down lines let us hypothesize that the discrepancy between the effects of loss- and gain-of-function is due to the action of unknown germin family proteins that are functionally redundant with ABP1.

Author contribution

Z.G., Mi.Ga., M.P., X.Z., Ma.Gl., L.L., J.M., I.V., H.H., J.H., M.Č., M. Z., L.H., M.F., T.V. and J.F. designed and conducted experiments and analyzed data. G.B. and Z.P. helped with performing experiments. R.H. and I.V. developed RG-tracker. Z.G., L.H. and T.X. contributed with the generation of the genetic material. Z.G., X.Z., Mi.Ga. and J.F. wrote the manuscript.

Declaration of Competing Interest

The authors report no declarations of interest.

Acknowledgments

We would like to acknowledge Bioimaging and Life Science Facilities at IST Austria for continuous support and also the Plant Sciences Core Facility of CEITEC Masaryk University for their support with obtaining a part of the scientific data. We gratefully acknowledge Lindy Abas for help with *ABP1::GFP-ABP1* construct design. This project has received funding from the European Research Council (ERC) under the European Union's Horizon 2020 research and innovation program [grant agreement no. 742985] and Austrian Science Fund (FWF) [I 3630-B25] to J. F.; DOC Fellowship of the Austrian Academy of Sciences to L.L.; the European Structural and Investment Funds, Operational Programme Research, Development and Education - Project „MSCAfellow@MUNI" [CZ.02.2.69/0.0/0.0/17_050/0008496] to M.P.. This project was also supported by the Czech Science Foundation [GA 20-20860Y] to M.Z and MEYS CR [project no.CZ.02.1.01/0.0/0.0/16_019/0000738] to M. Č.

Appendix A. Supplementary data

Supplementary material related to this article can be found, in the online version, at doi:https://doi.org/10.1016/j.plantsci.2020.110750.

References

[1] J. Brumos, L.M. Robles, J. Yun, T.C. Vu, S. Jackson, J.M. Alonso, A.N. Stepanova, Local auxin biosynthesis is a key regulator of plant development, Dev. Cell 47 (2018) 306–318, https://doi.org/10.1016/j.devcel.2018.09.022, e5.
[2] M. Adamowski, J. Friml, PIN-dependent auxin transport: action, regulation, and evolution, Plant Cell 27 (2015) 20–32, https://doi.org/10.1105/tpc.114.134874.
[3] B.O. Bargmann, S. Vanneste, G. Krouk, T. Nawy, I. Efroni, E. Shani, G. Choe, J. Friml, D.C. Bergmann, M. Estelle, K.D. Birnbaum, I.D.B. Inte, A Map of Cell Type-specific Auxin Responses, 2013, pp. 1–13, https://doi.org/10.1038/msb.2013.40.
[4] D. Weijers, D. Wagner, Transcriptional responses to the auxin hormone, Annu. Rev. Plant Biol. 67 (2016) 539–574, https://doi.org/10.1146/annurev-arplant-043015-112122.
[5] B. Steffens, C. Feckler, K. Palme, M. Christian, M. Böttger, H. Lüthen, The auxin signal for protoplast swelling is perceived by extracellular ABP1, Plant J. 27 (2001) 591–599, https://doi.org/10.1046/j.1365-313X.2001.01103.x.
[6] R.I. Dahlke, S. Fraas, K.K. Ullrich, K. Heinemann, M. Romeiks, T. Rickmeyer, G. Klebe, K. Palme, H. Lüthen, B. Steffens, Protoplast swelling and hypocotyl growth depend on different auxin signaling pathways, Plant Physiol. 175 (2017) 982–994, https://doi.org/10.1104/pp.17.00733.
[7] G.B. Monshausen, N.D. Miller, A.S. Murphy, S. Gilroy, Dynamics of auxin-dependent Ca 2+ and pH signaling in root growth revealed by integrating high-resolution imaging with automated computer vision-based analysis, Plant J. 65 (2011) 309–318, https://doi.org/10.1111/j.1365-313X.2010.04423.x.
[8] H.W. Shih, C.L. Depew, N.D. Miller, G.B. Monshausen, The cyclic nucleotide-gated channel CNGC14 regulates root gravitropism in arabidopsis thaliana, Curr. Biol. 25 (2015) 3119–3125, https://doi.org/10.1016/j.cub.2015.10.025.
[9] T. Paciorek, E. Zazímalová, N. Ruthardt, J. Petrásek, Y.-D. Stierhof, J. Kleine-Vehn, D.A. Morris, N. Emans, G. Jürgens, N. Geldner, J. Friml, Auxin inhibits endocytosis and promotes its own efflux from cells, Nature 435 (2005) 1251–1256, https://doi.org/10.1038/nature03633.
[10] S. Robert, J. Kleine-Vehn, E. Barbez, M. Sauer, T. Paciorek, P. Baster, S. Vanneste, J. Zhang, S. Simon, M. Čovanová, K. Hayashi, P. Dhonukshe, Z. Yang, S. Y. Bednarek, A.M. Jones, C. Luschnig, F. Aniento, E. Zažímalová, J. Friml, ABP1 mediates auxin inhibition of clathrin-dependent endocytosis in arabidopsis, Cell 143 (2010) 111–121, https://doi.org/10.1016/j.cell.2010.09.027.
[11] M. Kubeš, R. Napier, Non-canonical auxin signalling: fast and curious, J. Exp. Bot. 70 (2019) 2609–2614, https://doi.org/10.1093/jxb/erz111.
[12] M. Gallei, C. Luschnig, J. Friml, Auxin signalling in growth: schrödinger's cat out of the bag, Curr. Opin. Plant Biol. 53 (2020) 43–49, https://doi.org/10.1016/j.pbi.2019.10.003.

[13] O. Leyser, Auxin signaling, Plant Physiol. 176 (2018) 465–479, https://doi.org/10.1104/pp.17.00765.

[14] A.K. Spartz, S.H. Lee, J.P. Wenger, N. Gonzalez, H. Itoh, D. Inzé, W.A. Peer, A. S. Murphy, P.J. Overvoorde, W.M. Gray, The SAUR19 subfamily of SMALL AUXIN UP RNA genes promote cell expansion, Plant J. 70 (2012) 978–990, https://doi.org/10.1111/j.1365-313X.2012.04946.x.

[15] M. Fendrych, J. Leung, J. Friml, Tir1/AFB-Aux/IAA auxin perception mediates rapid cell wall acidification and growth of Arabidopsis hypocotyls, Elife 5 (2016) 1–18, https://doi.org/10.7554/eLife.19048.

[16] M. Fendrych, M. Akhmanova, J. Merrin, M. Glanc, S. Hagihara, K. Takahashi, N. Uchida, K.U. Torii, J. Friml, Rapid and reversible root growth inhibition by TIR1 auxin signalling, Nat. Plants 4 (2018) 453–459, https://doi.org/10.1038/s41477-018-0190-1.

[17] J. Dindas, S. Scherzer, M.R.G. Roelfsema, K. Von Meyer, H.M. Müller, K.A.S. Al-Rasheid, K. Palme, P. Dietrich, D. Becker, M.J. Bennett, R. Hedrich, AUX1-mediated root hair auxin influx governs SCFTIR1/AFB-type Ca2+ signaling, Nat. Commun. 9 (2018), https://doi.org/10.1038/s41467-018-03582-5.

[18] S. Simonini, J. Deb, L. Moubayidin, P. Stephenson, M. Valluru, A. Freire-Rios, K. Sorefan, D. Weijers, J. Friml, L. Østergaard, A noncanonical auxin-sensing mechanism is required for organ morphogenesis in arabidopsis, Genes Dev. 30 (2016) 2286–2296, https://doi.org/10.1101/gad.285361.116.

[19] A. Kuhn, S.R. Harborough, H.M. McLaughlin, B. Natarajan, I. Verstraeten, J. Friml, S. Kepinski, L. Østergaard, Direct ETTIN-auxin interaction controls chromatin states in gynoecium development, Elife 9 (2020) 1–18, https://doi.org/10.7554/eLife.51787.

[20] N. Dai, W. Wang, S.E. Patterson, A.B. Bleecker, The TMK subfamily of receptor-like kinases in Arabidopsis display an essential role in growth and a reduced sensitivity to auxin, PLoS One 8 (2013) 1–12, https://doi.org/10.1371/journal.pone.0060990.

[21] M. Cao, R. Chen, P. Li, Y. Yu, R. Zheng, D. Ge, W. Zheng, X. Wang, Y. Gu, Z. Gelová, J. Friml, H. Zhang, R. Liu, J. He, T. Xu, TMK1-mediated auxin signalling regulates differential growth of the apical hook, Nature 568 (2019) 240–243, https://doi.org/10.1038/s41586-019-1069-7.

[22] R. Huang, R. Zheng, J. He, Z. Zhou, J. Wang, Y. Xiong, T. Xu, Noncanonical auxin signaling regulates cell division pattern during lateral root development, Proc. Natl. Acad. Sci. U. S. A. 116 (2019) 21285–21290, https://doi.org/10.1073/pnas.1910916116.

[23] Q. Wang, G. Qin, M. Cao, R. Chen, Y. He, L. Yang, Z. Zeng, Y. Yu, Y. Gu, W. Xing, W.A. Tao, T. Xu, A phosphorylation-based switch controls TAA1-mediated auxin biosynthesis in plants, Nat. Commun. 11 (2020), https://doi.org/10.1038/s41467-020-14395-w.

[24] N. Leblanc, C. Roux, J.M. Pradier, C. Perrot-Rechenmann, Characterization of two cDNAs encoding auxin-binding proteins in Nicotiana tabacum, Plant Mol. Biol. 33 (1997) 679–689, https://doi.org/10.1023/a:1005757815212.

[25] S. Watanabe, S. Shimomura, Cloning and expression of two genes encoding auxin-binding proteins from tobacco, Plant Mol. Biol. 36 (1998) 63–74, https://doi.org/10.1023/A:1005999821066.

[26] H. Tian, D. Klambt, A.M. Jones, Auxin-binding protein 1 does not bind auxin within the endoplasmic reticulum despite this being the predominant subcellular location for this hormone receptor, J. Biol. Chem. 270 (1995) 26962–26969, https://doi.org/10.1074/jbc.270.45.26962.

[27] N. Leblanc, K. David, J. Grosclaude, J.M. Pradier, H. Barbier-Brygoo, S. Labiau, C. Perrot-Rechenmann, A novel immunological approach establishes that the auxin-binding protein, Nt-abp1, is an element involved in auxin signaling at the plasma membrane, J. Biol. Chem. 274 (1999) 28314–28320, https://doi.org/10.1074/jbc.274.40.28314.

[28] E.J. Woo, J. Marshall, J. Bauly, J.G. Chen, M. Venis, R.M. Napier, R. W. Pickersgill, Crystal structure of auxin-binding protein 1 in complex with auxin, EMBO J. 21 (2002) 2877–2885, https://doi.org/10.1093/emboj/cdf291.

[29] A.M. Jones, E.M. Herman, KDEL-containing auxin-binding protein is secreted to the plasma membrane and cell wall, Plant Physiol. 101 (1993) 595–606, https://doi.org/10.1104/pp.101.2.595.

[30] T. Xu, M. Wen, S. Nagawa, Y. Fu, J.-G. Chen, M.-J. Wu, C. Perrot-Rechenmann, J. Friml, A.M. Jones, Z. Yang, Cell surface- and rho GTPase-based auxin signaling controls cellular interdigitation in Arabidopsis, Cell 143 (2010) 99–110, https://doi.org/10.1016/j.cell.2010.09.003.

[31] T. Xu, N. Dai, J. Chen, S. Nagawa, M. Cao, H. Li, Z. Zhou, X. Chen, R. De Rycke, H. Rakusová, W. Wang, A.M. Jones, J. Friml, S.E. Patterson, A.B. Bleecker, Z. Yang, Cell surface ABP1-TMK auxin-sensing complex activates ROP GTPase signaling, Science 343 (2014) 1025–1028, https://doi.org/10.1126/science.1245125.

[32] P. Grones, J. Friml, Auxin transporters and binding proteins at a glance, J. Cell. Sci. 128 (2015) 1–7, https://doi.org/10.1242/jcs.159418.

[33] A. Tromas, N. Braun, P. Muller, T. Khodus, I.A. Paponov, K. Palme, K. Ljung, J. Y. Lee, P. Benfey, J.A.H. Murray, B. Scheres, C. Perrot-Rechenmann, The AUXIN BINDING PROTEIN 1 is required for differential Auxin responses mediating root growth, PLoS One 4 (2009) 1–11, https://doi.org/10.1371/journal.pone.0006648.

[34] X. Chen, S. Naramoto, S. Robert, R. Tejos, C. Löfke, D. Lin, Z. Yang, J. Friml, ABP1 and ROP6 GTPase signaling regulate clathrin-mediated endocytosis in Arabidopsis roots, Curr. Biol. 22 (2012) 1326–1332, https://doi.org/10.1016/j.cub.2012.05.020.

[35] P. Grones, X. Chen, S. Simon, W.A. Kaufmann, R. De Rycke, T. Nodzyński, E. Zažímalová, J. Friml, Auxin-binding pocket of ABP1 is crucial for its gain-of-function cellular and developmental roles, J. Exp. Bot. 66 (2015) 5055–5065, https://doi.org/10.1093/jxb/erv177.

[36] X. Chen, L. Grandont, H. Li, R. Hauschild, S. Paque, A. Abuzeineh, H. Rakusová, E. Benkova, C. Perrot-Rechenmann, J. Friml, Inhibition of cell expansion by rapid ABP1-mediated auxin effect on microtubules, Nature 516 (2014) 90–93, https://doi.org/10.1038/nature13889.

[37] S. Paque, G. Mouille, L. Grandont, D. Alabadí, C. Gaertner, A. Goyallon, P. Muller, C. Primard-Brisset, R. Sormani, M.A. Blázquez, C. Perrot-Rechenmann, AUXIN BINDING PROTEIN1 links cellwall remodeling, auxin signaling, and cell expansion in Arabidopsis, Plant Cell 26 (2014) 280–295, https://doi.org/10.1105/tpc.113.120048.

[38] Y. Gao, Y. Zhang, D. Zhang, X. Dai, M. Estelle, Y. Zhao, Auxin binding protein 1 (ABP1) is not required for either auxin signaling or Arabidopsis development, Proc. Natl. Acad. Sci. U. S. A. 112 (2015) 2275–2280, https://doi.org/10.1073/pnas.1500365112.

[39] J. Michalko, M. Dravecká, T. Bollenbach, J. Friml, Embryo-lethal phenotypes in early abp1 mutants are due to disruption of the neighboring BSM gene [version 1; referees: 3 approved], F1000Research 4 (2015), https://doi.org/10.12688/f1000research.7143.1.

[40] X. Dai, Y. Zhang, D. Zhang, J. Chen, X. Gao, M. Estelle, Y. Zhao, Embryonic lethality of Arabidopsis abp1-1 is caused by deletion of the adjacent BSM gene, Nat. Plants 1 (2015) 3–6, https://doi.org/10.1038/nplants.2015.183.

[41] T.A. Enders, S. Oh, Z. Yang, B.L. Montgomery, L.C. Strader, Genome sequencing of arabidopsis abp1-5 reveals second-site mutations that may affect phenotypes, Plant Cell 27 (2015) 1820–1826, https://doi.org/10.1105/tpc.15.00214.

[42] J. Michalko, M. Glanc, C. Perrot-Rechenmann, J. Friml, Strong morphological defects in conditional Arabidopsis abp1 knock-down mutants generated in absence of functional ABP1 protein, F1000Research 5 (2016) 86, https://doi.org/10.12688/f1000research.7654.1.

[43] M. Klode, R.I. Dahlke, M. Sauter, B. Steffens, Expression and subcellular localization of Arabidopsis thaliana auxin-binding protein 1 (ABP1), J. Plant Growth Regul. 30 (2011) 416–424, https://doi.org/10.1007/s00344-011-9203-2.

[44] J. Friml, A. Vieten, M. Sauer, D. Weijers, H. Schwarz, T. Hamann, R. Offringa, G. Jürgens, Efflux-dependent auxin gradients establish the apical-basal axis of Arabidopsis, Nature 426 (2003) 147–153, https://doi.org/10.1038/nature02085.

[45] S.J. Clough, A.F. Bent, Floral dip: a simplified method for Agrobacterium -mediated transformation of Arabidopsis thaliana, Plant J. 16 (1998) 735–743, https://doi.org/10.1046/j.1365-313x.1998.00343.x.

[46] J.E. Malamy, P.N. Benfey, Organization and cell differentiation in lateral roots of Arabidopsis thaliana, Development 124 (1997) 33–44.

[47] T. Czechowski, M. Stitt, T. Altmann, M.K. Udvardi, W.-R. Scheible, Genome-Wide Identification and Testing of Superior Reference Genes for Transcript Normalization in Arabidopsis, Plant Physiol. 139 (2005) 5 LP–17, https://doi.org/10.1104/pp.105.063743.

[48] D. von Wangenheim, R. Hauschild, M. Fendrych, V. Barone, E. Benková, J. Friml, Live tracking of moving samples in confocal microscopy for vertically grown roots, Elife 6 (2017), https://doi.org/10.7554/eLife.26792.

[49] J. Mathur, C. Koncz, Callus culture and regeneration, Methods Mol. Biol. 82 (1998) 31–34, https://doi.org/10.1385/0-89603-391-0:31.

[50] T. Ulmasov, J. Murfett, G. Hagen, T.J. Guilfoyle, Creation of a highly active synthetic AuxRE, Society 9 (1997) 1963–1971, https://doi.org/10.1105/tpc.9.11.1963.

[51] C. Després, C. Chubak, A. Rochon, R. Clark, T. Bethune, D. Desveaux, P.R. Fobert, The Arabidopsis NPR1 disease resistance protein is a novel cofactor that confers redox regulation of DNA binding activity to the basic domain/leucine zipper transcription factor TGA1, Plant Cell 15 (2003) 2181–2191, https://doi.org/10.1105/tpc.012849.

[52] S. Berg, D. Kutra, T. Kroeger, C.N. Straehle, B.X. Kausler, C. Haubold, M. Schiegg, J. Ales, T. Beier, M. Rudy, K. Eren, J.I. Cervantes, B. Xu, F. Beuttenmueller, A. Wolny, C. Zhang, U. Koethe, F.A. Hamprecht, A. Kreshuk, Ilastik: interactive machine learning for (Bio)image analysis, Nat. Methods 16 (2019) 1226–1232, https://doi.org/10.1038/s41592-019-0582-9.

[53] L. Hoermayer, J.C. Montesinos, P. Marhava, E. Benková, S. Yoshida, J. Friml, Wounding-induced changes in cellular pressure and localized auxin signalling spatially coordinate restorative divisions in roots, Proc. Natl. Acad. Sci. (2020), https://doi.org/10.1073/pnas.2003346117, 202003346.

[54] M. Sauer, J. Balla, C. Luschnig, J. Wisniewska, V. Reinöhl, J. Friml, E. Benková, Canalization of auxin flow by Aux/IAA-ARF-dependent feedback regulation of PIN polarity, Genes Dev. 20 (2006) 2902–2911, https://doi.org/10.1101/gad.390806.

[55] L. Abas, R. Benjamins, N. Malenica, T.T. Paciorek, J. Wiśniewska, J.C. Moulinier-Anzola, T. Sieberer, J. Friml, C. Luschnig, Intracellular trafficking and proteolysis of the Arabidopsis auxin-efflux facilitator PIN2 are involved in root gravitropism, Nat. Cell Biol. 8 (2006) 249–256, https://doi.org/10.1038/ncb1369.

[56] T. Hruz, O. Laule, G. Szabo, F. Wessendorp, S. Bleuler, L. Oertle, P. Widmayer, W. Gruissem, P. Zimmermann, Genevestigator V3: a reference expression database for the meta-analysis of transcriptomes, Adv. Bioinformatics 2008 (2008) 420747, https://doi.org/10.1155/2008/420747.

[57] S. Sabatini, D. Beis, H. Wolkenfelt, J. Murfett, T. Guilfoyle, J. Malamy, P. Benfey, O. Leyser, N. Bechtold, P. Weisbeek, B. Scheres, An auxin-dependent distal organizer of pattern and polarity in the Arabidopsis root, Cell. 99 (1999) 463–472, https://doi.org/10.1016/s0092-8674(00)81535-4.

[58] J. Friml, E. Benková, I. Blilou, J. Wisniewska, T. Hamann, K. Ljung, S. Woody, G. Sandberg, B. Scheres, G. Jürgens, K. Palme, AtPIN4 mediates sink-driven auxin gradients and root patterning in Arabidopsis, Cell 108 (2002) 661–673, https://doi.org/10.1016/S0092-8674(02)00656-6.

[59] E. Benková, M. Michniewicz, M. Sauer, T. Teichmann, D. Seifertová, G. Jürgens, J. Friml, Local, efflux-dependent auxin gradients as a common module for plant

organ formation, Cell 115 (2003) 591–602, https://doi.org/10.1016/S0092-8674(03)00924-3.
[60] W. He, J. Brumos, H. Li, Y. Ji, M. Ke, X. Gong, Q. Zeng, W. Li, X. Zhang, F. An, X. Wen, P. Li, J. Chu, X. Sun, C. Yan, N. Yan, D.Y. Xie, N. Raikhel, Z. Yang, A. N. Stepanova, J.M. Alonso, H. Guo, A small-molecule screen identifies L-Kynurenine as a competitive inhibitor of TAA1/TAR activity in ethylene-directed auxin biosynthesis and root growth in Arabidopsis, Plant Cell 23 (2011) 3944–3960, https://doi.org/10.1105/tpc.111.089029.
[61] M. Lavy, M. Estelle, Mechanisms of auxin signaling, Development 143 (2016) 3226–3229, https://doi.org/10.1242/dev.131870.
[62] Z. Ding, J. Friml, Auxin regulates distal stem cell differentiation in Arabidopsis roots, Proc. Natl. Acad. Sci. U. S. A. 107 (2010) 12046–12051, https://doi.org/10.1073/pnas.1000672107.
[63] M.L. Evans, H. Ishikawa, M.A. Estelle, Responses of Arabidopsis roots to auxin studied with high temporal resolution: comparison of wild type and auxin-response mutants, Planta 194 (1994) 215–222, https://doi.org/10.1007/BF00196390.
[64] H.M.O. Leyser, F.B. Pickett, S. Dharmasiri, M. Estelle, Mutations in the AXR3 gene of Arabidopsis result in altered auxin response including ectopic expression from the SAUR-AC1 promoter, Plant J. 10 (1996) 403–413, https://doi.org/10.1046/j.1365-313x.1996.10030403.x.
[65] K. Scheitz, H. Lüthen, D. Schenck, Rapid auxin-induced root growth inhibition requires the TIR and AFB auxin receptors, Planta 238 (2013) 1171–1176, https://doi.org/10.1007/s00425-013-1941-x.
[66] C. Luschnig, R.A. Gaxiola, P. Grisafi, G.R. Fink, EIR1, a root-specific protein involved in auxin transport, is required for gravitropism in Arabidopsis thaliana, Genes Dev. 12 (1998) 2175–2187, https://doi.org/10.1101/gad.12.14.2175.
[67] H. Rakusová, M. Fendrych, J. Friml, Intracellular trafficking and PIN-mediated cell polarity during tropic responses in plants, Curr. Opin. Plant Biol. 23 (2015) 116–123, https://doi.org/10.1016/j.pbi.2014.12.002.
[68] S.H. Su, N.M. Gibbs, A.L. Jancewicz, P.H. Masson, Molecular mechanisms of root gravitropism, Curr. Biol. 27 (2017) R964–R972, https://doi.org/10.1016/j.cub.2017.07.015.
[69] H. Han, H. Rakusová, I. Verstraeten, Y. Zhang, J. Friml, SCF TIR1 / AFB auxin signaling for bending termination, Plant Physiol. Prev. 183 (2020) 37–40, https://doi.org/10.1104/pp.20.00212.
[70] W.M. Gray, A. Östin, G. Sandberg, C.P. Romano, M. Estelle, High temperature promotes auxin-mediated hypocotyl elongation in Arabidopsis, Proc. Natl. Acad. Sci. U. S. A. 95 (1998) 7197–7202, https://doi.org/10.1073/pnas.95.12.7197.
[71] A. Peaucelle, R. Wightman, H. Höfte, The control of growth symmetry breaking in the Arabidopsis hypocotyl, Curr. Biol. 25 (2015) 1746–1752, https://doi.org/10.1016/j.cub.2015.05.022.
[72] K. Takahashi, K.I. Hayashi, T. Kinoshita, Auxin activates the plasma membrane H +-ATPase by phosphorylation during hypocotyl elongation in Arabidopsis, Plant Physiol. 159 (2012) 632–641, https://doi.org/10.1104/pp.112.196428.
[73] E. Scarpella, D. Marcos, J. Friml, T. Berleth, Control of leaf vascular patterning by polar auxin transport, Genes Dev. 20 (2006) 1015–1027, https://doi.org/10.1101/gad.1402406.
[74] C. Verna, S.J. Ravichandran, M.G. Sawchuk, N.M. Linh, E. Scarpella, Coordination of tissue cell polarity by auxin transport and signaling, Elife 8 (2019) 1–30, https://doi.org/10.7554/eLife.51061.
[75] A. Hay, M. Barkoulas, M. Tsiantis, ASYMMETRIC LEAVES1 and auxin activities converge to repress BREVIPEDICELLUS expression and promote leaf development in Arabidopsis, Development 133 (2006) 3955–3961, https://doi.org/10.1242/dev.02545.
[76] C.S. Galvan-Ampudia, M.M. Julkowska, E. Darwish, J. Gandullo, R.A. Korver, G. Brunoud, M.A. Haring, T. Munnik, T. Vernoux, C. Testerink, Halotropism is a response of plant roots to avoid a saline environment, Curr. Biol. 23 (2013) 2044–2050, https://doi.org/10.1016/j.cub.2013.08.042.
[77] M. Zwiewka, T. Nodzyński, S. Robert, S. Vanneste, J. Friml, Osmotic stress modulates the balance between exocytosis and clathrin-mediated endocytosis in Arabidopsis thaliana, Mol. Plant 8 (2015) 1175–1187, https://doi.org/10.1016/j.molp.2015.03.007.
[78] W. Liu, R.-J. Li, T.-T. Han, W. Cai, Z.-W. Fu, Y.-T. Lu, Salt stress reduces root meristem size by nitric oxide-mediated modulation of auxin accumulation and signaling in Arabidopsis, Plant Physiol. 168 (2015) 343–356, https://doi.org/10.1104/pp.15.00030.
[79] J.I. Kim, D. Baek, H.C. Park, H.J. Chun, D.-H. Oh, M.K. Lee, J.-Y. Cha, W.-Y. Kim, M.C. Kim, W.S. Chung, H.J. Bohnert, S.Y. Lee, R.A. Bressan, S.-W. Lee, D.-J. Yun, Overexpression of Arabidopsis YUCCA6 in potato results in high-auxin developmental phenotypes and enhanced resistance to water deficit, Mol. Plant 6 (2013) 337–349, https://doi.org/10.1093/mp/sss100.
[80] Q. Ke, Z. Wang, C.Y. Ji, J.C. Jeong, H.-S. Lee, H. Li, B. Xu, X. Deng, S.-S. Kwak, Transgenic poplar expressing Arabidopsis YUCCA6 exhibits auxin-overproduction phenotypes and increased tolerance to abiotic stress, Plant Physiol. Biochem. 94 (2015) 19–27, https://doi.org/10.1016/j.plaphy.2015.05.003.
[81] P. Marhava, L. Hoermayer, S. Yoshida, P. Marhavý, E. Benková, J. Friml, Re-activation of stem cell pathways for pattern restoration in plant wound healing, Cell 177 (2019) 957–969, https://doi.org/10.1016/j.cell.2019.04.015, e13.
[82] T. Vernoux, J. Kronenberger, O. Grandjean, P. Laufs, J. Traas, PIN-FORMED 1 regulates cell fate at the periphery of the shoot apical meristem, Development 127 (2000) 5157–5165.
[83] D. Reinhardt, T. Mandel, C. Kuhlemeier, Auxin regulates the initiation and radial position of plant lateral organs, Plant Cell 12 (2000) 507–518, https://doi.org/10.1105/tpc.12.4.507.
[84] D. Reinhardt, E.R. Pesce, P. Stieger, T. Mandel, K. Baltensperger, M. Bennett, J. Traas, J. Friml, C. Kuhlemeier, Regulation of phyllotaxis by polar auxin transport, Nature. 426 (2003) 255–260, https://doi.org/10.1038/nature02081.
[85] M. Furutani, Y. Nakano, M. Tasaka, MAB4-induced auxin sink generates local auxin gradients in Arabidopsis organ formation, Proc. Nat. Acad. Sci. U. S. A 2013 (2013), https://doi.org/10.1073/pnas.1316109111.
[86] M.G. Heisler, C. Ohno, P. Das, P. Sieber, G.V. Reddy, J.A. Long, E.M. Meyerowitz, Patterns of auxin transport and gene expression during primordium development revealed by live imaging of the Arabidopsis inflorescence meristem, Curr. Biol. 15 (2005) 1899–1911, https://doi.org/10.1016/j.cub.2005.09.052.
[87] F. Besnard, Y. Refahi, V. Morin, B. Marteaux, G. Brunoud, P. Chambrier, F. Rozier, V. Mirabet, J. Legrand, S. Lainé, E. Thévenon, E. Farcot, C. Cellier, P. Das, A. Bishopp, R. Dumas, F. Parcy, Y. Helariutta, A. Boudaoud, C. Godin, J. Traas, Y. Guédon, T. Vernoux, Cytokinin signalling inhibitory fields provide robustness to phyllotaxis, Nature 505 (2014) 417–421, https://doi.org/10.1038/nature12791.
[88] T. Berleth, T. Sachs, Plant morphogenesis: long-distance coordination and local patterning, Curr. Opin. Plant Biol. 4 (2001) 57–62, https://doi.org/10.1016/S1369-5266(00)00136-9.
[89] K. Wabnik, J. Kleine-Vehn, J. Balla, M. Sauer, S. Naramoto, V. Reinöhl, R.M. H. Merks, W. Govaerts, J. Friml, Emergence of tissue polarization from synergy of intracellular and extracellular auxin signaling, Mol. Syst. Biol. 6 (2010), https://doi.org/10.1038/msb.2010.103.
[90] M. Glanc, M. Fendrych, J. Friml, Mechanistic framework for cell-intrinsic re-establishment of PIN2 polarity after cell division, Nat. Plants 4 (2018) 1082–1088, https://doi.org/10.1038/s41477-018-0318-3.
[91] N. Geldner, J. Firml, Y.D. Stierhof, G. Jürgens, K. Palme, Auxin transport inhibitors block PIN1 and vessicle trafficing, Nature 413 (2001) 425–428.
[92] I.A. Paponov, J. Dindas, E. Król, T. Friz, V. Budnyk, W. Teale, M. Paponov, R. Hedrich, K. Palme, Auxin-induced plasma membrane depolarization is regulated by AUXIN transport and not by AUXIN BINDING PROTEIN1, Front. Plant Sci. 9 (2019), https://doi.org/10.3389/fpls.2018.01953.
[93] R. Hertel, K.S. Thomson, V.E.A. Russo, In-vitro auxin binding to particulate cell fractions from corn coleoptiles, Planta 107 (1972) 325–340, https://doi.org/10.1007/BF00386394.
[94] M. Löbler, D. Klämbt, Auxin-binding protein from coleoptile membranes of corn (Zea mays L.). II. Localization of a putative auxin receptor, J. Biol. Chem. 260 (1985) 9854–9859.
[95] Y. Effendi, S. Rietz, U. Fischer, G.F.E. Scherer, The heterozygous abp1/ABP1 insertional mutant has defects in functions requiring polar auxin transport and in regulation of early auxin-regulated genes, Plant J. 65 (2011) 282–294, https://doi.org/10.1111/j.1365-313X.2010.04420.x.
[96] N. Braun, J. Wyrzykowsk, P. Muller, K. David, D. Couch, C. Perrot-Rechenmann, A.J. Fleming, Conditional repression of Auxin Binding Protein1 reveals that it coordinates cell division and cell expansion during postembryonic shoot development in Arabidopsis and tobacco, Plant Cell 20 (2008) 2746–2762, https://doi.org/10.1105/tpc.108.059048.
[97] A. Tromas, S. Paque, V. Stierlé, A.L. Quettier, P. Muller, E. Lechner, P. Genschik, C. Perrot-Rechenmann, Auxin-Binding Protein 1 is a negative regulator of the SCF TIR1/AFB pathway, Nat. Commun. 4 (2013), https://doi.org/10.1038/ncomms3496.
[98] A.M. Jones, Auxin-dependent cell expansion mediated by overexpressed auxin-binding protein 1, Science (80-.) 282 (1998) 1114–1117, https://doi.org/10.1126/science.282.5391.1114.
[99] J.M. Bauly, I.M. Sealy, H. Macdonald, J. Brearley, S. Droge, S. Hillmer, D. G. Robinson, M.A. Venis, M.R. Blatt, C.M. Lazarus, R.M. Napier, Overexpression of auxin-binding protein enhances the sensitivity of guard cells to auxin, Plant Physiol. 124 (2000) 1229–1238, https://doi.org/10.1104/pp.124.3.1229.
[100] K. Palme, T. Hesse, N. Campos, C. Garbers, M.F. Yanofsky, J. Schell, Molecular analysis of an auxin binding protein gene located on chromosome 4 of arabidopsis, Plant Cell 4 (1992) 193–201, https://doi.org/10.1105/tpc.4.2.193.
[101] W. Diekmann, M.A. Venis, D.G. Robinson, Auxins induce clustering of the auxin-binding protein at the surface of maize coleoptile protoplasts, Proc. Natl. Acad. Sci. U. S. A. 92 (1995) 3425–3429, https://doi.org/10.1073/pnas.92.8.3425.
[102] R.M. Napier, K.M. David, C. Perrot-Rechenmann, A short history of auxin-binding proteins, Plant Mol. Biol. 49 (2002) 339–348.
[103] J.M. Dunwell, J.G. Gibbings, T. Mahmood, S.M. Saqlan Naqvi, Germin and germin-like proteins: evolution, structure, and function, Crit. Rev. Plant Sci. 27 (2008) 342–375, https://doi.org/10.1080/07352680802333938.